

Dual operative Radar for Vehicle To Vehicle and Vehicle To Infrastructure Communication



Pasquale Striano

Centre for Signal and Image Processing
Department of Electronic and Electrical Engineering
University of Strathclyde
Glasgow

This dissertation is submitted for the degree of
Doctor of Philosophy

2020

This thesis is the result of the author's original research. It has been composed by the author and has not been previously submitted for examination which has led to the award of a degree.

The copyright of this thesis belongs to the author under the terms of the United Kingdom Copyright Acts as qualified by University of Strathclyde Regulation 3.50. Due acknowledgement must always be made of the use of any material contained in, or derived from, this thesis.

Abstract

The research presented in this Thesis deals with the concepts of joint radar and communication system for automotive application. The novel systems developed include a joint radar and communication system based on the fractional Fourier transform (FrFT) and two interference mitigation frameworks.

In the joint radar and communication system the FrFT is used to embed the data information into a radar waveform in order to obtain a signal sharing Linear Frequency Modulation (LFM) characteristics while allowing data transmission. Furthermore, in the proposed system multi user operations are allowed by assigning a specific order of the FrFT to each user. In this way, a fractional order division multiplexing can be implemented allowing the allocation of more than one user in the same frequency band with the advantage that the range resolution does not depend on the number of the users that share the same frequency band but only from the assigned of the FrFT. Remarkably, the predicted simulated radar performance of the proposed joint radar and communication system when using Binary Frequency Shift Keying (BFSK) encoding is not significantly affected by the transmitted data.

In order to fully describe the proposed waveform design, the signal model when the bits of information are modulated using either BFSK or Binary Phase Shift Keying (BPSK) encoding is derived. This signal model will result also useful in the interference mitigation frameworks.

In multi user scenarios to prevent mutual radar interference caused by users that share the same frequency band at the same time, each user has to transmit waveforms that are uncorrelated with those of other users. However, due to spectrum limitations, the uncorrelated property cannot always be satisfied even by using fractional order division multiplexing, thus interfer-

ence is unavoidable. In order to mitigate the interference, two frameworks are introduced. In a joint radar communication system, the radar also has access to the communication data. With a near-precision reconstruction of the communication signal, this interference can be subtracted. In these two frameworks the interfering signal can be reconstructed using the derived mathematical model of the proposed FrFT waveform.

In the first framework the subtraction between the received and reconstructed interference signals is carried out in a coherent manner, where the amplitude and phase of the two signals are taken into account. The performance of this framework is highly depend on the correct estimation of the Doppler frequency of the interfering user. A small error on the Doppler frequency can lead to a lack of synchronization between the received and reconstructed signal. Consequently, the subtraction will not be performed in a correct way and further interference components can be introduced.

In order to solve the problem of the lack of the synchronization an alternative framework is developed where the subtraction is carried out in non-coherent manner. In the proposed framework, the subtraction is carried out after that the received radar signal and the reconstructed interference are processed, respectively. The performance is tested on simulated and real signals. The simulated and experimental results show that this framework is capable of mitigating the interference from other users successfully.

Table of contents

List of figures	ix
List of tables	xiv
Symbols	xv
1 Introduction	1
1.1 Preface	1
1.2 Motivations	2
1.3 Original Contributions	3
1.4 Publications	4
1.5 Thesis Organization	5
2 Automotive radar	8
2.1 Basic concepts	9
2.1.1 Radar Range Equation	10
2.1.2 Processing Gain	12
2.1.3 Pulse compression	13
2.1.4 Radar Data Matrix	14
2.1.5 Doppler Spectrum	16
2.2 Automotive Radar System	16
2.2.1 Classification	18
2.2.2 Waveform for Automotive Radar	19
2.2.3 Continuous Wave and Pulsed Wave Radars	19
2.2.4 Continuous Waveform	20
2.2.5 Unmodulated CW	22

Table of contents

2.2.6	Linear Frequency Waveform	23
2.2.7	Triangular LFM waveform	26
2.2.8	Frequency Shift Keying (FSK) Waveform	28
2.2.9	Multiple Frequency Shift Keying	31
2.2.10	Fast Chirp LFM (FCLFM)	34
2.2.11	Orthogonal Frequency Division Multiplexing	36
2.3	Conclusion	37
3	Time-Frequency representation	39
3.1	Ambiguity Function	40
3.2	Canonical AF Definition	40
3.3	AF Cuts and Properties	41
3.4	Short-Time Frequency Transformation	45
3.5	Bilinear Time-Frequency Transforms	47
3.6	Fractional Fourier transform	47
3.7	Definition	48
3.8	FrFT Properties	49
3.9	FrFT Implementations	51
3.9.1	Discrete FrFT	52
3.9.2	Fast Approximation of FrFT	52
3.10	Applications of FrFT in Signal processing	53
3.10.1	Communication	53
3.10.2	Radar applications	54
3.11	Conclusion	55
4	Joint Radar and Communication Systems	57
4.1	Sharing Radar and Communication	58
4.2	State of art systems and applications for joint radar and communication systems	61
4.2.1	Spread Spectrum techniques	62
4.2.2	Dual radar communication function based on phased array	65
4.2.3	Joint radar and communication system based on OFDM	66

Table of contents

4.2.4	Joint radar and communication system based on Orthogonal Time Frequency Space (OTFS)	72
4.2.5	Joint radar and communication system based on fractional Fourier transform (FrFT)	72
4.3	Mutual Radar Interference mitigation techniques	74
4.4	Interference mitigation for communication system	77
4.5	Conclusion	78
5	Joint Radar and Communication system for automotive environment	82
5.1	Proposed framework design	83
5.1.1	Communication Receiver	89
5.1.2	Frequency domain representation	90
5.2	Conclusion	98
6	Performance of the proposed joint radar and communication system	101
6.1	Radar performance	103
6.2	User discrimination	111
6.3	Multi target scenarios	114
6.4	Multi User scenario	116
6.5	Detection Performance versus SINR	119
6.6	Communication performance	121
6.6.1	Single User scenarios	122
6.6.2	Link Budget	123
6.6.3	Multi User scenarios	124
6.7	Conclusion	126
7	Interference Mitigation Strategies for the proposed system	129
7.1	Coherent Interference Framework	130
7.2	Non-coherent Interference Mitigation Framework	131
7.3	Performance of the proposed frameworks	133
7.4	Assessment of non-coherent interference mitigation	137

Table of contents

7.5	Non-Coherent Interference Mitigation On Simulated Signal . .	139
7.6	Non-Coherent Interference Mitigation on Real Signal	142
7.7	Conclusion	148
8	Conclusion and Future work	151
8.1	Future Work	154
Appendix A	Design of signal-sharing for radar and communica-	
	tion	157
References		159

List of figures

2.1	Major elements of the radar transmission/ reception process. . .	9
2.2	Matched filter output of 2.2a an unmodulated pulse and 2.2b an LFM waveform.	14
2.3	Slow-Time Fast-Time Data matrix.	15
2.4	Doppler spectrum for one range bin, viewed by a stationary target.	16
2.5	Advanced Driver Assistant System (ADAS) applications. . . .	17
2.6	Radar Waveform.	19
2.7	Monofrequency CW radar system.	21
2.8	Instantaneous frequency versus time for an LFM waveform. . .	24
2.9	Frequency of transmitted and received LFM as a function of time.	26
2.10	Frequency of transmitted and received triangular LFMs as a function of time.	27
2.11	Solutions of the beat frequencies problem, 2.11a when one target is present, 2.11b when two targets are present.	28
2.12	Frequency Shift Keying (FSK) waveform.	29
2.13	Multiple Frequency Shift Keying (MFSK).	32
2.14	Fast Chirp LFM (FCLFM).	35
2.15	OFDM block with symbols time T and cycle prefix time T_{CP} . . .	37
3.1	Ambiguity function of an LFM waveform, with a time-bandwidth by 2228.	44
3.2	The two cuts of an LFM pulse, 3.2a zero-Doppler cut, 3.2b zero delay cut. The time-bandwidth product is set at 2228. . .	45

List of figures

3.3	Illustration of STFT processing on the signal $x(t)$ from [44].	46
3.4	FrFT as a rotation in the time-frequency plane.	49
3.5	Time-Frequency representation using STFT of a Gaussian pulse after applying FrFT of different orders.	50
4.1	An example of joint radar and communication system.	60
4.2	Vehicular communication and ranging applications.	63
4.3	Ambiguity function of a joint radar and communication system based on OFMD [39].	67
4.4	Range profile calculated with the classical correlation based approach [130].	68
4.5	Range profile calculated with the approach proposed in [130].	69
4.6	Spectrum when two target at the same distance, but with two different velocities are present [129].	69
4.7	Block scheme of the OFDM system architecture [132].	70
4.8	Spectrogram of a FrFT CoRadar waveform with 7 sub carriers [42].	71
4.9	Communication performance on varying $\text{SNR}_{\text{comms}}$ and for dif- ferent number of chirp sub carriers [43].	73
4.10	Spectrogram obtained from FrFT based Co-Radar pulses with four sub carriers and different SNR radar, 4.10a SNR is set at 2.95 dB, 2.11b the SNR is set at 14.28 dB [43].	73
4.11	Example interference scenarios for automotive radar.	75
5.1	Block diagram of (top) monostatic radar and (bottom) the Communication of the FrFT based on a joint radar communi- cation basic configuration.	83
5.2	Envelope of the signal with two different orders of the FrFT and when a BFSK encoding is used, in 5.2a α is set at 0.3 while in 5.2b the order of the FrFT is set at 0.8.	86
5.3	Spectrograms of a Coherent Processing Interval.	88
5.4	Representation of the waveform in time domain.	88
5.5	Mean Square Error (MSE) of the amplitude 5.5a and phase 5.5b when the BFSK encoding scheme is used.	95

List of figures

5.6	Analytical and simulated PSDs when the BFSK modulation is used.	95
5.7	Mean Square Error (MSE) of the amplitude 5.7a and phase 5.7b when the BFSK encoding scheme is used.	97
5.8	Analytical and simulated PSDs when the BPSK modulation is used.	97
6.1	Ambiguity Function when the BFSK modulation is used. . . .	105
6.2	Ambiguity Function when the BPSK modulation is used. . . .	105
6.3	Zero-Doppler cut of the BFSK, BPSK, and LFM waveforms AF.	106
6.4	Zero-delay cut of the BFSK and BPSK waveforms AF.	106
6.5	SLL when the BFSK encoding scheme and LFM waveform are used.	107
6.6	SLL when the BPSK encoding and LFM are used.	108
6.7	Variance when the BFSK and BPSK encoding scheme are used.	109
6.8	Energy for different zero-Doppler cuts when the FrFT is applied on BFSK encoding scheme and when an LFM waveform is transmitted.	110
6.9	Receiver Operating Characteristic curves between P_D and design DP_{FA}	112
6.10	P_{FA} values versus design DP_{FA}	112
6.11	Cross-Correlation between the main and interference users for different values of α_{diff}	113
6.12	Multi target environment, when 4 targets are present.	115
6.13	Range-Doppler detection when 4 targets are present.	115
6.14	Range-Doppler map in multi user scenarios.	117
6.15	Range-Doppler detection in multi user scenarios.	118
6.16	Range-Doppler map, with LFMF waveform.	118
6.17	ROC curves in multi user scenarios.	121
6.18	Bit Error Rate versus SNR_{comms} when the BFSK encoding is used.	123
6.19	Bit Error Rate versus $SINR_{comms}$ when the BFSK encoding is used.	126

List of figures

7.1	Interference mitigation framework where the subtraction is carried out in coherent manner.	131
7.2	Interference mitigation framework where the subtraction is carried out in non-coherent manner.	132
7.3	SIR_{out} obtained when both frameworks are applied against the offset frequency $\delta_{\tilde{f}_D}$	134
7.4	SIR_{out} obtained when both frameworks are applied against the offset amplitude δ_C	135
7.5	SIR_{out} obtained when both frameworks are applied against the offset frequency $\delta_{\tilde{f}_D}$ considering that the interference signal is reconstructed using the analytical model of the proposed joint radar and communication system.	136
7.6	SIR_{out} obtained when both frameworks are applied against the offset amplitude δ_C considering that the interference signal is reconstructed using the analytical model of the proposed joint radar and communication system.	136
7.7	ROC curves obtained after interference mitigation, where in 7.7a each parameter is estimated, while in 7.7b the parameters are perfectly estimated	138
7.8	Power Spectral Density of the simulated signal before and after interference mitigation.	140
7.9	Spectrograms of the received signal 7.9a before and 7.9b after interference mitigation. The figures are normalized with the respect to the maximum values obtained by 7.9a.	141
7.10	Acquisition geometry of the laboratory-based experimental campaign.	142
7.11	Power Spectral Density of the real signal before and after interference mitigation.	143
7.12	Spectrograms of the received signal 7.12a before and 7.12b after interference mitigation. The figures are normalized with the respect to the maximum values obtained by 7.12a.	144
7.13	Spectrum of the received and simulated signal.	145

List of figures

7.14 Spectrograms of the signal scattered by a person 7.14a before and 7.14b after interference mitigation. The figures are normalized with the respect to the maximum values obtained by 7.14a.	146
7.15 Spectrograms of the signal scattered by a person 7.15a before and 7.15b after interference mitigation. The figures are normalized with the respect to the maximum values obtained by 7.15a.	147
A.1 Architecture design.	158

List of tables

Symbols	xiv
2.1 Technology and Performance Features [144].	17
2.2 Frequency bands for automotive radar in Europe.	18
2.3 Summary of fulfilled and missed requirements, of waveforms used in automotive radar.	38
3.1 Summary of fulfilled and missed requirements of the Time- Frequency representation.	55
4.1 Applications of the CRSS technology.	59
4.2 Radar performance parameters [42]	74
4.3 Summary of different joint radar and communication systems.	79
5.1 Further Properties of the FrFT [94].	91
6.1 System Parameter	104
6.2 Location of the targets	114
6.3 Interference power	117
6.4 Simulated Users Parameter	120
6.5 Link budget parameters	123
6.6 Simulated Users Parameter	124
7.1 System Parameters for a low computational cost	139
7.2 Maximum values before interference mitigation	148
7.3 Maximum values after interference mitigation	148

Symbols

Roman Symbols

A	Amplitude of the received radar signal
$\mathcal{A}_{Ca}(\cdot, \cdot)$	Ambiguity Function
B	Bandwidth
B_{LFM}	Bandwidth of LFM waveform
\hat{C}	Estimated amplitude of the interference signal
C_k	Amplitude of the interfering user
C_{spr}	Vector obtained after the CDMA
P_t	Power developed by the transmitter
DP_{FA}	Desired Probabilities of False Alarm
DP_I	Radar processing applying on reconstructed interference
DP_{T+I}	Radar processing applying on the received signal
\mathbf{E}	Engenvectors' matrix
E	Energy of the signal
\mathcal{F}_α	DFrFT matrix
\tilde{f}_D	Doppler frequency calculated on single path
$f(\cdot)$	Instantaneous frequency

Symbols

f_D	Doppler frequency
f_s	Sampling frequency
$\mathfrak{F}^{-1}\{\cdot\}$	Inverse Fourier Transform
$f_{c_{A,B}}$	Two carrier frequencies
f_b	Beat frequency
f_c	Carrier frequency
$f_{b_{down}}$	Beat frequency associated to a down-LFM waveform
\tilde{f}_{D_i}	Doppler frequency of the interfering user
\mathbf{F}_{ilt}	Output of the RRC filter
f_M	Mark frequency
\mathfrak{F}^α	fractional Fourier transform operator
\hat{f}_D	Estimated Doppler frequency of the interference signal
f_S	Space frequency
f_{step}	Frequency step using in FSKW
f_R	Received frequency
f_T	Transmitted frequency
$\mathfrak{F}\{\cdot\}$	Fourier Transform
f_τ	Range shift
$f_{b_{up}}$	Beat frequency associated to an up-LFM waveform
G_g	number of random bits
$G_{ch_{Inter}}$	Interference Transmit Gain Value
$G_{ch_{Radar}}$	Radar Transmit Gain Value

Symbols

$G_{ch_{Receive}}$	Receive Gain Value
$G_{t,r}$	Transmitter and receiver antenna gains
$h(t)$	Impulse response
\mathbf{h}_{RRC}	Time response of the RRC filter
\hat{I}	Reconstructed interference signal
$\hat{\mathcal{J}}_{rec}(\cdot)$	Reconstructed interference signal
\mathbf{I}_b	Vector obtained after the interleaver
I	Identity operator
\mathcal{J}	Sum of the reconstructed interference in the non-coherent framework
K_α	Kernel transform
L	Samples in fast-time
L_p	length of PN code
L_s	Loss factor
$M_{IF}(u)$	Integrated function
N_b	number of bits of information
N_I	Number of interfering users
N_s	Number of samples per symbol using in BFSK
N_T	Number of the targets
N_{trials}	Number of Monte Carlo runs
N_{wave}	Number of the pulses
\mathbf{P}	PN vector given by L_p bits

Symbols

P_{Int}	Power of interfering signal
P_{Com}	Communication power
P_{D}	Probability of Detection
P_{FA}	Probabilities of False Alarm
P_n	Power of the noise
P_r	Received power radar
P_{radar}	Received radar power
$Q_{1,2}$	Order of the pilot sequence used for the synchronization
\mathfrak{R}	Received radar signal plus received interference signal
R	Range
R_{Int_k}	Distance from the interfering user to the radar
R_0	Range at $t = 0$
R_s	Multirate filter
\mathfrak{s}_{rx}	Receiving radar signal
\mathfrak{s}_{tx}	Transmitting Unmodulated CW signal
S	Filter Span in Symbol
SINR_{Com}	SINR at communication side
SIR_{In}	SIR before the interference mitigation
SIR_{out}	SIR after the interference mitigation
SNR_c	Coherent SNR
SNR_{nc}	Non-coherent SNR
$\text{SNR}_{\text{comms}}$	SNR on communication side

Symbols

$\text{SNR}_{\text{radar}}$	SNR on radar side
$\tilde{S}_{rr}(f)$	Power Spectral Density of the reconstructed interference signal
$S_{rr}(f)$	Power Spectral Density of the received interference signal
$\tilde{\mathbf{S}}_{\text{sym}_{\text{BFSK},\text{BPSK}}}$	Sequence of symbols obtained when a BFSK or BPSK modulation are applied
S_{STFT}	Short-time Frequency transformation
$\hat{s}(u_n)$	Square pulse centred in t_n
\tilde{T}_{WAVE}	Time of signal after the FrFT
t	Slow time
T_{WAVE}	Time of signal after delete samples
T_{FrFT}	Threshold applied after the FrFT
T_{PRI}	PRI
t_p	Width of the transmitted pulse
t_s	Sampling time
u	FrFT domain
u'	Spatial time
$U_{\text{FSK,PSK}}$	Length of waveform after that the FrFT is applied
v_r	Velocity component along the radial between the radar and the target
\mathbf{x}_α	Discrete FrFT vector
\mathbf{x}_b	Vector that contains N_b data information
\mathbf{X}_α	FrFT waveform with α order after the sample delete
$\tilde{\mathbf{X}}_\alpha$	FrFT waveform with α order after the FrFT

Symbols

$\tilde{\mathbf{x}}_{bL_p}$	Sequence obtained when the interleaver is applied on data information
$x[\cdot]$	Arbitrary discrete signal
$\tilde{\mathbf{x}}_g$	Vector that contains G_g random bits
$x(t)$	Transmitted signal

Greek Symbols

α	Order fractional Fourier transform
α_{diff}	difference of the orders of the FrFT
β	Roll-off factor
$\Delta\phi_{\mathbf{b}}$	Difference beat phase
$\delta_{\mathcal{C}}$	Offset of amplitude of the interference signal
$\delta_{\tilde{f}_D}$	Offset of Doppler frequency of the interference signal
Δf_D	Doppler frequency resolution
η	fast time
$\mathfrak{f}_{tx,rx}$	Transmitted and received FSKW
$\zeta_{tx}(\cdot)$	Transmitted LFM waveform
Λ	Diagonal Eigenvalues
λ	Wavelength
$\hat{\zeta}$	Normalized LFM pulse
ν	Spatial frequency
ϕ	Phase of a signal
$\phi_{\mathbf{b}}$	Phase of a beat signal

Symbols

σ_{SLLs}^2	Variance of the SLLs
σ_{radar}	RCS of the radar
Δ_R	Range resolution
τ	Propagation delay calculated on dual path
$\tilde{\tau}$	Delay calculated on single path
$\hat{\tau}$	Estimated delay of the interference signal
ϱ	Time-bandwidth product
$\vartheta(\cdot)$	Rotation angle associated with the fractional order
$\tilde{\zeta}_{tx}(\cdot)$	Transmitted and received baseband LFM waveform

Subscripts

$(\cdot)_i$	i-th target
$(\cdot)_k$	k-th interfering user
$(\cdot)_M$	Main user

Superscripts

$(\cdot)^*$	Complex conjugate
\circ	Convolution operator
$(\cdot)^T$	Transpose matrix operation

Acronyms/Abbreviations

AF	Ambiguity Function
ADAS	Advanced Driver Assistant System
AFT	Affine Fourier Transform
AM	Amplitude Modulation

Symbols

ASK	Amplitude Shift Keying
ATC	Air Traffic Control
AWGN	Additive white Gaussian noise
BER	Bit Error Rate
BFSK	Binary Frequency Shift Keying
BPSK	Binary Phase Shift Keying
CRSS	Communication and Radar Spectrum Sharing
CDM	Code Division Multiplexing
CA-CFAR	Cell-averaging CFAR
CE	Constant Envelope
RCCM	Range Cell Migration Correction
CFAR	Constant False Alarm Rate
CPI	Coherent Processing Interval
CW	Continuous Wave
DFrFT	Discrete FrFT
DFT	Discrete Fourier Transform
DSSS	Direct-Sequence Spread Spectrum
EM	Electromagnetic
FCLFM	Fast Chirp LFM
FDM	Frequency Division Multiplexing
FrFT	fractional Fourier transform
FSK	Frequency Shift Keying

Symbols

FSKW	Frequency Shift Keying Waveform
FT	Fourier transform
GHz	Gigahertz
GNSS	Global Navigation Satellite System
Hz	Hertz
IFT	inverse Fourier transform
ISI	Inter-Symbol Interference
ITS	Intelligent Transportation System
KPI	Key Performance Indicators
LFM	Linear Frequency Modulated
LHCP	Left Hand Circular Polarized
LFM	Linear Frequency Modulation
LOS	Line of Sight
LPI	Low-probability of Intercept
LRR	Long Range Radar
LTE	Long-Term Evolution
MFSK	Multiple Frequency Shift Keing
MIMO	Multiple Input Multiple Output
mmWave	Millimeter Wave
MRR	Medium Range Radar
MSE	Mean Square Error
NI-USRP	National Instruments Universal Software Defined Radio

Symbols

NASA	National Aeronautics and Space Administration
NR	New Radio
OFDM	Orthogonal Frequency Division Multiplexing
PAPR	Peak-to-Average Power Ratio
PN	Pseudo Noise
PR	Pseudo random
PRF	Pulse Repetition Frequency
PRI	Pulse Repetition Time
PSK	Phase Shift Keying
RCMC	Range Cell Migration Correction
RADAR	RAdio Detecting And Ranging
RCS	Radar Cross Section
RHCP	Right Hand Circular Polarized
ROC	Receiver Operating Characteristic
RRC	Root Raised Cosine
SAR	Synthetic Aperture Radar
SDR	Software Defined Radio
SINR	Signal-to-Interference-plus-Noise Ratio
SIR	Signal-to-Interference Ratio
SLL	Sidelobe Level
SNR	Signal-to-Noise Ratio
SRR	Short Range Radar

Symbols

SLD	Square Law Detector
STFT	Short-time Fourier transform
SWaP	Size, Weight and Power
TDD	Time-division Duplex
TDM	Time Division Multiplexing
TFMCW	Trapezoidal Frequency Modulation Continuous Wave
T/R	Transmit/receive device
UAV	Unmanned Aerial Vehicle
V2V	Vehicle to Vehicle
V2X	Vehicle-to-Everything

Chapter 1

Introduction

1.1 Preface

Road traffic injuries are a major but neglected global public health problem, requiring concerted efforts for effective and sustainable prevention. In [96], it was presented that the number of people killed in road traffic crashes each year is estimated at almost 1.2 million, while the number injured could be as high as 50 million. The appraisal of the main responsible accident factors indicates different solutions to adopt in order to reduce the total number of crashes. The most important and efficient solution is to raise awareness in society. However, they also emphasize the concept of intelligent vehicles and smart city in order to improve the visibility of the driver, provide road state knowledge, or just to reduce the reaction time against an accident through automatic brake controls.

The European standard for Intelligent Transportation Systems (ITS) [86] and the international standard IEEE 802.11p [63], are the reference standards in this field. Their aim is to establish an intelligent network among vehicles and the infrastructure, such to provide the Vehicle-to-Vehicle (V2V) and Vehicle-to-Infrastructure (V2I) communication. This network could be used to share information such as payment, road status, weather forecasts, with other drivers.

Nonetheless, the idea of using an intelligent network to perform a traffic safety system is considered as an indirect method, since the locations of the vehicles

can be implicitly determined by the communication among the vehicles that belong to this network. An obvious drawback of this system is related to the vehicles that do not belong to the network or possible objects obstructing the road; in these situations, the obstacles and vehicles cannot be detected.

In order to overcome this issue, a direct method can be applied using sensors as radar, camera, lidar. From the earliest days, the use of radar is oriented to detect and track targets accurately. The capability to operate in hostile weather and day and night are two great advantages of the use of electromagnetic waves compared with other sensors.

The separation of the radar and communication functions is a waste of the hardware and the spectrum is not used in an efficient manner. Additionally, it has been demonstrated that the radar spectral efficiency can be improved incrementing the bandwidth or reusing the radar bandwidth to perform communication operation [84] [45]. Besides, a joint radar and communication applications are feasible due to recent advances in digital signal processing unit, such that the computational cost arises from the baseband signal processing unit from such a merged system can be easily performed. The mains advantages of a joint radar communication system are that both functions share the same hardware, transmitter, receiver, antennas, as well as the radio-electromagnetic spectrum; thus, the efficiency of the spectrum is improved.

1.2 Motivations

The aim of this thesis is to develop a new joint radar communication system based on the fractional Fourier transform (FrFT) for automotive applications. Additionally, in an automotive environment where more than one vehicle shares the same channel at the same time strong mutual radar interference can arise leading to a degradation of the radar and communication performance. In order to reduce the interference, two frameworks for interference mitigation are developed. The objectives of the research presented in this thesis are: to use the FrFT to embed the data information into a radar waveform; to use the different order of the FrFT to allocate more than one user in the same frequency band. The radar performance of the proposed joint radar

and communication system is evaluated and compared to that when a Linear Frequency Modulated (LFM) pulse is transmitted. The radar performance of the proposed system is evaluated considering the ability of the proposed waveform to distinguish multiple targets allocated at the same distance or have different distance and Doppler frequencies. In addition, the radar performance is evaluated even in multi user scenarios, where the targets are transmitting a radar communication signal. In this scenario a degradation of the detection performance is achieved. In an automotive environment, a radar sensor is used to increase security, consequently, in order to improve the detection performance additionally processing is required. Thus, two interference mitigation frameworks based on joint radar and communication system are presented. The main difference between these two frameworks is that in the first the interference is mitigated by applying a coherent subtraction between the received and reconstructed signals, while in the second framework the subtraction is carried out in a non-coherent manner. The performance of these two frameworks are compared respect to the Signal to Interference plus Noise Ratio (SINR) against different values by offset frequency and amplitude.

1.3 Original Contributions

The research detailed in this thesis includes original contributions to the field of joint radar and communication system for automotive applications. The original contributions can group in two different groups. In the first group, a new joint radar and communication system, based on the fractional Fourier transform, is presented. In the second group, in order to alleviate the mutual radar interference, two frameworks for interference mitigation are presented and described. The main contributions are as follows:

- A new joint radar and communication system, based on the FrFT for automotive application, is developed. So considering its related framework, the FrFT is used to generate a signal sharing LFM feature, while allowing communication and radar functions to run simultaneously by using the same hardware and the same spectrum.

- In order to allow more than one user to share the same channel at the same time a fractional order division multiplexing is proposed.
- The closed form derivation of the analytical signal model and the Power Spectral Density (PSD) of the proposed joint radar and communication system is derived, when the bits are mapped into symbols through a BFSK and BPSK encoding scheme.
- A coherent interference mitigation framework is proposed where the subtraction between the reconstructed and received interference is carried out, by considering the amplitude and phase of these two signals.
- A non-coherent interference mitigation framework is presented where the interference is mitigated in a non-coherent way. This means that the subtraction between the reconstructed interference and the received one, is carried out only considering the amplitude.
- The proposed joint radar and communication system is developed on SDR device and the real data are achieved in a controlled laboratory environment.

The first three contributions are presented in chapter 5, while last three ones are presented in chapter 7

1.4 Publications

Journal Paper

- P. Striano, C.V. Ilioudis, C. Clemente, J. Soraghan (2019), Communicating radar using frequency-shift keying and fractional Fourier transform for automotive applications, in The Journal of Engineering, vol. 2019, no. 19, pp. 6016-6020.

Conference Papers

- P. Striano, C. V. Ilioudis, C. Clemente, J. Soraghan, (2019) Performance of a Communicating Radar using FSK and Fractional Fourier Transform for Automotive Applications, 2019 IEEE Radio and Wireless Symposium (RWS), Orlando, FL, USA, pp.1-4

- P. Striano, C. V. Ilioudis, C. Clemente, J. Soraghan, (2019) Fractional Fourier Transform based Joint Radar Communication system for Multi-User Automotive Applications, 2019 IEEE Radar Conference (RadarConf), Boston, MA, USA, pp.1-6
- C. V. Ilioudis, J. Cao, I. Theodorou, P. Striano, W. Coventry, C. Clemente, J. Soraghan, (2019), GNSS Based Passive Radar for UAV Monitoring, 2019 IEEE Radar Conference (RadarConf), Boston, MA, USA, pp.1-6
- P. Striano, C. V. Ilioudis, J. Cao, C. Clemente, J. Soraghan, (2020), Interference Mitigation for a joint radar communication system based on the FrFT for Automotive Applications, 2020 IEEE International Radar Conference (RADAR), Washington, DC, USA, pp. 1-6.
- P. Striano, C. V. Ilioudis, J. Cao, C. Clemente, J. Soraghan, (2020), Assessment of Micro-Doppler based road targets recognition based on co-operative multi-sensor automotive radar applications, 2020 IEEE Radar Conference (RadarConf20), Florence, Italy, pp.1-5

1.5 Thesis Organization

The remainder of the thesis is divided into eight chapters as follows:

Chapter 2 introduces the key concepts of radar systems, describing basic and advanced operational modes. In the second part of the chapter, the fundamentals automotive radar system are described.

Chapter 3 is dedicated to advanced time-frequency transforms. First, the concept of the Ambiguity Function is introduced. Later, the concept of time-frequency analysis is introduced with commonly time-frequency signal representations is also discussed. Additionally, an extensive analysis of FrFT is presented. Specifically, the properties, implementations, and applications of FrFT in communication and radar systems are discussed in more detail.

Chapter 4 introduces the motivation that leads to share radar and communication functions. First, the different frameworks to provide radar and communication functions, to run simultaneously using the same hardware

and sharing the same spectrum. In last part of the chapter a review of the frameworks to alleviate the mutual interference for radar and communication system was presented.

Chapter 5 presents a new joint radar and communication system based on the FrFT for automotive applications. Then the analytical model and the PSD of the proposed system are derived when the bits are mapped in symbols using a BFSK or BPSK encoding scheme.

Chapter 6 demonstrates the capability of the proposed system to embed data information into a radar waveform and at the same time the characteristics of an LFM pulse are obtained. Thus, the radar performance of the proposed system does not depend highly on data information. Additionally, the simulated results demonstrate the capability of the proposed system to distinguish different targets in an ambiguous manner in multi target scenarios. In last part of the chapter, communication performance will show the capability of the proposed system to work in different types of channels ensuring an acceptable Bit Error Rate (BER).

Chapter 7 presents two novel interference mitigation frameworks based on the proposed joint radar and communication system. In both frameworks, the interference signal is reconstructed and then mitigated from the received radar signal. In the first framework, the interference is mitigated in a coherent manner, where the amplitude and phase of both signals are taken into account. While in the second framework, the interference is alleviated in a non-coherent manner, where only the amplitude of the two signals is taken into account. Additionally, the performance of these two proposed frameworks is evaluated in terms of the Signal Interference Ratio (SIR) obtained when the interference has been mitigated, SIR_{out} against different values of offset frequency and amplitude. This performance is evaluated considering two scenarios. In the first scenario, the received radar signal and reconstructed signal one are obtained using the proposed joint radar and communication system, Section 5.1. In the second scenario, the received interference signal is generated by the Matlab function while the reconstructed one is obtained by using the signal model of the proposed joint radar and communication system.

Chapter 8 presents a summary and conclusions of the thesis, providing an

Chapter 1. Introduction

overview of possible future directions of this work.

Chapter 2

Automotive radar

The word RADAR was coined in 1940 by the United States Navy as an acronym for RAdio Detection and Ranging [113]. The term radio refers to the use of electromagnetic (EM) waves with wavelength in the so-called radio wave portion of the spectrum. The detection and ranging part of the acronym is accomplished by timing the delay between transmission of a pulse of radio energy and its subsequent return.

Modern radar systems are sophisticated systems that not only detect targets and determine target range, but also identify, track, image and classify targets while suppressing strong unwanted interference from the environment and countermeasures. Modern radars are used in an expanding range of applications, from the traditional military and civilian tracking of aircraft and vehicles to two- and three-dimensional mapping, collision avoidance, Earth resources monitoring, automotive, and many others.

The use of radar technology in commercial vehicle applications can provide great benefits in safety and driver assistance. Radar can be used for forward and side obstacle detection, and collision warning as well as extended applications including Advanced Driver Assistance Systems (ADAS). In automotive environment also other sensors like ultrasounds, camera, and Lidar are used. However, a radar system offers advantages due to its capacity to enable a detailed representation of the environment, independent of weather conditions. In this chapter, the basic concepts of radar systems are introduced, highlighting those particularly relevant to the scope of this thesis. The chapter will

focus on describing the fundamental principles of automotive radars, describing their capabilities, characteristics and typical waveforms. The remainder of the chapter is organized as follows. Section 2.1 describes the basic concepts of a radar system including radar range equation, processing gain such as matched filter and pulse integration, slow time/fast time matrix and Doppler spectrum. While the automotive radar, its applications and the different waveforms are presented in Section 2.2.

2.1 Basic concepts

Radar is an electrical system exploiting radiofrequency (RF) electromagnetic waves transmitted towards a particular region of interest and collecting and analysing EM waves that are reflected by objects in that region. A simple radar system must include the following subsystems: a transmitter, one or more antennas, a receiver, and a signal processing unit. A representation of a radar system is illustrated in Fig. 2.1. The transmitter subsystem generates the EM waves. The antenna is the subsystem that takes as input these EM waves from the transmitter and introduces them into the atmosphere. The transmit/receive (T/R) device has the function of connecting the transmitter and receiver to the antenna and it protects the sensitive receiver components. The EM waves that are reflected by an object that propagates back to the radar system are captured by the antenna [113]. The receiver subsystem takes as input the received echoes from the antenna and introduces them into the signal processing unit. Finally, the received signals are analysed by the signal

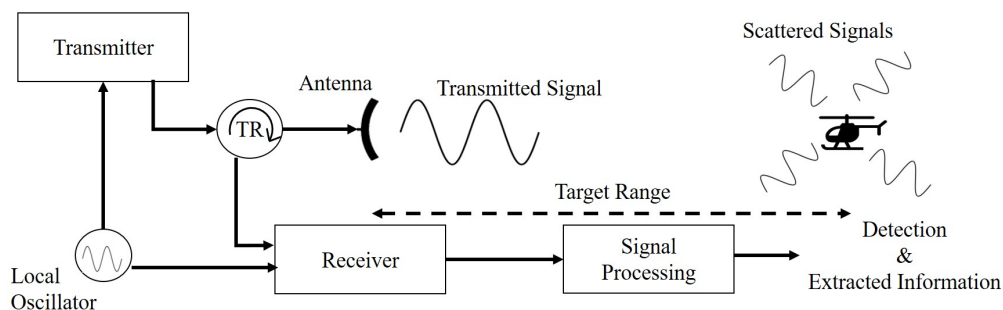


Fig. 2.1. Major elements of the radar transmission/ reception process.

processing unit.

The range, R , to a detected target can be determined based on the time, τ . Where τ is the time that EM waves take to propagate to that target and back. The relationship between the range and time is given by

$$R = \frac{c\tau}{2} \quad (2.1)$$

where c is the speed of light in free space. Since the waves travel to a target and back, the round trip time is divide by two in order to obtain the time that waves took to reach the target.

Range resolution, Δ_R , is the ability of a radar system to distinguish between targets that are very close range. In the literature two more common metrics are used to define resolution [112]:

1. The Rayleigh criterion, which defines resolution as the separation between the peak and the first null;
2. The width of the mainlobe at specific point below the peak, most commonly such at -3 dB point.

For an unmodulated pulse, the range resolution is defied as the separation between the peak and the first null. In this case, the range resolution is defined as [111]

$$\Delta_R = \frac{ct_p}{2} \quad (2.2)$$

where t_p is the width of the transmitted waveform. The range resolution defined in (2.2) depends on the width of the transmitted waveform. However, the resolution can be improved dramatically when proper waveforms are transmitted and signal processing is applied. It will be discussed in Section 2.1.3.

2.1.1 Radar Range Equation

The radar range equation predicts the received radar power. The formulation of the radar equation was given by Ugo Tiberio [37] and provides a useful

relationship between all the elements in a radar system:

$$P_{\text{radar}} = \frac{P_t G_t G_r \sigma_{\text{radar}} \lambda^2}{(4\pi)^3 R^4 L_s} \quad (2.3)$$

where P_t is the power developed by the transmitter, G_t and G_r are the transmit and the receiver antenna gains respectively, σ_{radar} is the Radar Cross Section (RCS) which depends on different parameters as (size of the target, operating frequency, material of which the target is made, the incident angle, the polarization, and the reflected angle), λ is the wavelength, $L_s > 1$ is a loss factor.

Considering a simple radar scenario where the received signal is affected only by the noise, the Signal to Noise Ratio (SNR) can be written as

$$\text{SNR} = \frac{P_{\text{radar}}}{P_n} = \frac{P_t G_t G_r \sigma_{\text{radar}} \lambda^2}{(4\pi)^3 R^4 L_s P_n} \quad (2.4)$$

where P_n is the power of the noise. The power, P_n , of the thermal noise in a radar receiver is given by

$$P_n = kT_s B = kT_0 F B \quad (2.5)$$

where

- k is Boltzmann's constant (1.38×10^{-23} watt-sec/K)
- T_0 is the standard temperature (290 K)
- T_s is the system noise temperature ($T_s = T_0 F$)
- B is the instantaneous receiver bandwidth in Hz
- F is the noise figure of the receiver subsystem (unitless).

The detection range at which a given target can be detected with a given SNR is obtained solving (2.4)

$$R = \left[\frac{P_t G_t G_r \sigma_{\text{radar}} \lambda^2}{(4\pi)^3 \text{SNR} P_n L_s} \right]^{\frac{1}{4}} \quad (2.6)$$

The detection range given in (2.6) depends on radar parameters, target, environment and geometry.

2.1.2 Processing Gain

In radar theory, the probability of detection is related to the SNR rather than the exact waveform of the received signal. This means that on the receiver side, the main interest is that to maximize the SNR rather than in preserving the shape of the signal. In order to obtain a high SNR value, in literature, two main approaches known as matched filter and pulse integration are widely used. A matched filter is a filter that provides the maximum output SNR when the signal is corrupted by the white Gaussian noise. White noise means that the power spectrum of the noise is uniformly distributed over the entire frequency domain, and Gaussian noise indicates that the probability density function of the amplitude of the noise is a Gaussian distribution.

Matched filter

The impulse response of a matched filter is defined by the particular signal to which the filter is matched. The maximum SNR at the output of the filter is obtained when the signal to which the filter was matched, plus white noise, is passed through it.

The impulse response, $h(t)$, that maximizes the SNR at the output of the filter is given by [75]

$$h(t) = x^*(\tau - t) \quad (2.7)$$

where $x(t)$ is the transmitted signal while $(\cdot)^*$ is the complex conjugate. As it can be seen the impulse response is linearly related to the time-inverted complex conjugate of the transmitted signal.

In radar processing, this filter is widely used due to its ability to detect the presence of the transmitted signal in the received one.

Pulse Integration

Another common signal processing technique for achieving higher SNR is the integration of multiple received echoes scattered by the same target. These

echoes can be integrated in a coherent or non-coherent manner. In a coherent integration, the sum is carried out employing both amplitude and phase information. The SNR resulting from the coherent integration, SNR_c is [113]

$$\text{SNR}_c(N_{\text{wave}}) = N_{\text{wave}}\text{SNR}(1) \quad (2.8)$$

with N_{wave} number of echoes integrated by a radar sensor, while $\text{SNR}(1)$ is the SNR obtained with a single echo. As we can see from (2.8), when a coherent integration is carried out the SNR increases by a factor N_{wave} . The coherent integration can be carried out only if the N_{wave} echoes have a predictable phase relationship. It is true when a target is in the same range bin over the entire Coherent Processing Interval (CPI).

In a non-coherent integration, the echoes are summed taking into account only the amplitude information of the scattered echoes. When a non-coherent integration is carried out the SNR_{nc} is not defined unequivocally

$$\text{SNR}_{nc}(N_{\text{wave}}) \in \left[\sqrt{N_{\text{wave}}}\text{SNR}(1), N_{\text{wave}}\text{SNR}(1) \right] \quad (2.9)$$

The non-coherent integration of N_{wave} echoes provides an integration gain less than N_{wave} , but greater than about $\sqrt{N_{\text{wave}}}$. Equation 2.9 suggests that when the received echoes are summed between them taking into account only the amplitude, the gain does not scale linearly to the number of the pulses that are summed. The limit of the integration depends on time that a target takes to move from two consecutive range bins.

2.1.3 Pulse compression

As we can see from (2.2) the range resolution of unmodulated pulse depends on the time duration of the signal. Additionally, in order to obtain a high SNR value a long transmitted waveform has to be transmitted. Consequently, a trade-off between the SNR and range resolution is required [113].

In order to solve the coupling between the energy and range resolution a pulse compression technique can be applied. This technique allows to obtain at the same time high SNR and fine resolution.

In a pulse compression, the resolution is defined using the -3 dB resolution

definition, consequently, the range resolution can be written as:

$$\Delta_R = \frac{ct_p}{2} \approx \frac{c}{2B} \quad (2.10)$$

The range resolution given by (2.10) does not depend on the duration of the transmitted waveform, but on its bandwidth. Consequently, when this technique is applied a fine range resolution and a high SNR can be simultaneously obtained.

In Fig. 2.2 the matched filter output of an unmodulated square pulse, Fig. 2.2a, and of a compressed pulse such as LFM are illustrated. These two signals have the same bandwidth. Comparing the width of the mainlobe shown in Fig. 2.2a with Fig. 2.2b we can see that the width of an LFM is smaller than the one obtained when a square pulse is used. Consequently, when a pulse compression is applied a fine range resolution is obtained. Additionally, Fig. 2.2b shows that sidelobes appear due to the fact that the total energy of the signal does not change. Meaning that a sharper mainlobe leads to the more significant presence of sidelobes.

2.1.4 Radar Data Matrix

On receiver side, before that the radar processing unit is applied, the received signal is organized in a fast-time slow-time matrix.

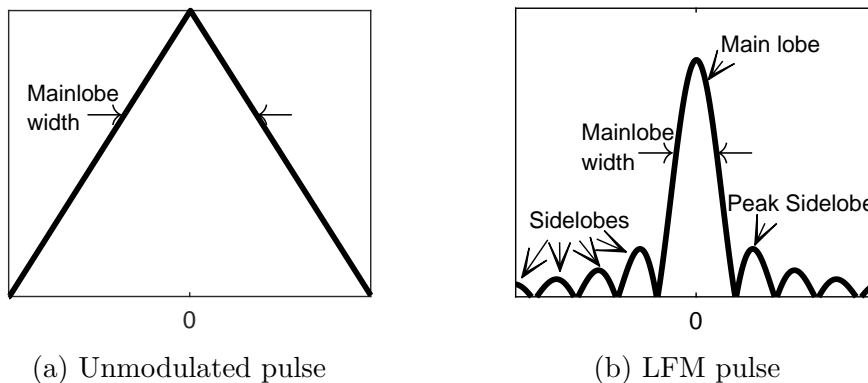


Fig. 2.2. Matched filter output of 2.2a an unmodulated pulse and 2.2b an LFM waveform.

In a pulsed radar configuration, the transmitter emits a pulse every T_{PRI} seconds where this interval is known as Pulse Repetition Time (PRI). The inverse of the PRI is called Pulse Repetition Frequency (PRF).

The received signal is sampled in an interval time that corresponds to the minimum and the maximum of the desired range. The sampling is performed at a sampling rate $f_s = 1/t_s$, where t_s is the sampling time. After this operation, L samples are obtained. These samples fill a rangeline which can be arranged as a column in a matrix as illustrated in Fig. 2.3. The samples related to the second sampling interval build a new rangeline which is inserted in the two-dimensional matrix. That operation is repeated until all the N_{wave} pulses emitted from the transmitter are received at the radar. After this stage, a 2-D matrix of LN_{wave} samples is obtained as illustrated in Fig. 2.3. The total amount time $N_{wave}T_{PRI}$ represented by data matrix is called Coherent Processing Interval. The vertical and horizontal dimensions of matrix Fig. 2.3 are called fast-time or range dimension and slow-time or pulse number dimension, respectively.

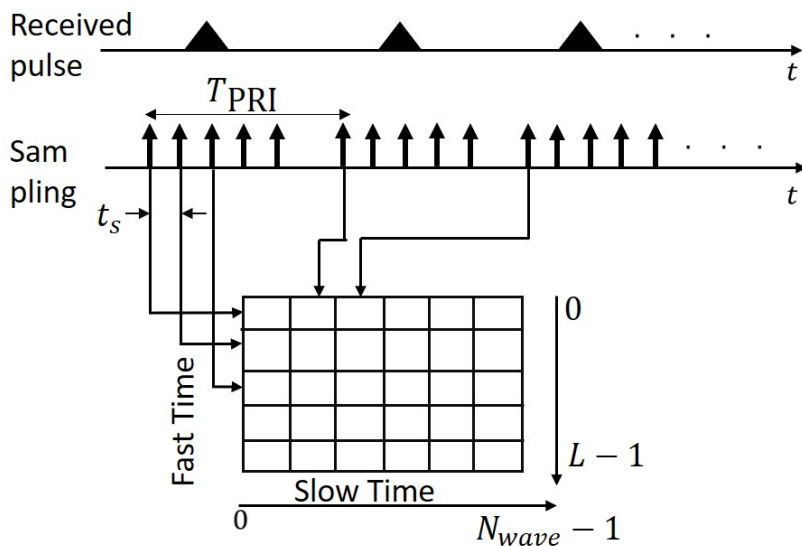


Fig. 2.3. Slow-Time Fast-Time Data matrix.

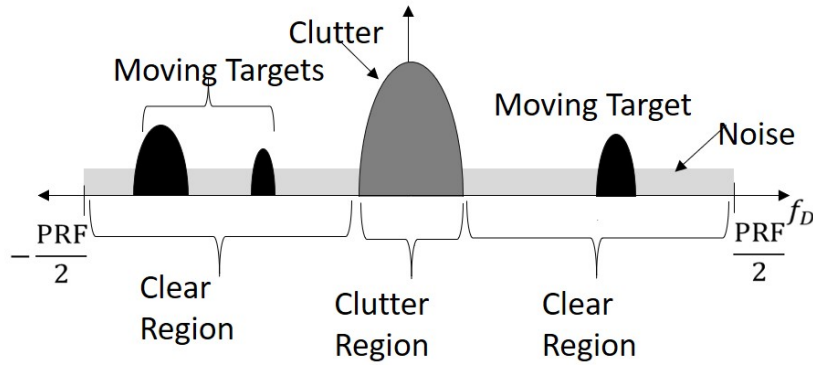


Fig. 2.4. Doppler spectrum for one range bin, viewed by a stationary target.

2.1.5 Doppler Spectrum

The received frequency of an echo scattered by a moving target will differ from the transmitted frequency. The difference between the transmitted and received frequencies is called Doppler frequency, and it is defined as [75]

$$f_D = -\frac{2v_r}{\lambda} \quad (2.11)$$

where v_r is the relative velocity between a target and the radar. Equation 2.11 is true if the radar works in hypothesis of stop and go.

Measurement and processing of Doppler data in a pulsed radar begin with the fast time/slow time matrix as defined in Section 2.1.4. An example of the Doppler spectrum obtained applying a fast Fourier transform (FFT) on a single row of the matrix is illustrated in Fig. 2.4, where it shows a notional generic Doppler spectrum as observed from a stationary radar for a single range bin containing clutter, noise, and three moving targets. The spectrum is periodical with periodicity PRF, due to this in Fig. 2.4 only the portion between $[-\frac{\text{PRF}}{2}, \frac{\text{PRF}}{2}]$ is illustrated.

2.2 Automotive Radar System

Automotive radar systems are responsible for the detection of objects and obstacles, and determining their position, and speed relative to the vehicle.

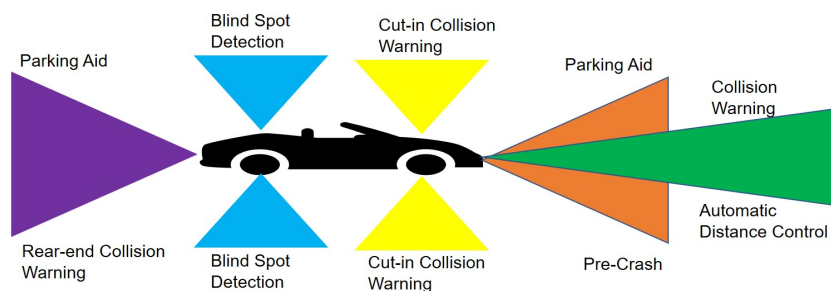


Fig. 2.5. Advanced Driver Assistant System (ADAS) applications.

The development of signal processing techniques along with progress in the mmWave semiconductor technology plays a key role in automotive radar systems [95]. In addition to radar, automotive platforms also rely on different sensors such as laser, video, ultrasound. A comparison between all sensors is listed in Table 2.1, [144]. As we can see among these sensors, radar offers the ability to reach long distance ahead of the car in poor visibility conditions, while also being able to measure the relative velocity and range between the vehicles. Additionally, low false alarms is obtained, consequently, it can be used to increase the security on the road. Furthermore, the radar has the capability to distinguish the objects in angle. Last capability means that in a narrow streets the objects can be distinguish in azimuth.

Table 2.1: Technology and Performance Features [144].

Performance Feature	Ultrasound	Laser	Video	Radar
Long Range Capability	Poor	Good	Good	Good
Target Discrimination	Poor	Fair	Good	Good
Minimizing False Alarms	Poor	Fair	Fair	Good
Temperature Stability	Poor	Good	Good	Good
Darkness Penetration	Good	Good	Poor	Good
Adverse Weather Penetration	Poor	Poor	Poor	Good
Low Cost Hardware Possibility	Good	Fair	Poor	Good
Low Cost Signal Processing	Good	Good	Poor	Good

2.2.1 Classification

Both autonomous and human-driven cars are increasingly using radars to improve drivers' comfort and safety. For each individual function, a different sensor specification is needed. This can lead to a very high number of different radar sensor specifications, each designed to address the appropriate distance range or field of view.

As we can see from Fig. 2.5 in an automotive environment different radar systems can be used for different applications like Blind Spot Detection, Parking Aid, Collision Warning. An ADAS groups these applications in three different types of radars:

- Long Range Radar (LRR): for applications where a narrow-beam forward-looking view is required, like Adaptive Cruise Control and Emergency Braking System;
- Medium Range Radar (MRR): for applications with a medium distance and speed profile, like cross traffic alert;
- Short Range Radar (SRR): for applications sensing in direct proximity of the vehicle, like blind spot detection, rear collision warning, lane change assistance, cross traffic alerts, and parking assistance.

Typical frequency bands used in automotive radar are listed in Table 2.2. The European Commission has proposed the internationally available 79 GHz band as a replacement in its “79 GHz Project” [1]. Along with minimal limitation regarding the emitted power level and a smaller form factor for the sensors, it offers a wide signal bandwidth up to 4 GHz and higher range resolution. Higher frequencies are not only helpful for the development of smaller sensors,

Table 2.2: Frequency bands for automotive radar in Europe.

Frequency band	CW Bandwidth
24 GHz to 24.25 GHz	250 MHz
21 GHz to 26 GHz	5 GHz
76 GHz to 77 GHz	1 GHz
77 GHz to 81 GHz	4 GHz

they also help to improve the range and radial velocity resolution of the radar, allowing it to identify objects that are closely spaced.

2.2.2 Waveform for Automotive Radar

Following, the basic Key Performance Indicators (KPI) of waveform design for automotive applications are discussed including range resolution, velocity resolution, and SNR. In order to meet these requirements for automotive applications, a radar sensor must be capable of measuring a target's range and velocity simultaneously, very accurately and unambiguously even in multi target scenarios.

Furthermore, the measurement time should be relatively short because of the need for short reaction time in brake and throttle control systems. These key objectives and technical features are obtained by sophisticated waveform designs that will be described in the following.

2.2.3 Continuous Wave and Pulsed Wave Radars

A radar system can use different types of waveforms. Fig. 2.6 shows that the radar waveforms are separated into Continuous Wave (CW) and pulsed wave. CW and pulsed waveforms are both able to host a wide variety of different forms of modulation. The CW family of waveforms comprises: Unmodulated CW, Frequency Modulation CW and Phase Modulation CW; while pulsed radar can be: Fixed Frequency, Intrapulse Modulation and Pulse to Pulse Modulation

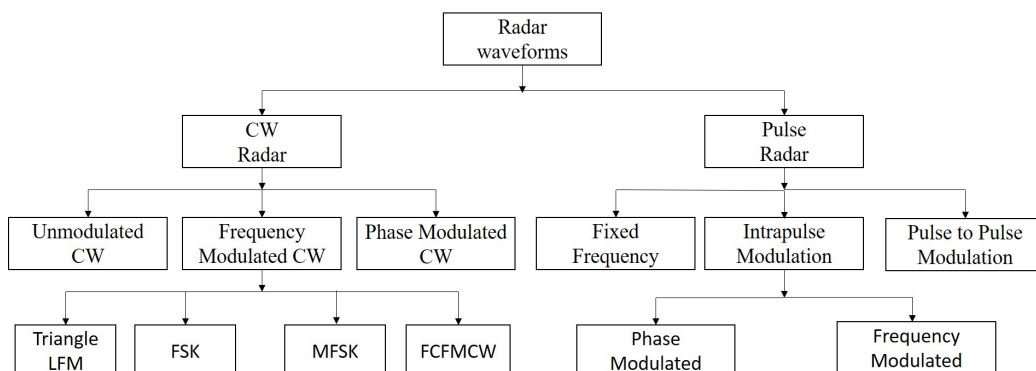


Fig. 2.6. Radar Waveform.

Modulation, see Fig. 2.6. This wide variety of waveform types provides the radar designer with a range of options allowing performance optimisation of specific applications.

The main difference between the CW and pulse radar is that in the CW, the transmitter and receiver are continuously operated without interruption, while in the pulsed radar, the transmitter and receiver do not operate at the same time.

For CW radar the transmitter is continuously transmitting a signal with a fixed frequency while the receiver is continuously receiving echoes that are scattered by targets [113]. Additionally, to avoid the phenomenon of the leakage due to not perfect isolation between the transmitter and receiver, the transmitter emits a signal with low power and hence this radar is used for short-range applications, such as automotive radar.

A pulsed radar transmits a train of EM pulses of finite duration known as pulse width t_p . When the transmitter is switched on the receiver is switched off and vice versa. In this system, the transmitter and receiver are perfectly isolated hence the transmitter can emit a high power EM wave. A pulsed radar is used for long-range applications such as surveillance.

2.2.4 Continuous Waveform

As described in Section 2.2.3 in a CW radar a signal is transmitted and received without interruption, consequently, these systems have a duty cycle of 100%. The duty cycle is given by the product of the pulse width t_p and PRF. In other words, it is defined as the proportion of time during which the transmitter radar is operated. The received radar signals are down-converted directly into baseband by using as reference the transmitted frequency f_T . The difference between the frequency of the received signal f_R and the transmitted f_T is called beat frequency f_b , which is technically influenced by the waveform itself, by the propagation delay τ associated with the target range R and the Doppler frequency f_D :

$$f_b = f_R - f_T \quad (2.12)$$

When a radar illuminates a stationary target, the frequency of the echo signal is unchanged from the transmitted. However, if a target is moving, then the

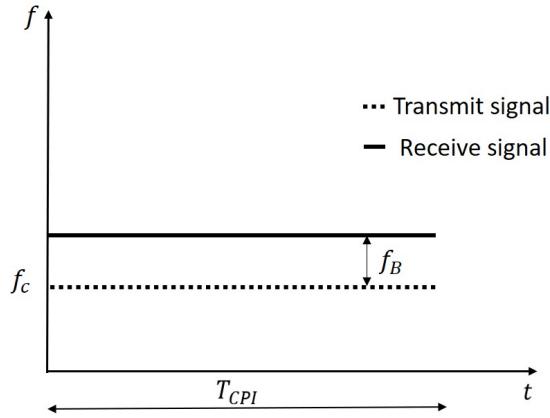


Fig. 2.7. Monofrequency CW radar system.

frequency of the echo signal is altered due to the Doppler effect as described in Section 2.1.5. The velocity of the moving target can be determined by detecting of Doppler frequency, f_D . Owing to the target movement, the time-dependent target range $R(t)$ changes lightly, but continuously in the so-called slow-time. Thus, the propagation delay $\tau(t)$ is not constant any longer and it becomes time dependent

$$R(t) = R_0 + v_r t \quad (2.13)$$

where R_0 is the distance between the radar and the target when $t = 0$.

By using (2.1), follows that the propagation delay can be written as

$$\tau(t) = \frac{2}{c} R(t) = \frac{2}{c} (R_0 + v_r t) \quad (2.14)$$

The effect of the presence of relative motion translates in a Doppler shift that is therefore useful to describe/discriminate moving target. If a frequency-modulated signal is transmitted and a moving target is present, then the beat frequency f_b depends on the propagation delay, τ , and the Doppler frequency, f_D (2.11), simultaneously.

This aspect introduces a technical challenge in the measurement of unambiguous range and velocities.

2.2.5 Unmodulated CW

When a sinusoidal signal is transmitted the carrier frequency f_c is constant during the coherent measurement time T_{CPI} . The transmitted and received signals are illustrated in Fig. 2.7.

The transmitted signal with carrier frequency f_c can be written as

$$\mathbf{s}_{tx}(t) = \cos(2\pi f_c t) \quad (2.15)$$

with f_c carrier frequency. When a stationary target is present, the received frequency is equal to the transmitted one. If a target with radial velocity v_r is present, the received radar signal can be written as

$$\mathbf{s}_{rx}(t) = \cos(2\pi f_c [t - \tau(t)]) \quad (2.16)$$

Given (2.14) follows that

$$\begin{aligned} \mathbf{s}_{rx}(t) &= \cos \left\{ 2\pi \left[f_c t - f_c \frac{2}{c} (R_0 + v_r t) \right] \right\} \\ &= \cos \left\{ 2\pi \left[\left(f_c - f_c \frac{2}{c} v_r \right) t - f_c \frac{2}{c} R_0 \right] \right\} \end{aligned} \quad (2.17)$$

The beat signal is obtained down converting (2.17) by using the carrier frequency, it is

$$\mathbf{b}(t) = \cos \left(2\pi f_c \frac{2}{c} (R_0 + v_r(t)) \right) \quad (2.18)$$

Equation 2.18 shows that in the frequency domain a peak rises at frequency beat

$$f_b = 2f_c \frac{v_r}{c} = f_D \quad (2.19)$$

As it can be seen when an unmodulated CW signal is transmitted the Doppler frequency is the same as the beat frequency. While the phase of the received signal consists of a constant term proportional to target range, R , i.e.

$$\phi_b = 2\pi f_T c \frac{2}{c} R_0 = 4\pi \frac{R_0}{\lambda} \quad (2.20)$$

The Doppler frequency resolution depends on the observation time T_{CPI} :

$$\Delta f_D = \frac{1}{T_{CPI}} \quad (2.21)$$

The described monofrequency CW waveform has very good performance in velocity measurement. A drawback of such waveform is that it is unable to detect stationary targets or measure range. It is due to the fact that the range is ambiguous to a wavelength (2.20).

2.2.6 Linear Frequency Waveform

To fulfill the general performance requirement in automotive radar and to measure the target range and radial velocity simultaneously even in multi target scenarios an LFM waveform can be transmitted. LFM is a very popular choice in modern radar systems, because it can achieve high range resolution (see Section 2.1.3) holding in the advantage that the hardware can keep relatively simple.

The complex baseband signal with unitary amplitude is:

$$\tilde{\zeta}_{tx}(\eta) = e^{\pm j\pi \frac{B_{LFM}}{t_p} \eta^2} \quad 0 \leq \eta \leq t_p \quad (2.22)$$

where B_{LFM} , t_p , and η are the bandwidth, the duration of the waveform and fast time, respectively. The ratio B_{LFM}/t_p is the slope of the instantaneous frequency, and it is called sweep rate. A positive sweep rate indicates an up-LFM, whereas a negative indicates a down-LFM with the same bandwidth. The time varying phase $\phi(\eta)$ of an LFM waveform is a quadratic function

$$\phi(\eta) = \pi \frac{B_{LFM}}{t_p} \eta^2 \quad 0 \leq \eta \leq t_p \quad (2.23)$$

while the instantaneous frequency is defined as the derivation of the phase (2.23),

$$f(\eta) = \frac{1}{2\pi} \frac{d\phi(\eta)}{d\eta} = \frac{B_{LFM}}{t_p} \eta \quad 0 \leq \eta \leq t_p \quad (2.24)$$

An interesting property of an LFM pulse is that the instantaneous frequency, (2.24), is linear with the time. Consequently, an LFM waveform sweeps

through B_{LFM} Hz in t_p seconds. An example of time frequency representation of an LFM waveform is shown in Fig. 2.8.

The transmitted signal can now be expressed as

$$\zeta_{tx}(\eta) = e^{j\left(2\pi f_c \eta \pm \pi \frac{B_{LFM}}{t_p} \eta^2\right)} \quad 0 \leq \eta \leq t_p \quad (2.25)$$

The first term inside of the exponential function corresponds to phase shift due to the carrier frequency, while the second term is due to the modulated frequency. The transmitted frequency is given by

$$f_T(\eta) = f_c \pm \frac{B_{LFM}}{t_p} \eta \quad (2.26)$$

The received radar signal scattered by a moving target can be written as

$$\zeta_{rx}(\eta) = e^{j\left(2\pi f_c(\eta - \tau(\eta)) \pm \pi \frac{B_{LFM}}{t_p} (\eta - \tau(\eta))^2\right)} \quad (2.27)$$

The beat signal is obtained by applying a mixer between the transmitted signal and the complex conjugate of the received signal. This operation is

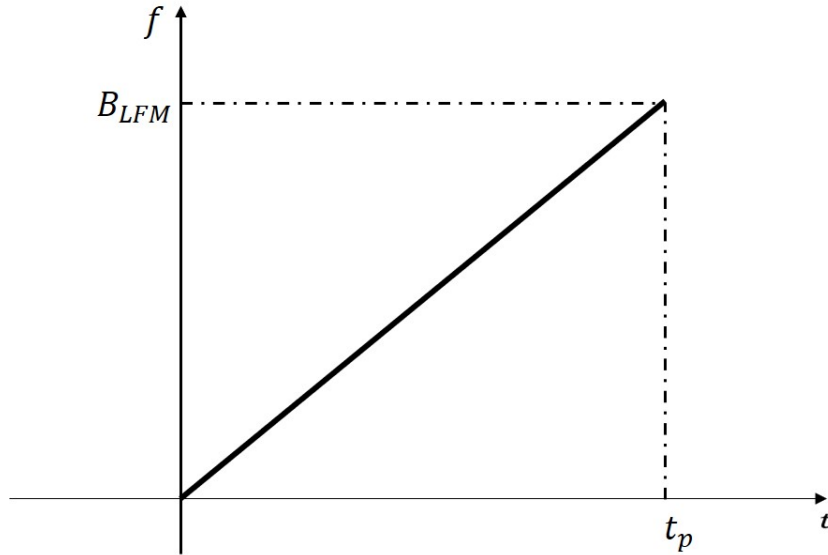


Fig. 2.8. Instantaneous frequency versus time for an LFM waveform.

known as stretch processing, obtaining:

$$\begin{aligned}
 \mathbf{b}(\eta) &= \zeta_{rx}(\eta)\zeta_{tx}^*(\eta) = e^{j\left(2\pi f_c(\eta-\tau(\eta))\pm\pi\frac{B_{LFM}}{t_p}(\eta-\tau(\eta))^2\right)} e^{-j\left(2\pi f_c\eta\pm\pi\frac{B_{LFM}}{t_p}\eta^2\right)} \\
 &= e^{j\left(2\pi f_c\eta-2\pi f_c\tau(\eta)\pm\pi\frac{B_{LFM}}{t_p}(\eta^2+\tau^2(\eta)-2\eta\tau(\eta))\right)} e^{-j\left(2\pi f_c\eta\pm\pi\frac{B_{LFM}}{t_p}\eta^2\right)} \\
 &= e^{j\left(-2\pi f_c\tau(\eta)\pm\pi\frac{B_{LFM}}{t_p}\tau^2(\eta)\mp 2\pi\frac{B_{LFM}}{t_p}\tau(\eta)\eta\right)}
 \end{aligned} \tag{2.28}$$

The second terms of the exponential in (2.28) can be assumed to be sufficiently small due to c and can be neglected. In addition, by substituting (2.14) in the first and third term we obtain

$$\mathbf{b}(\eta) = e^{j\left(-4\pi f_c\frac{R_0}{c}-2\frac{f_c}{c}v_r(\eta)\mp 2\frac{B_{LFM}}{t_p}\frac{R_0}{c}\eta\mp 4\frac{B_{LFM}}{t_p}\frac{v_r}{c}\eta^2\right)} \tag{2.29}$$

Assumed the sweeps are sufficiently short, the terms dependent on second power of η can be assumed to be negligible. The expression can be now rewrite into

$$\mathbf{b}(\eta) = e^{j\left(-4\pi f_c\frac{R_0}{c}-2\frac{f_c}{c}v_r\eta\mp 2\frac{B_{LFM}}{t_p}\frac{R_0}{c}\eta\right)} \tag{2.30}$$

It is now assumed that the radial velocity of the target is sufficiently small so that the range R_0 remains constant for each sweep. The first term inside of the exponential is assumed a constant phase term for all sweep number, and ignored. Thus the beat signal can be written as

$$\mathbf{b}(\eta) = e^{j\left(\frac{-4\pi f_c v_r}{c}\mp 2\frac{B_{LFM}}{t_p}\frac{R_0}{c}\right)\eta} \tag{2.31}$$

The beat signal shows that in frequency domain a peak is present at

$$f_b = -\frac{2}{\lambda}v_r \mp \frac{B_{sw}}{t_p}\frac{2}{c}R_0 = f_D \mp f_\tau \tag{2.32}$$

In a moving target scenario, the measured beat frequency f_b contains two components, one from the range shift f_τ and another one from the Doppler frequency f_D (see Fig. 2.9). When an LFM waveform is transmitted the range and Doppler of a target cannot be solved in an unambiguous manner,

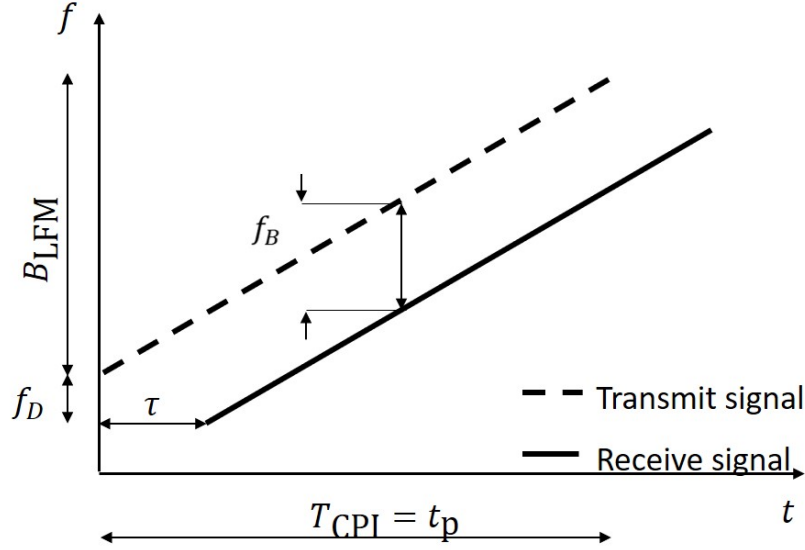


Fig. 2.9. Frequency of transmitted and received LFM as a function of time.

because the beat frequency depends simultaneously on range and Doppler frequency.

2.2.7 Triangular LFM waveform

When a radar system transmits an LFM waveform the range and velocity cannot be solved simultaneously. In order to accomplish an unambiguous measurement of the range and Doppler frequency an up-and-down-LFM can be used. The LFMs are transmitted sequentially in a serial concatenation as illustrated in Fig. 2.10. In this system, two beat frequencies relative to an up-LFM and down-LFM are obtained.

$$\begin{aligned}
 f_{b_{up}} &= f_D + f_\tau = -\frac{2}{\lambda}v_r - \frac{2}{c} \frac{B_{LFM}}{t_p} R_0 \\
 f_{b_{down}} &= f_D - f_\tau = -\frac{2}{\lambda}v_r + \frac{2}{c} \frac{B_{LFM}}{t_p} R_0
 \end{aligned} \tag{2.33}$$

In a scenario where a single target is present, two beat frequencies $f_{b_{up}}$ and $f_{b_{down}}$ will be measured separately in the up-and-down-LFM echo waveform. Hence, a system (2.33) given by two independent linear equations, i.e. one for

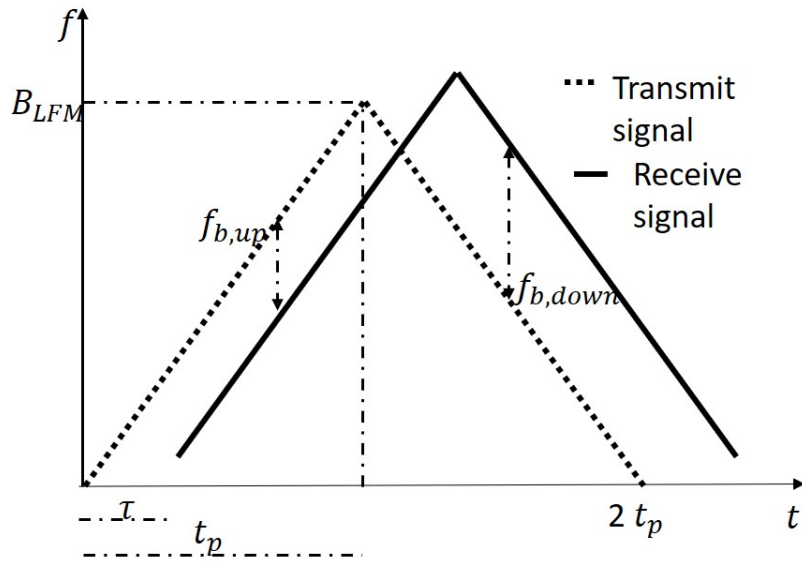


Fig. 2.10. Frequency of transmitted and received triangular LFM as a function of time.

the up-LFM and the other for down-LFM, can be solved. Based on these two equations, the target range R_0 and the radial velocity v_r can be estimated in an unambiguous way. In this system, the number of the up and down beats depends on the number of the targets. Consequently, in a scenario where two targets are present, two up beats $f_{b_{up}}$ and two down beats $f_{b_{down}}$ are obtained thus four possible targets can be detected. To better understand, a graphical solution is shown in Fig. 2.11 illustrating the cases with one or two targets. As we can see from Fig. 2.11a when a single target is present a single intersection point is obtained. While when two targets are present four intersection points are obtained as illustrated in Fig. 2.11b. Consequently, when more than one target is present this waveform is not available to detect the real targets due to the presence of the ghost targets. Hence, in multi target scenarios, the ghost targets are present, because it is not possible to associate between the measured beat frequencies in the up-LFM case and the beat frequencies in the down-LFM case. This issue can only be avoided if the transmit signal is further extended by two additional up-and down-LFM waveforms with different bandwidth. However, in automotive scenario a short

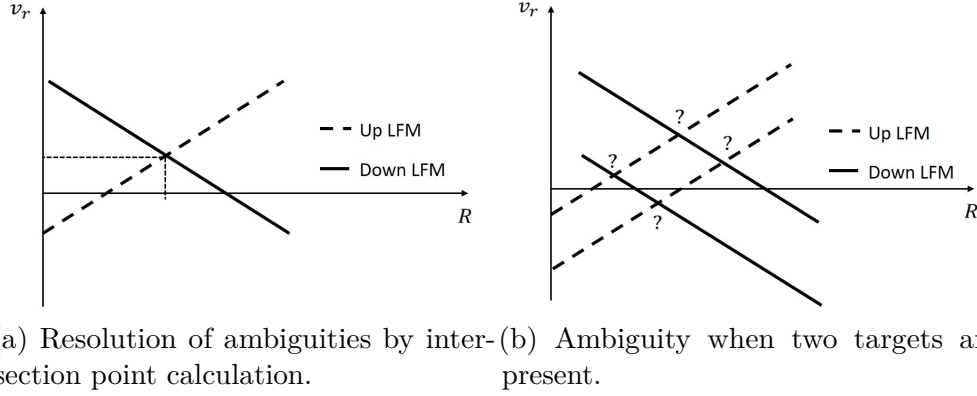


Fig. 2.11. Solutions of the beat frequencies problem, 2.11a when one target is present, 2.11b when two targets are present.

duration signal has been transmitted. Thus, this waveform does not fit for an automotive scenario.

2.2.8 Frequency Shift Keying (FSK) Waveform

The requirement of an unambiguous measurement in multi target scenarios in the LFM is not completely fulfilled. Additionally, LFM requires long measurements as within each LFM return there is a single measurement point. Thus, an alternative procedure able to measure the target range R_0 and radial velocity v_r simultaneously even in multi target situations is required.

An alternative procedure is to modulate a CW signal using two discrete carrier frequencies f_{c_A} and f_{c_B} . The two modulated signals A and B are transmitted in an alternated form as illustrated in Fig. 2.12. The two carrier frequencies are chosen such that a small frequency step $f_{step} = f_{c_B} - f_{c_A}$ is obtained. This waveform is known as Frequency Shift Keying Waveform (FSKW). The two signals can be written as:

$$\begin{aligned}
 f_{tx,A}(t) &= e^{j2\pi f_{c_A} t} \text{rect} \left[\frac{t - (2i+1)T_{Step}}{T_{Step}} \right] & i = 0, \dots, (N-1)/2 \\
 f_{tx,B}(t) &= e^{j2\pi f_{c_B} t} \text{rect} \left[\frac{t - 2iT_{Step}}{T_{Step}} \right] & i = 0, \dots, (N-1)/2
 \end{aligned} \tag{2.34}$$

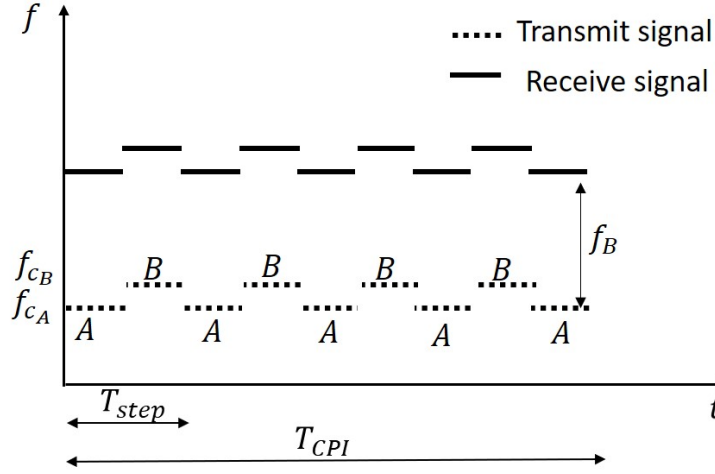


Fig. 2.12. Frequency Shift Keying (FSK) waveform.

The received radar signals are

$$\begin{aligned}
 f_{rx,A}(t) &= e^{j2\pi f_{cA}(t-\tau(t))} \text{rect} \left[\frac{t - \frac{2R}{c} - (2i+1)T_{Step}}{T_{Step}} \right] \\
 f_{rx,B}(t) &= e^{j2\pi f_{cB}(t-\tau(t))} \text{rect} \left[\frac{t - \frac{2R}{c} - 2iT_{Step}}{T_{Step}} \right] \\
 i &= 0, \dots, \frac{N-1}{1}
 \end{aligned} \tag{2.35}$$

The respectively beat signals are:

$$\begin{aligned}
 \mathbf{b}_A(t) &= e^{-j2\pi f_{cA}\tau(t)} = e^{-j2\pi(f_{cA}\frac{2}{c}R_0 + f_{cA}\frac{2}{c}v_r t)} = e^{j2\pi(f_{DA} - f_{cA}\frac{2}{c}R_0)} \\
 \mathbf{b}_B(t) &= e^{-j2\pi f_{cB}\tau(t)} = e^{-j2\pi(f_{cB}\frac{2}{c}R_0 + f_{cB}\frac{2}{c}v_r t)} = e^{j2\pi(f_{DB} - f_{cB}\frac{2}{c}R_0)}
 \end{aligned} \tag{2.36}$$

Equation 2.36 shows that the two beat frequencies are given by the two terms. The first term is the Doppler frequency while the second term is a constant phase which depends on the target range and on transmitted frequency. Due to the small frequency step in the transmit signal follows that

$$f_b = f_{DA} = f_{DB} = -\frac{2}{\lambda}v_r \tag{2.37}$$

Hence, a single target will be detected at the same Doppler frequency position, but with the different phase information. Let ϕ_A and ϕ_B be the phase angles

of the target in the two separated spectra. The difference between the two phases is

$$\begin{aligned}\Delta\phi_{\mathbf{b}} &= \phi_{\mathbf{b}_A} - \phi_{\mathbf{b}_B} = -2\pi f_{c_A} \frac{2R_0}{c} + 2\pi f_{c_B} \frac{2R_0}{c} = \\ &2\pi \frac{2R_0}{c} (f_{c_B} - f_{c_A}) = 2\pi \frac{2R_0}{c} f_{\text{step}}\end{aligned}\quad (2.38)$$

thus the range measured can be computed by (2.38) as

$$R_0 = \frac{c\Delta\phi_{\mathbf{b}}}{4\pi f_{\text{step}}}\quad (2.39)$$

The range R_0 is calculated from each target separately from the measured phase difference $\Delta\phi_{\mathbf{b}}$ for each of the corresponding Doppler frequency pairs where a target has been detected as in (2.39).

Additionally, in (2.39) is shown that the maximum range depends on f_{step} . So to obtain long range small values of f_{step} are required. However, the step frequency f_{step} must be adjusted with respect to an unambiguous phase angle

$$2\pi f_{\text{step}} \frac{2}{c} R_{\text{max}} \leq 2\pi\quad (2.40)$$

Based on the FSK waveform, the target R_0 and the radial velocity v_r can be measured simultaneously and unambiguously even in multi target situations. Target resolution is processed in the Doppler frequency axis only. There is a small limitation for the FSK waveform. It is due to the fact that if a target has been detected at a specific line in the Doppler spectrum, then it is assumed during the range estimation procedure that a single object with the range R_0 has contributed to this detection. Hence, if there are two objects measured at the same spectral line, then the result of the range estimation procedure is meaningless. It means that the FSK waveform does not resolve targets in range.

For automotive radar applications, all stationary targets with different range R_0 will be observed on the same spectral line in the Doppler spectrum. These targets cannot be resolved in range direction.

2.2.9 Multiple Frequency Shift Keying

When an LFM CW waveform is transmitted a system cannot simultaneously estimate range and radial velocity in a single ramp, we need multi-ramp waveform. However, in multi target scenarios, spectral peaks from multiple ramps have to be associated to find the range and radial velocity for a certain target.

In order to overcome this issue, a hybrid waveform of a FSK and LFM known as Multiple Frequency Shift Keying (MFSK) waveform can be transmitted [117]. It offers an unambiguous solution for range and radial velocity measurements simultaneously. The transmit waveform consists in this case of two linear frequency modulation up-LFM waveforms (the intertwined signal sequences are called A and B). The two LFM waveforms have the same slope and bandwidth. They will be transmitted in an intertwined sequence ($ABABAB\dots$), where the stepwise frequency modulated sequence A is used as a reference signal while the second up-LFM waveform is shifted in frequency with f_{shift} . The combined and intertwined waveform concept is illustrated in Fig. 2.13. The transmitted signal A for common MFSK can be written as

$$\zeta_{tx,A}(\eta_A) = e^{j2\pi(f_{T,A}+mf_{incr})\eta_A} \quad \eta_A \in [2mT_{step}, (2m+1)T_{step}] \quad (2.41)$$

With $m = 0, \dots, N-1$ where N is the number of the step. Similarly, signal B can be written as

$$\zeta_{tx,B}(\eta_B) = e^{j2\pi(f_{T,B}+mf_{incr})\eta_B} \quad \eta_B \in [(2m+1)T_{step}, (2m+2)T_{step}] \quad (2.42)$$

The received radar signal can be written as

$$\begin{aligned} \zeta_{rx,A}(\eta_A) &= e^{j2\pi(f_{T,A}+mf_{incr})(\eta_A-\tau(\eta_A))} \\ \zeta_{rx,B}(\eta_B) &= e^{j2\pi(f_{T,B}+mf_{incr})(\eta_B-\tau(\eta_B))} \end{aligned} \quad (2.43)$$

The beat signals are

$$\begin{aligned} \mathbf{b}_A(\eta_A) &= e^{-j2\pi(f_{T,A}+mf_{incr})\tau(\eta_A)} \\ \mathbf{b}_B(\eta_B) &= e^{-j2\pi(f_{T,B}+mf_{incr})\tau(\eta_B)} \end{aligned} \quad (2.44)$$

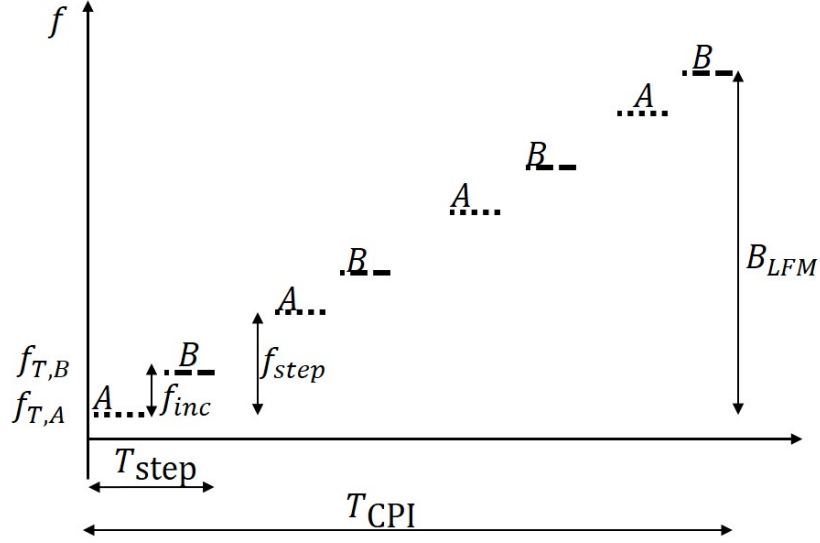


Fig. 2.13. Multiple Frequency Shift Keying (MFSK).

Substituting (2.14) in (2.44), follows the \mathbf{b}_A and \mathbf{b}_B are

$$\begin{aligned}\mathbf{b}_A(\eta_A) &= e^{-j2\pi(f_{T,A}+mf_{incr})\tau(\eta_A)} = e^{-j2\pi\left(f_{T,A}\frac{2R_0}{c} + \frac{2v_r}{c}f_{T,A}\eta_A + \frac{2R_0}{c}mf_{incr} + \frac{2v_r}{c}f_{incr}m\eta_A\right)} \\ \mathbf{b}_B &= e^{-j2\pi(f_{T,B}+mf_{incr})\tau(\eta_B)} = e^{-j2\pi\left(f_{T,B}\frac{2R_0}{c} - f_{T,B}\frac{2v_r}{c}\eta + mf_{incr}\frac{2R_0}{c} - mf_{incr}\frac{2v_r}{c}\eta_B\right)}\end{aligned}\quad (2.45)$$

where $f_{inere} = \frac{B_{LFM}}{N}$ and $T_{CPI} = NT_{step}$. Hence

$$\begin{aligned}\mathbf{b}_A(\eta_A) &= e^{j2\pi\left(-\frac{2R_0}{c}f_{T,A} + f_{D,A}\eta_A - \frac{2R_0}{c}m\frac{B_{LFM}}{NT_{CPI}}T_{CPI} - \frac{2v_r}{c}mf_{inere}\eta_A\right)} \\ \mathbf{b}_B(\eta_B) &= e^{j2\pi\left(-\frac{2R_0}{c}f_{T,B} + f_{D,B}\eta_B - \frac{2R_0}{c}m\frac{B_{LFM}}{NT_{CPI}}T_{CPI} - \frac{2v_r}{c}mf_{inere}\eta_B\right)}\end{aligned}\quad (2.46)$$

where $f_{D,A} = \frac{-2v_r}{c}f_{T,A}$, $f_{D,B} = \frac{-2v_r}{c}f_{T,B}$. In this case, the two Doppler frequencies are the same, because f_{step} is too small. Additionally, the beat signals at each stepping cycle are sampled at $\eta_A = (2m+1)T_{step}$ and $\eta_B = (2m+2)T_{step}$,

and the sampled data of the beat signals are obtained.

$$\begin{aligned}
 \mathbf{b}_A(\eta_A) &= e^{j2\pi \left[-\frac{2R_0}{c} f_{T,A} + f_D(2m+1)T_{step} - \frac{2R_0}{c} m \frac{B_{LFM}}{T_{CPI}} T_{step} - \frac{2v_r}{c} f_{inere} m(2m+1)T_{step} \right]} \\
 &= e^{j2\pi \left[-\frac{2R_0}{c} f_{T,A} + f_D T_{step} 2m + f_D T_{step} - \frac{2R_0}{c} m \frac{B_{LFM}}{T_{CPI}} T_{step} - \frac{2v_r}{c} f_{inere} T_{step} 2m^2 - \frac{2v_r}{c} f_{inere} T_{step} m \right]} \\
 &= e^{j2\pi \left[2m T_{step} \left(f_D - \frac{2R_0}{c} \frac{B_{LFM}}{T_{CPI}} \right) + f_D T_{step} - \frac{2R_0}{c} f_{T,A} \right]}
 \end{aligned} \tag{2.47}$$

In similar way, the beat signal $\mathbf{b}_B(\eta_B)$ is

$$\begin{aligned}
 \mathbf{b}_B(\eta_B) &= e^{j2\pi \left[-\frac{2R_0}{c} f_{T,B} + f_D(2m+2)T_{step} - \frac{2R_0}{c} m \frac{B_{LFM}}{T_{CPI}} T_{step} - \frac{2v_r}{c} f_{inere} m(2m+2)T_{step} \right]} \\
 &= e^{j2\pi \left[-\frac{2R_0}{c} f_{T,B} + f_D T_{step} 2m + 2f_D T_{step} - \frac{2R_0}{c} m \frac{B_{LFM}}{T_{CPI}} T_{step} - \frac{2v_r}{c} f_{inere} T_{step} 2m^2 - \frac{2v_r}{c} f_{inere} T_{step} 2m \right]} \\
 &= e^{j2\pi \left[2m T_{step} \left(f_D - \frac{2R_0}{c} \frac{B_{LFM}}{T_{CPI}} \right) + 2f_D T_{step} - \frac{2R_0}{c} f_{T,B} \right]}
 \end{aligned} \tag{2.48}$$

The beat frequency obtained by (2.47) is the same to that obtained by (2.48) follows

$$f_{\mathbf{b}} = \frac{2}{\lambda} v_r - \frac{2}{c} \frac{B_{LFM}}{T_{CPI}} R_0 \tag{2.49}$$

While the phase of the two beat frequencies at the target position is expressed as $\phi_{\mathbf{b}_A}$ and $\phi_{\mathbf{b}_B}$, respectively. Their difference denoted as $\Delta\phi_{\mathbf{b}}$, is

$$\Delta\phi_{\mathbf{b}} = \phi_B - \phi_A = 2\pi \left(\frac{2T_{step}}{\lambda} v_r - \frac{2f_{shift}}{c} R_0 \right) \tag{2.50}$$

Using (2.49) and (2.50), the range and velocity of the target are estimated. In multi target scenarios on the spectrogram the number of peaks in each frequency spectrum is the same as the number targets. In addition, the peaks are at the same locations in both returns so there are not ghost targets. The MFSK waveform meets the performance requirements for automotive radar system almost perfectly. The measurements of the target range R_0 and the radial velocity v_r are carried out simultaneously and unambiguously even in multi target situations. The latter aspect is very important in the complex traffic and road environment. The targets resolution in range and velocity

are defined by the system parameters, i.e. the sweep bandwidth B_{LFM} and the LFM duration t_p . Maximum target range R_{max} and the maximum radial velocity $v_{r,max}$ determine the maximum beat frequency $f_{b,max}$.

In addition, in the MFSK signal the frequency step f_{step} between both alternating transmitted signals is responsible for an unambiguous phase measurement with respect to the phase interval $[-\pi; \pi)$

$$\left| 2\pi \left(T_{step} \frac{2}{\lambda} v_{r,max} - f_{step} \frac{2}{c} R_{max} \right) \right| \leq \pi \quad (2.51)$$

To assure that the radar echo signal is always down-converted by the corresponding transmit frequency, the time duration T_{step} for a single step in the transmit waveform, in automotive environment, is chosen to be $10\mu s$, which is much longer the maximum propagation delay τ_{max} .

2.2.10 Fast Chirp LFM (FCLFM)

The MFSK waveform fulfils the automotive radar requirements almost in a perfect way. The range is calculated measuring phase difference $\Delta\phi_b$, consequently in order to achieve high accuracy a high SNR is required. With the aim to improve the radar measurement accuracy and system performance, a Fast Chirp LFM (FCLFM) waveform is proposed. FCLFM transmit scheme is illustrated in Fig. 2.14. As we can see in a single CPI consecutive LFM waveforms are transmitted, the duration of each one is t_p . In this way, the target's range R_0 and the radial velocity v_r are estimated by two independent frequency measurements, but without any phase estimation. In this case, the measurement accuracy is much higher, and the system performance is improved. On the other hand, the computational complexity increases as well.

The beat frequency f_b for each LFM depends on the target range R_0 and on the radial velocity v_r in the same way as described in (2.32)

$$f_b = -\frac{2}{\lambda} v_r + \frac{B_{sw}}{t_p} \frac{2}{c} R_0 \quad (2.52)$$

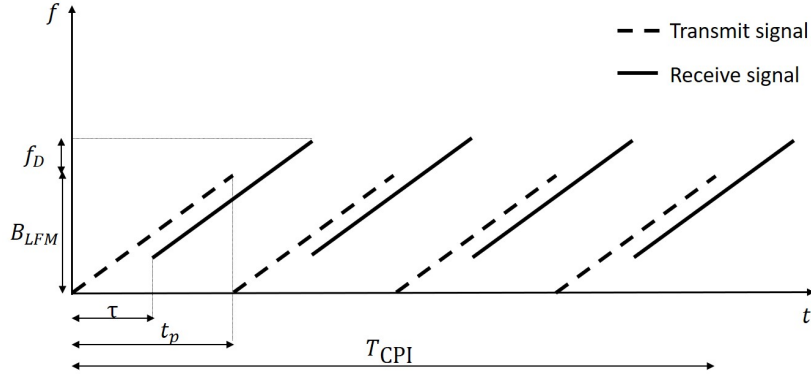


Fig. 2.14. Fast Chirp LFM (FCLFM).

From (2.52) we can see that the beat frequency is given from the sum of two terms: radial velocity and target range where the range is proportional to the $\frac{B_{sw}}{t_p}$ that in this case can assume very large values, because t_p is very short. Therefore, the target range R_0 is the dominating component in the f_b . The first step of the signal processing procedure is the determination of the beat frequency f_b for each individual up-LFM signal. After the down conversion process has been applied to a single LFM waveform, the baseband signal of each LFM is transformed into frequency domain by the FFT. The resulting complex valued signal spectrum of each LFM waveform is stored in a single column of a matrix. At this point in the signal processing procedure, targets with different range R_0 are already resolved in range direction by the measured beat frequency. The second step of the signal processing procedure is the determination of the Doppler frequency f_D based on range gate specific second FFT application. After this second processing step, targets are resolved in Doppler frequency f_D . Radial velocity is directly calculated from the measured beat frequency f_b inside of each chirp signal.

$$R_0 = \frac{t_p}{B_{LFM}} \frac{c}{2} (f_b - f_D) \quad (2.53)$$

The considered waveform is based on a sequence of LFM waveforms and very short LFM duration. The LFM length is chosen in accordance to the maximum Doppler frequency to avoid any ambiguity in Doppler measurement. The frequency resolution is inversely proportional to the observation time. In

cases in which the Doppler frequency f_D is measured, this is the time duration T_{CPI} for the entire sequence of N_{wave} LFM waveforms with a duration t_p each

$$\Delta f_D = \frac{1}{N_{wave}t_p} = \frac{1}{T_{CPI}} \quad (2.54)$$

Therefore, the frequency modulation with rapid LFM achieves similar range and Doppler resolution as LFM and the ambiguity of range and Doppler is solved [16]. The cost, of course, is the time required to transmit and receive N_{wave} waveforms instead of one LFM, and the computational load of processing N_{wave} rows of samples along slow-time axis.

An important advantage of the rapid chirp transmit signal is the fact that the beat frequency f_b obviously has a positive sign due to the dominating range component in the beat frequency in all measurement cases, meaning that there is no longer need for a quadrature channel. The FCLFM described above meets the performance requirements on automotive radar systems. The simultaneous measurement of target range and radial velocity is very accurate since only frequency measurement are involved. Furthermore, the determination of target parameters is unambiguous even in multi target situations. In addition, a real two-dimensional resolution of targets is possible due two-dimensional processing in beat frequency f_b and in Doppler frequency f_D direction separately. Thus, it is possible to handle multiple target cases.

2.2.11 Orthogonal Frequency Division Multiplexing

Orthogonal Frequency Division Multiplexing (OFDM) is a digital multi-carrier modulation scheme that extends the concept of single sub-carrier modulation by using multiple sub-carriers within the same single channel. It can be viewed as another multi frequency waveform that offers unique features of the joint implementation of automotive radar and V2V communications as it will be discussed in chapter 4. For the radar operation, the orthogonality between OFDM subcarriers is ensured by choosing carrier spacing, $\Delta \bar{f}$, more than maximum Doppler shift, and the cycle prefix, T_{CP} , duration is selected greater than the longest round-trip delay, see Fig. 2.15. The range profile is estimated through frequency domain channel estimation. OFDM radar processing along

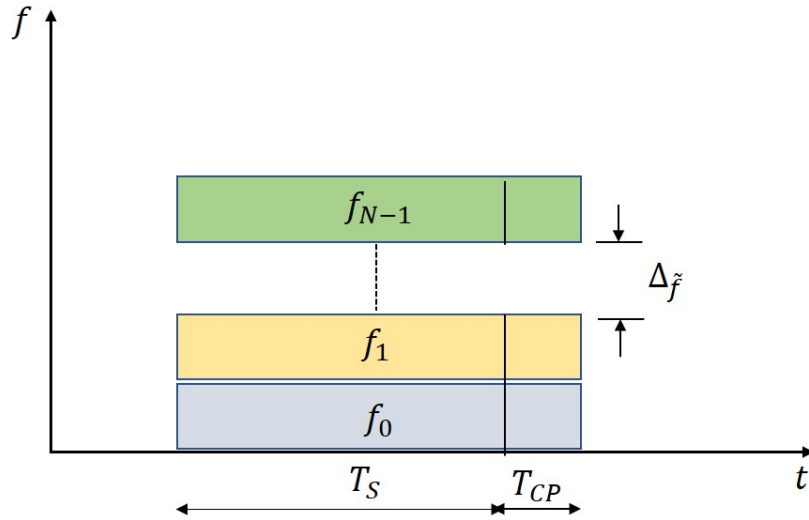


Fig. 2.15. OFDM block with symbols time T and cycle prefix time T_{CP} .

with simulation results is explained in [130]. However, OFDM-radar systems lack high resolutions compared to the FMCW radars.

2.3 Conclusion

In this chapter, the basics of a radar sensor and the automotive radar system have been presented. Additionally, the design of an automotive radar waveform has been introduced and illustrated. In an automotive environment, a waveform must solve the problem of ambiguity in range and Doppler measurements and shall be robust in multi-target scenarios. Six different CW designs of waveforms have been discussed. In Table 2.3 an overview of the fulfilled and missed requirements of the automotive waveform described in this chapter is given. The MFSK, FCLFM, and OFDM waveforms have shown better capabilities. These three waveforms meet the performance requirements for an automotive radar system almost perfectly. Using these waveforms, the target has been solved in range and velocity in an unambiguous manner, that is very important in the complex traffic and road environment. The MFSK and FCLFM are very similar where a similar signal to LFM is transmitted, while in OFDM a CW signal is transmitted and a different portion of the total bandwidth is assigned at each user. The OFDM will be discussed in chapter 4. The main

Table 2.3: Summary of fulfilled and missed requirements, of waveforms used in automotive radar.

Property	CW	LFM	FSK	MFSK	FCLFM	OFDM
Simultaneous measurements of R and v_r	\times	✓	✓	✓	✓	✓
Resolution in range	\times	✓	\times	✓	✓	✓
Resolution in velocity	✓	✓	\times	✓	✓	✓
Accuracy	✓	✓	\times	✓	✓	✓
Measurement time	✓	\times	✓	✓	✓	✓
Ghost targets	✓	\times	✓	✓	✓	✓
Complexity	✓	✓	✓	✓	\times	\times

differences between MFSK and FCLFM are that, in MFSK a single waveform is transmitted while in FCLFM consecutive LFM waveforms are transmitted. The MFSK waveform is obtained combining two up-LFM waveforms with the same slope, but they are shifted in frequency domain. In order to generate a MFSK waveform a complex hardware than FCLFM is required. On the other hand, in order to estimate the radar parameters, when a FCLFM waveform is transmitted the range and velocity are both estimated applying the FFT twice, so that a MFSK is transmitted, the range is estimated applying a stretch processing while the velocity is computed taking into account the phase of the received signal. Thus, in order to estimate the radar parameters when a FCLFM waveform is transmitted a complex hardware have to be used, but due to the fact that the phase of the signal is not involved, the accuracy of the estimated parameters is higher than when the MFSK waveform is used.

In the first part of this chapter an overview of the basic concept of a radar system has been given. While, in last part different radar waveforms used in an automotive environment have been details described. However, in this chapter, the signal processing is view as 1-dimensional signal. In signal processing, time-frequency analysis is a body of techniques and methods used for characterizing and manipulating signals whose statistics change in time. Due to this in the next chapter, on overview of the signal processing in time-frequency analysis will be given.

Chapter 3

Time-Frequency representation

Signal processing can be found in many applications and its primary goal is to provide underlying information on specific problems for the purpose of decision making. The signals, as a function of time, may be considered as a representation with perfect time resolution, however, the time domain lacks the frequency description of the signals. The Fourier transform (FT) of the signal cannot depict how the spectral content of the signal changes with time, which is critical in many non-stationary signals in practice. In real-world as in an automotive environment, the signals have frequency contents that change over time. In this situations, it is not always best to use simple sinusoids as basis functions and characterize a signal by its frequency spectrum. Hence, the time variable is introduced in the Fourier based analysis in order to provide a proper description of the spectral content changes as a function of time.

The aim of this chapter is to give an overview of the time-frequency as Ambiguity Function (AF), Short-time Fourier transform (STFT), Bilinear Time-Frequency Transforms, and fractional Fourier transform. The AF is used for characterizing radar performance in target resolution and the Side Lobe Levels (SLLs) of a waveform. The STFT is basically a moving window Fourier transform. By examining the frequency domain content of the signal as the time window is moved, a 2D time-frequency distribution called the spectrum is generated. The spectrogram contains information on the frequency content of the signal at different time instances. In this thesis, the FrFT is used to

embed, directly, data information into radar waveform. Due to this, in last part of the chapter the FrFT is detail presented and discussed.

The remainder of the chapter is organized as follows. The AF is introduced in Section 3.1 while the canonical AF definition is given in Section 3.2. Additionally, in Section 3.3 the importance AF as a performance evaluation tool for radar system is described. In Section 3.4 the Short-time Fourier transform is introduced while in Section 3.5 the Bilinear Time-Frequency transform is presented. Last in Section 3.6 the FrFT is introduced as a generalization of the conventional FT, while its properties are presented in Section 3.8. Additionally, in Section 3.9 the implementation of FrFT in discrete signals is presented. Finally, the various application of the FrFT in communication system and in radar signal processing are discussed in Section 3.10.

3.1 Ambiguity Function

As discussed in Section 2.1.2, the matched filter is a fundamental tool in radar signal processing. However, it cannot provide information when the system receives a signal from a non-stationary target [75].

In order to provide information even when a non-stationary target is present the AF has been introduced [75]. The radar AF can provide insight about how different radar waveforms may be suitable for the various radar applications. Moreover, it is also used to determine the range and Doppler resolution for a specific radar waveform. Following a review of the most common radar related AF definitions is held.

3.2 Canonical AF Definition

In 1967, Woodward P. introduced the general AF concept, aiming to characterize how well a system could identify the target's range and velocity parameters, based on the transmission of a known waveform. The general definition of the AF is given as [113]

$$\mathcal{A}_{Ca}(\tau, f_D) \int_{-\infty}^{\infty} x(t)x^*(t - \tau)e^{j2\pi f_D t} dt \quad (3.1)$$

As it can be seen from (3.1) the AF is a 2D function of delay time τ and Doppler frequency f_D . Where τ and f_D are the delay time and Doppler frequency shift of the received signal in comparison with the transmitted one, respectively. As can be seen by (3.1) the AF describes the response of a filter matched to $x(t)$ when the signal is received with a delay τ and a Doppler shift f_D relative to the nominal values expected by the filter. The particular form of the AF is determined entirely by the complex waveform $x(t)$. In the concept of radar systems positive τ implies a target farther from the radar than the reference ($\tau = 0$) position. While a negative τ indicates that a target is located close to the radar. Moreover, positive and negative Doppler shift, i.e. $f_D > 0$ and $f_D < 0$, indicate that the target is moving toward or in opposite direction from the radar.

The AF is also used to describe the interference caused by the range and/or Doppler shift of a target when compared to a reference target of equal RCS called nominal targets. Therefore the AF at nonzero points, i.e. all other points except the origin, represents returns from some range and Doppler different from those for the nominal target, while returns from nominal target are located at the origin of the AF.

3.3 AF Cuts and Properties

By its definition (3.1), the AF of an arbitrary signal returns complex values. In radar processing, the modulus of the AF, i.e. $|\mathcal{A}_{Ca}|$, is widely used to describe performance characteristic of the examined signal. Following the absolute value of the AF in (3.1) will be considered to review some of its major properties.

In order to provide very important properties associated with the expected resolution and ambiguities in the time and Doppler domain, separately, one-dimensional cuts of the AF are commonly used. First, consider the cut along the delay axis or the so called zero-Doppler cut. Setting $f_D = 0$ the AF formula in (3.1) can be rewritten as:

$$|\mathcal{A}_{Ca}(\tau, 0)| = \left| \int_{-\infty}^{\infty} x(t)x^*(t - \tau)dt \right| \quad (3.2)$$

The zero-Doppler cut, (3.2), of the signal $x(t)$ can be expressed as the inverse Fourier transform (IFT) of the signal's power spectrum:

$$\int_{-\infty}^{\infty} x(t)x^*(t - \tau)dt = \mathfrak{F}^{-1}\{|\mathfrak{F}\{x(t)\}|^2\} \quad (3.3)$$

where $\mathfrak{F}\{\cdot\}$ and $\mathfrak{F}^{-1}\{\cdot\}$ denote the FT and IFT, respectively.

The second AF cut is along the Doppler frequency axis also called zero-delay cut. Setting $\tau = 0$ the formula AF in (3.1) can be written as

$$|\mathcal{A}_{Ca}(0, f_D)| = \left| \int_{-\infty}^{\infty} |x(t)|^2 e^{j2\pi f_D t} dt \right| \quad (3.4)$$

The zero-delay cut of the AF is a function only the magnitude of the signal, as it can be seen in (3.4), and is equal to the FT of its squared magnitude. In other words, this cut remains unchanged to any phase or frequency modulation in $x(t)$.

Additionally, some further properties of the AF are described as follows:

1. **Maximum Value:** The maximum of the AF of any signal will be located at the origin of its axes:

$$|\mathcal{A}_{Ca}(\tau, f_D)| \leq |\mathcal{A}_{Ca}(0, 0)| = E \quad (3.5)$$

Thus, when the filter is matched in Doppler to the echo and is sampled at a delay corresponding to the target range, the response will be maximum. If the filter is not matched or is sampled at a different delay, then the response will be less than or equal to the maximum.

2. **Symmetry about the origin:** The AF of any signal will be symmetric at its origin:

$$|\mathcal{A}_{Ca}(\tau, f_D)| = |\mathcal{A}_{Ca}(-\tau, -f_D)| \quad (3.6)$$

3. **Volume invariance:** The AF of any signal with finite energy E will have a finite volume equal to E^2 :

$$\int_{-\infty}^{\infty} |\mathcal{A}_{Ca}(\tau, f_D)|^2 = E^2 \quad (3.7)$$

This property implies that, in the design of waveforms, the energy after the AF can be only moved around the AF surface.

The direct consequence of the properties given in (3.5) and (3.7) is that the AF of an any signal should have finite peak value equal to E and a finite volume also equal to E^2 at the same time. As a direct consequence of these properties is that reducing the “height” of the AF in certain regions, e.g. close to the centre to increase the resolution, will push the volume in other areas leading to secondary sidelobes in the delay-Doppler plane. Sidelobes in the AF are undesired as any non-zero values other than its origin represent a potential range and Doppler shifts that could be mistaken for the correct one. In chapter 2, it has been shown that the LFM waveform is widely used in automotive radar. Consequently, the AF of an LFM waveform is presented.

LFM Waveform

Consider the normalized LFM $\hat{\zeta}$ waveform defined by:

$$\hat{\zeta}_{tx}(\eta) = \frac{1}{\sqrt{t_p}} e^{j\left(2\pi f_c \eta \pm \pi \frac{B_{LFM}}{t_p} \eta^2\right)} \quad -\frac{t_p}{2} \leq \eta \leq \frac{t_p}{2} \quad (3.8)$$

Substituting (3.8) in (3.1) the AF of the LFM is given as:

$$|\mathcal{A}_{Ca}(\tau, f_D)| = \left| \left(1 - \frac{|\tau|}{t_p}\right) \frac{\sin\left(\pi t_p \left(f_D + \frac{B_{LFM}}{t_p} \tau\right) \left(1 - \frac{|\tau|}{t_p}\right)\right)}{\pi t_p \left(f_D + \frac{B_{LFM}}{t_p} \tau\right) \left(1 - \frac{|\tau|}{t_p}\right)} \right| \quad (3.9)$$

The zero-Doppler AF cut can be calculated by 3.2 as:

$$|\mathcal{A}_{Ca}(\tau, 0)| = \left| \left(1 - \frac{|\tau|}{t_p}\right) \frac{\sin\left(\pi B_{LFM} \tau \left(1 - \frac{|\tau|}{t_p}\right)\right)}{\pi B_{LFM} \tau \left(1 - \frac{|\tau|}{t_p}\right)} \right| \quad (3.10)$$

From (3.10) it can be extracted that if the time-bandwidth of the pulse is large, i.e. $t_p B_{LFM} \gg 4$, the first null of the zero-Doppler cut is located at $\tau_{null} \approx 1/B_{LFM}$. An example of the AF, of an LFM pulse when the product time-bandwidth is set at 2228, is illustrated in Fig. 3.1. As we can see, the energy of the AF is essentially concentrated along the diagonal ridge, causing lower sidelobes outside the ridge. The zero-delay AF cut can be calculated

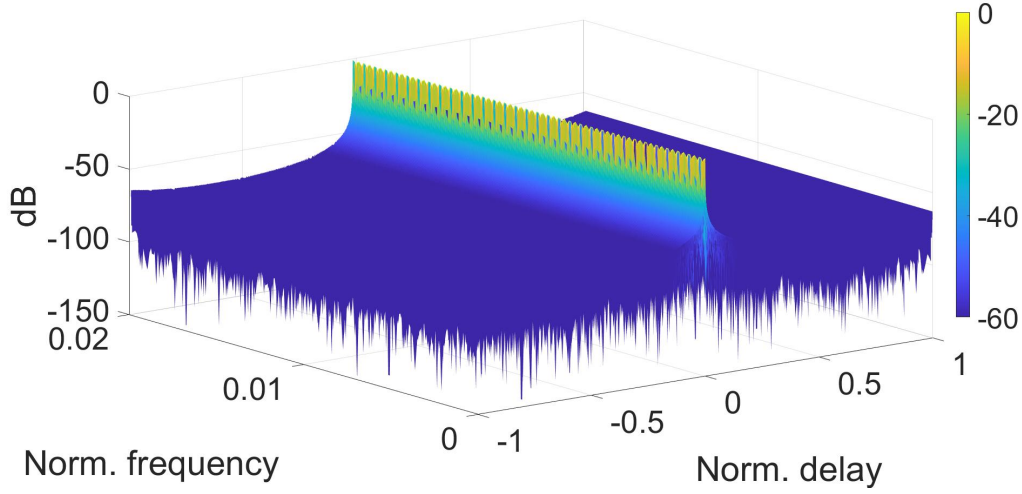


Fig. 3.1. Ambiguity function of an LFM waveform, with a time-bandwidth by 2228.

by (3.2) as:

$$|\mathcal{A}_{Ca}(0, f_D)| = \left| \frac{\sin(\pi f_D \tau)}{\pi f_D \tau} \right| \quad (3.11)$$

As mentioned previously in this Section, the zero-delay cut only depends on the modulus of the signal $|x(t)|$. As it can be seen in (3.11), any signal with a square modulus has a zero-delay cut described by a sinc function.

The two cuts obtained by (3.9) are illustrated in Fig. 3.2. As we can see from zero-Doppler cut, Fig. 3.2a, and zero-delay cut, Fig. 3.2b, is that in both cuts the peak sidelobe ratio is -13.2 dB.

Comparing the arguments of the sine functions in equation 3.9 and equation 3.10 we can see that a Doppler shift by δ_{f_D} translates the peak of the response along the time delay by an amount equal to $-(\delta_{f_D}/B_{\text{LFM}}t_p)$. This means that an LFM waveform exhibits a coupling between range and Doppler. The range Doppler coupling leads to an error in the estimated range. However, it can be eliminated by repeating the measurements with an LFM opposite slope.

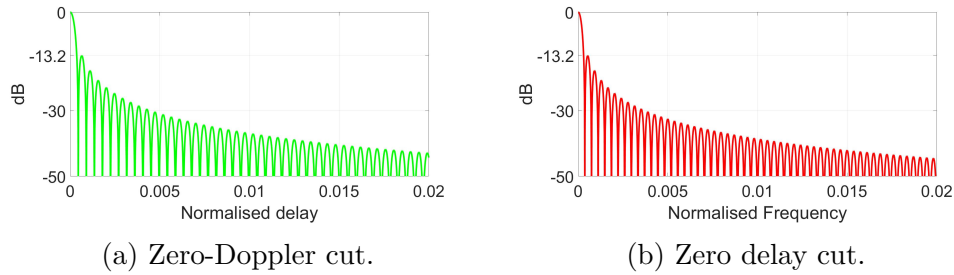


Fig. 3.2. The two cuts of an LFM pulse, 3.2a zero-Doppler cut, 3.2b zero delay cut. The time-bandwidth product is set at 2228.

3.4 Short-Time Frequency Transformation

The Fourier transform introduced in the nineteenth century has become one of the most widely used in signal-analysis tools across many disciplines of science and engineering. However, when a signal varies over time the FT does not clearly indicate how the frequency content of a signal changes over time. One of the most known time frequency representations of a time signal is Short-time Fourier transform [18]. The STFT of a generic non-stationary signal $x(t)$ is a linear transformation given by

$$S_{STFT}(t, f) = \int_{-\infty}^{\infty} x(t')w^*(t' - t)e^{-i2\pi ft'} dt' \quad (3.12)$$

where $w(\cdot)$ is a window function centred at zero delay [53]. The basic principle of STFT is the computation of FT onto shorter signal segments obtained by moving the window centre t' along the signal time duration, as illustrated in Fig. 3.3 from [44]. The magnitude display $|S_{STFT}(t, f)|$ is called the spectrogram. It shows how the frequency spectrum varies as a function of the horizontal time axis.

STFT has two major advantages. First, according to its definition, STFT is simple enough, as it is equal to the computation of multiple FT. The second advantage is the absence of cross terms. The cross terms are not present, because the STFT derived directly from the Fourier transform.

The definition of the STFT can also be expressed in the frequency domain by manipulating (3.12), with the result:

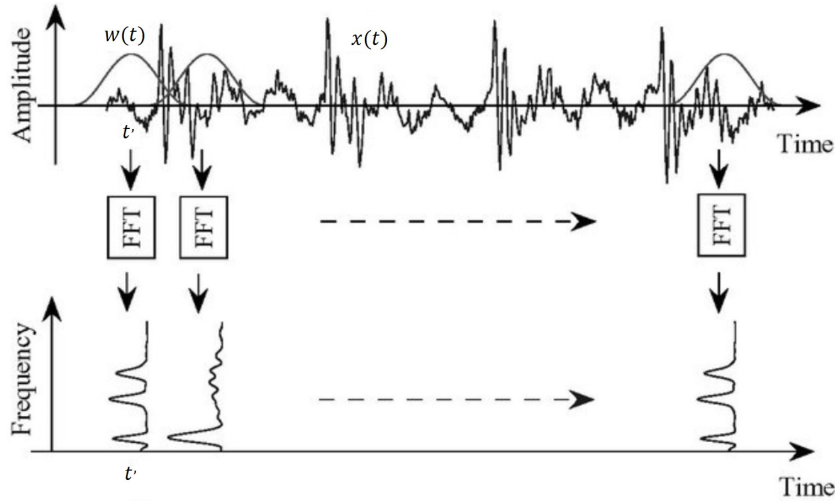


Fig. 3.3. Illustration of STFT processing on the signal $x(t)$ from [44].

$$S_{STFT}(t, f) = \frac{1}{2\pi} e^{-i2\pi ft} \int_{-\infty}^{\infty} X(f') W^*(f' - f) e^{-i2\pi f' t} df' \quad (3.13)$$

With $W(f)$ is the Fourier transform of $w(t)$. The dual relationship between (3.12) and (3.12) is apparent. In addition, the following observations can be done:

1. Signal components with durations shorter than the duration of the window will tend to obtain smeared out;
2. The window width in time and the window width in frequency are inversely proportional to each other by the uncertainty principle. Therefore, good resolution in time (small time window) necessary implies poor resolution in frequency (large frequency window). Conversely, good resolution in frequency implies poor resolution in time;
3. The window width in each domain remains fixed as it is translated.

3.5 Bilinear Time-Frequency Transforms

The power spectrum of a signal $x(t)$ is the magnitude square of its FT, $|X(f)|^2$. It can also be expressed as the FT of the autocorrelation function of $x(t)$.

$$|S(f)|^2 = \int_{-\infty}^{\infty} R(\tau)e^{-j2\pi f\tau} d\tau \quad (3.14)$$

with $R(\tau)$ autocorrelation function defined as

$$R(\tau) = \int_{-\infty}^{\infty} x(t)x^*(t - \tau)dt \quad (3.15)$$

The power spectrum indicates how the signal energy is distributed in the frequency domain. While the FT, $S(f)$ is a linear function of $x(t)$, the power spectrum is a quadratic function of $x(t)$.

The STFT derived directly from the FT and it is classified as a linear transforms. On the other hand, the power spectrum is a quadratic function and the cross-terms are present.

3.6 Fractional Fourier transform

The fractional Fourier transform was firstly introduced in [88] as a technique to help in solving certain classes of ordinary and practical equations with application in quantum mechanics. Later, it was rediscovered by [135], [72], [82] [92] for application in optic and by Almeida in signal processing. The fractional Fourier transform is a generalization of the ordinary Fourier transform with an order α . If the Fourier transform operator is denoted by \mathfrak{F} , then the α -th order fraction Fourier transform operator is denoted by $\mathfrak{F}^\alpha(\cdot)$. The zero-th order fractional Fourier transform operator $\mathfrak{F}^0(\cdot)$ is equal to the identity operator I , while the first-order FrFT operator $\mathfrak{F}^1(\cdot)$ is equal to the ordinary Fourier transform operator.

3.7 Definition

Let $x(t)$ be an arbitrary signal defined in the time domain, the α -th ordered FrFT of $x(t)$ is given by [92]:

$$x_\alpha(u) = \mathfrak{F}^\alpha\{x(t)\} = \int_{-\infty}^{\infty} K_\alpha(u, t)x(t)dt \quad (3.16)$$

where u is the domain in which $x_\alpha(u)$ is defined and K_α is the Kernel of the transform defined as [92]:

$$K_\alpha[u, t] = \begin{cases} A_\alpha e^{j\pi(u^2+t^2)B_\alpha} e^{-j\pi 2utC_\alpha} & \text{if } \vartheta \neq m\pi \\ \delta[u - t] & \text{if } \vartheta = 2m\pi \\ \delta[u + t] & \text{if } \vartheta = 2m\pi + \pi \end{cases} \quad (3.17)$$

where $A_\alpha = |C_\alpha|^{\frac{1}{2}} e^{-i(\pi \operatorname{sgn}(\sin \vartheta)/4 - \vartheta/2)}$ and $\vartheta = \alpha \frac{\pi}{2}$ is the rotation angle and depends on the order α , $\delta[\cdot]$ is the Dirac delta function and $m \in \mathbb{Z}$. While B_α and C_α are:

$$\begin{aligned} B_\alpha &= \cot(\vartheta) \\ C_\alpha &= \csc(\vartheta) \end{aligned} \quad (3.18)$$

As it can be seen from the kernel in (3.17), the FrFT can be parametrised by an angle ϑ which is the rotation angle between the time domain t and u , where u is the phase space where the signal after the FrFT is defined. This is best understood by referring to Fig. 3.4 which shows the phase space spanned by the time axes t and frequency f . Oblique axes making angle ϑ constitute domains where the α -th order of the FrFT lives. The kernel equation (3.17) shows that for angles that are not multiples of π , the FrFT can be described by following steps:

1. A product by a chirp;
2. A FT scaled by $\csc \vartheta$;
3. Another product by a chirp;
4. A product by a complex amplitude factor

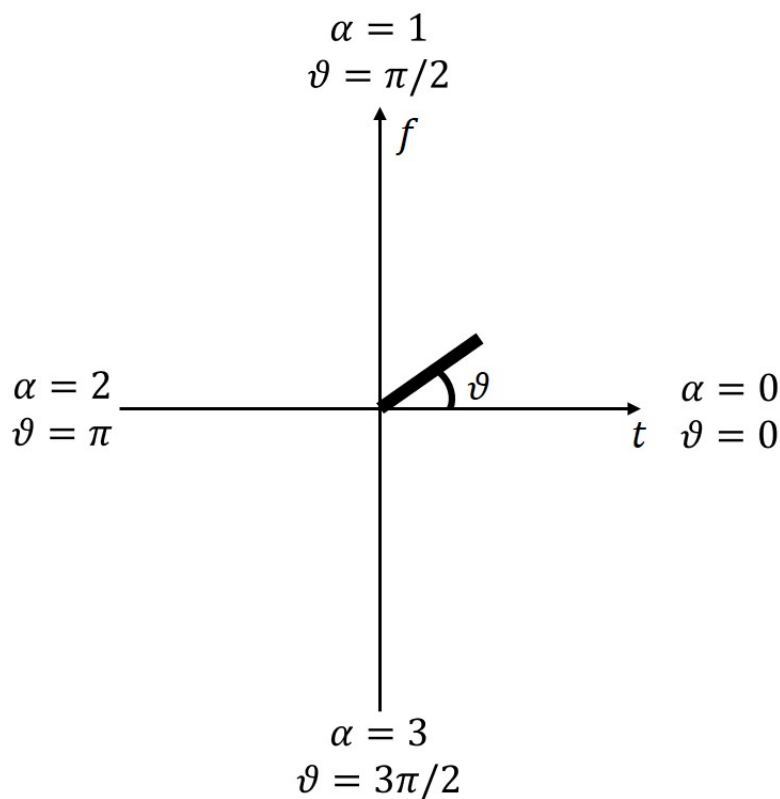


Fig. 3.4. FrFT as a rotation in the time-frequency plane.

In summary, the FrFT is an invertible linear transform, continuous in the angle ϑ , which satisfies the basic conditions for it to be meaningful as a rotation in the time-frequency plane. This rotation is better illustrated in Fig. 3.5 where the STFT of a complex Gaussian pulse is illustrated after FrFT of different orders has been applied on the pulse. As we can see when the order is 0 and 2 the signal is defined in time domain, while when α is equal to 1 and 3 the FrFT corresponds to a FT, for other different orders of the FrFT the signal is rotated in time-frequency domain. As we can see for each order of the FrFT a different signal is obtained.

3.8 FrFT Properties

In the literature, the various properties of the FrFT have been investigated [92] [99]. In the following paragraphs the most important properties of FrFT will be

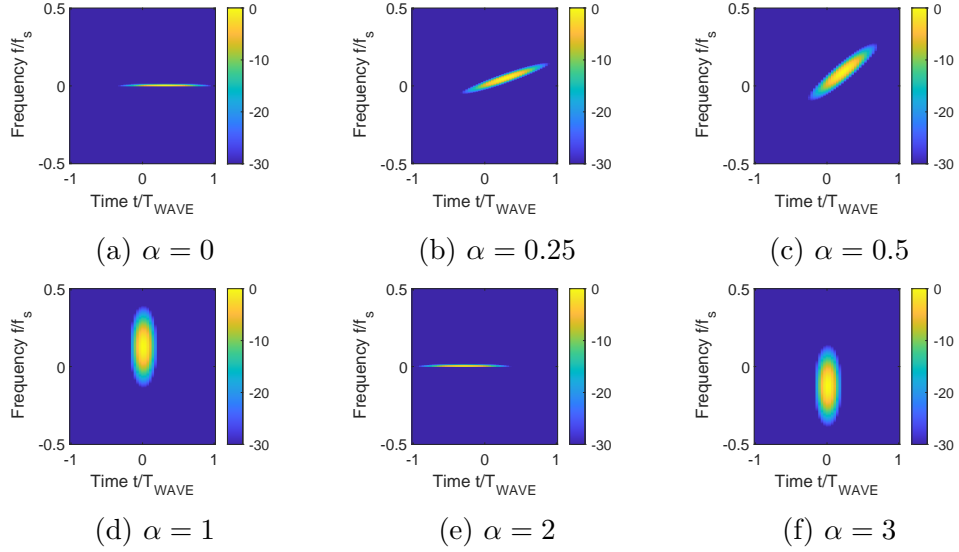


Fig. 3.5. Time-Frequency representation using STFT of a Gaussian pulse after applying FrFT of different orders.

presented and discussed.

Linearity: Similar to the original FT, the FrFT is a linear transform, i.e.:

$$\mathfrak{F}^\alpha \left\{ \sum_k h_k f_k(t) \right\} = \sum_k h_k \mathfrak{F}^\alpha \{ f_k(t) \} \quad (3.19)$$

where h_k is a constant and $f_k(t)$ is an arbitrary function.

Integer Order: The integer orders of the FrFT return well-know functions as listed:

$$\mathfrak{F}^4 = \mathfrak{F}^0 = I \quad (\text{Identity Function}) \quad (3.20)$$

$$\mathfrak{F}^1 = \mathfrak{F} \quad (\text{Fourier transform}) \quad (3.21)$$

$$\mathfrak{F}^2 = P \quad (\text{Parity Operator}) \quad (3.22)$$

$$\mathfrak{F}^3 = \mathfrak{F}^{-1} = (\mathfrak{F})^{-1} \quad (\text{inverse Fourier transform}) \quad (3.23)$$

where the parity operation of an arbitrary signal $x(t)$ is obtained by $P\{x(t)\} = x(-t)$.

Index additivity: Sequential FrFTs are equivalent to a FrFT with an order

equal to the summation of all the orders, i.e.:

$$\mathfrak{F}^{\alpha_1} \mathfrak{F}^{\alpha_2} = \mathfrak{F}^{\alpha_1 + \alpha_2} \quad (3.24)$$

Repetition: From (3.20) and (3.23) it can be easily derived that

$$\mathfrak{F}^{4m+\alpha} = \mathfrak{F}^{\alpha} \quad \forall m \in \mathbb{Z} \quad (3.25)$$

Inverse: From (3.20) and (3.24) it also follows that the inverse of a FrFT of an order α is a FrFT of order $-\alpha$

$$(\mathfrak{F}^{\alpha})^{-1} = \mathfrak{F}^{-\alpha} \quad (3.26)$$

Commutativity and Associativity: Sequential FrFTs follow both the commutativity and associativity properties, i.e.

$$(\mathfrak{F}^{\alpha_1} \mathfrak{F}^{\alpha_2}) \mathfrak{F}^{\alpha_3} = \mathfrak{F}^{\alpha_1} (\mathfrak{F}^{\alpha_3} \mathfrak{F}^{\alpha_2}) \quad (3.27)$$

Parseval's Theorem: Similar to FT, FrFT satisfies the Parseval's theorem which implies that a signal will contain the same energy before and after FrFT is applied.

$$\int_{-\infty}^{\infty} x(t)y^*(t)dt = \int_{-\infty}^{\infty} \mathfrak{F}^a\{x(t)\}\mathfrak{F}^a\{y^*(t)\}du \quad (3.28)$$

where $x(t)$ and $y(t)$ are arbitrary signals and u is the variable of fractional domain in which $\mathfrak{F}^a\{x(t)\}$ and $\mathfrak{F}^a\{y^*(t)\}$ are defined.

3.9 FrFT Implementations

The discussion on FrFT has only covered application on continuous signals as it can be also seen in the definition provided in (3.16). In the following paragraphs, the two mainly used approaches for implementation of FrFT in discrete signals will be discussed.

3.9.1 Discrete FrFT

Assume an arbitrary discrete signal described by the vector \mathbf{x} :

$$\mathbf{x} = [x[1], x[2], \dots, x[N]]^T \quad (3.29)$$

The discrete fractional Fourier transform (DFrFT) of \mathbf{x} is defined as the vector $\mathbf{x}_\alpha = \mathcal{F}_\alpha \mathbf{x}$, i.e., the vector populated as:

$$\mathbf{x}_\alpha[n] = \sum_{k=1}^N \mathcal{F}_\alpha[n, k] \mathbf{x}[k], \quad n = 0, \dots, N \quad (3.30)$$

where \mathcal{F}_α is the $N \times N$ DFrFT matrix. Moreover, the DFrFT matrix can be decomposed as:

$$\mathcal{F}_\alpha = \mathbf{E} \mathbf{\Lambda}^\alpha \mathbf{E}^T \quad (3.31)$$

where \mathbf{E} is the eigenvectors' matrix and $\mathbf{\Lambda}^\alpha$ is the diagonal eigenvalues matrix of discrete FT (DFT), i.e. $\mathcal{F} = \mathbf{E} \mathbf{\Lambda} \mathbf{E}^T$. In general, if N is large, the DFrFT can be employed as an approximation of the continuous FrFT. However, more direct and less complex methods have been proposed for the approximation of continuous FrFT as it will be discussed below.

3.9.2 Fast Approximation of FrFT

To define the fast approximation of FrFT the definition given in [12] is used. The algorithms discussed in [12] are algorithms that approximate the continuous FrFT in the sense that they map samples of the signal to samples of the continuous FrFT. This comes to a difference with the FFT, introduced in [11] which is a much lower in complexity technique of implementing the DFT. Thus, when the computation of the DFT of a vector \mathbf{x} with length N is applied using matrix multiplication, i.e. $\mathfrak{F}(\mathbf{x}) = \mathcal{F}(\mathbf{x})$ the technique will have a complexity of $\mathcal{O}(N^2)$. On the other hand, FFT offers a much lower complexity of $\mathcal{O}N \log(N)$ [141]. While FFT and inverse FFT (IFFT) can be used to perform fast calculation of DFrFT of order $\alpha = 1$ and $\alpha = 3$ respectively, there is not a know genuine fast FrFT (FFrFT) that satisfies all the conditions in (3.19)-(3.28) [12] [125].

3.10 Applications of FrFT in Signal processing

Similar to the traditional FT, FrFT has many applications in Digital Signal Processing (DSP) covering even larger field due to its higher degree of freedom which can allow further optimisation and thus achieving better performance. In this Section an overview of the applications in communication and radar fields is given as follows

3.10.1 Communication

In a communication system, the Orthogonal Frequency Division Multiplexing (OFDM) is widely used. The main advantage is that by taking carriers that are orthogonal in the frequency domain one may avoid that the symbols mutually interfere each other in the frequency domain. In wireless communication channels, the channel frequency response is rapidly time varying and the Doppler spread may cause interchannel interference. In [81] the discrete FrFT is used instead of the DFT in multi carrier systems. Performance of this technique is significantly improved since the time-frequency plane can be rotated in a way to compensate undesired modulation of the signals introduced by high velocity of the other users and/or by multipath component shifted from the Line Of Sight (LOS) components. This technique is generalized for general linear canonical form of the transform (Affine Fourier transform (AFT)) in [34]. This form showed an improved flexibility with respect to the FrFT-based scheme. These chirps based modulations and associated AFT schemes were identified as a suitable basis for multi carrier communication such as aeronautical and satellite [127]. Additionally, in [66] a minimum mean squared error receiver based on the FrFT for Multiple Input Multiple Output (MIMO) systems with space time processing over Rayleigh faded channels was presented. The numerical analysis of the proposed receiver showed improved performance; outperforming the simple minimum means squared error receiver in Rayleigh faded channel. Furthermore, chirp modulation spread spectrum based on the FrFT was proposed for demodulation of multiple access system [73]. The numerical analysis showed that the FrFT based receiver is more

flexible and efficient system for multiple access by reducing the designed complexity of the system.

3.10.2 Radar applications

The FrFT has also been extensively used in radar applications. Namely, FrFT based techniques for SAR images have been proposed in [3] [17] [97] [55]. Moreover, the authors in [24] [25] [26] showed how FrFT can be useful in performing high resolution SAR processing. In [101] an algorithm was proposed in which the azimuth compression and Range Cell Migration Correction (RCMC) are jointly carried out using FrFT.

In [77] the authors proposed an optimisation of OFDM radar signals based on FrFT showing that the proposed design offer better wideband AF shape as well as higher range and velocity resolution compared to traditional OFDM. Moreover, in [23] a novel waveform design scheme based on FrFT was introduced showing that the generated waveforms are suitable for radar applications. These novel libraries showed to provide significant advantages in terms of delay resolution, interference and sidelobe level reduction. Increased performance is shown in terms of orthogonality and reuse of waveform for the same canonical sequence, but with different fractional orders when higher values of chip sampling rate are used [22]. In order to analyse the orthogonality properties of the library the authors in [22] assumed that two waveforms are orthogonal if their cross-correlation is below the side-lobe level of the original waveform. In [28] two optimisation algorithms were introduced for maximizing the Signal to Interference plus Noise Ratio (SINR) in a collocated MIMO radar system taking into account constant modulus and similarity constraints. Both algorithms have been shown good performance trading however with high complexity. Furthermore, an efficient-low complexity technique to reconstruct FrFT based waveforms under Constant Envelope (CE) constraints was presented in [56], while in [57] three CE-FrFT based waveforms of different fractional order were validated experimentally in terms of orthogonality. The experimental and simulation results suggest that the proposed technique offers an efficient method for generating multiple waveforms suitable for MIMO radar system offering good orthogonality levels while also retaining good

Table 3.1: Summary of fulfilled and missed requirements of the Time-Frequency representation.

Property	AF	STFT	PSD	FrFT
Capacity to distinguish the targets in range and Doppler	✓	✗	✗	✗
Computational complexity	✓	✓	✓	✗
Trade off Resolution	✗	✓	✓	✗
Rotate the signal in time-frequency domain	✗	✗	✗	✓
Frequency over time	✗	✓	✗	✗

localization performance. In [124], it was proposed a method of radar signal feature extraction based on FrFT, where the experimental results have shown that the performance of the eigenvector proposed by its method is excellent, effective and feasible.

3.11 Conclusion

In this chapter, five time-frequency transformations have been presented. A summary of the analysis so as to highlight the advantages and shortcomings of the different time-frequency methods is given in Table 3.1. As we can see the AF is able to distinguish the target in range and Doppler, thus will be used to evaluate the radar performance of the waveform that will be presented in chapter 5. The STFT is widely used to analyse non-stationary signals, determining how the spectral content of signals changes over time. This transform localizes the signal in time using a window. The main disadvantage is the using of a fixed window size. On one hand, long windows have better frequency resolution, but poor time resolution. On the other hand, short windows provide better time resolution, but lower frequency resolution. The PSD will be used to show how the energy is located in the frequency domain. Finally, the FrFT will be used due to its capacity to be applied at the modulated signal in frequency. In addition, in this thesis it will be used to rotate the baseband signal, obtained after the communication functions in time-frequency domain. It will be discussed in chapter 5. In addition, in

this chapter it has been shown that using the different orders of the FrFT different signals are obtained in time-frequency domain. In an automotive environment, in order to prevent the mutual radar interference each user has to transmit waveforms that are uncorrelated with those of other users. In last part of the chapter, it has been shown that when the order of the FrFT changes a different signal is obtained. So, in order to allocate more than one user in the same frequency band at the same time, a fractional multiplexing order can be applied. However, to prevent the mutual radar interference only two opposite orders, of the FrFT, can be used. Due to it in chapter 6 the mutual radar interference will be analysed.

The main drawbacks of the FrFT are that the Inverse FrFT (IFrFT) can be applied profitably, only when the time signal start has been estimated correctly. Comparing the Discrete FrFT with Discrete FT, as demonstrated in Section 3.9.2, the Discrete FrFT cannot be computed by applying a Fast discrete FrFT. Thus means that the Discrete FrFT is more complexed than the FFT.

Chapter 4

Joint Radar and Communication Systems

As economies and societies have become more mobile and information centric there has been an explosion in mobile radio use, and wireless communications became a necessary part of human life [91]. The high demand for wireless services and the shortage of new spectral resources has recently motivated the necessity of new spectrum allotments or a re-design of current systems to effectively manage coexistence between different types of technologies. Spectrum sharing technology between a radar sensor and communication function has emerged.

In this chapter, the motivation that leads to share radar and communication functions is illustrated. Then an overview of the different joint radar and communication systems present in literature is reported. Finally, an overview of the different approaches to mitigate the mutual radar interference caused by other users that operate in the same frequency band at the same time is given. The remainder of the chapter is organized as follows. The rationale behind a joint radar and communication systems is presented in Section 4.1. In Section 4.2 the state of the art of the joint radar and communication system is described. Finally, Section 4.3 describes the different approaches presented in literature to mitigate multiple radars in automotive environment.

4.1 Sharing Radar and Communication

In order to satisfy the growing consumer demand for higher data rates, wireless communication has pushed the carrier frequencies towards bands traditionally assigned to radar systems. The spectrum, extending from below 1 MHz to above 100 GHz, represents a precious resource, meaning that the spectrum will be more and more congested and contested.

In contrast to the rapid growth of spectral demand, a measurement of spectrum occupancy at a given location as a function of direction, frequency, time, and polarisation would be likely to show that the instantaneous spectrum occupancy is underutilized. The reason for these apparent contradictions is that existing allocation is rather inefficient. It, therefore, follows that there is great potential and needs for techniques that use spectrum in a more intelligent and adaptive manner.

In USA due to the new Federal spectrum architecture, [91], spectrum sharing technology has emerged as a developing research topic for both radar and communication communities. Hence, cooperation between these two established technologies has become a fertile ground for research.

Spectrum sharing involves a primary user, whom the bandwidth is licensed to, and a secondary user that utilizes the same spectrum band without endangering any mission of both sides [58]. Until recently, in order to prevent any interference among different systems, a certain frequency band was assigned exclusively to a technology like radar or wireless.

Technical challenges of spectrum sharing involve both accurately sensing radio environment, and transmitting signals accordingly. Challenges of spectrum sharing in communication system are widely investigated in [98], [13], [46], and [79]. Although the effects to RF interference in radar system concerning spectrum sharing has been investigated in the past, [119], more work needs to be done to understand drawbacks and fundamental limits of spectrum sharing in radar and communication systems coexistence.

To this end, research efforts are well under way to address the issue of Communication and Radar Spectrum Sharing (CRSS). There are two main research directions in CRSS:

1. Radar and Communication coexistence

2. Joint Radar and Communication system.

In the first category, the two systems can operate without unduly interfering with each other. In this category, solutions are proposed to mitigate the interference caused by the communication system on the radar. Although, it is assumed that the communication system is operating cognitively, the proposed solutions are developed by assuming that the interference mitigation responsibility is on radar itself without any level of explicit cooperation among the radar and the communication system. In the second category, a system can simultaneously perform radar and communication functions at the same time. Hence, it is the most sophisticated category and it, potentially, leads to the highest gains for both radar and communication systems operating in the same frequency band and at the same time. In this category, both radar and communication systems cooperatively alleviate the effects of interference to each other which necessitates the joint design of both systems for interference mitigation. An example of the joint radar and communication system is illustrated in Fig. 4.1, where the user on the left acts as a monostatic radar transceiver (transmitter and receiver), while simultaneously functioning as a communication transmitter. The user on the right is a communication receiver. A joint radar and communication system contributes to reducing the number of antennas [136], system size, weight and power consumption [78], as well as alleviating concerns for electromagnetic compatibility and spectrum congestion issues [155]. This type of system has been extended to numerous novel applications, including vehicular networks, indoor positioning, and secret communications [145], [147], and [9].

In Table 4.1 the potential application scenarios of CRSS from both civilian

Table 4.1: Applications of the CRSS technology.

Civilian Applications	Radar-comms coexistence, V2X network, WiFi localization, UAV comms and sensing, RFID, Medial sensors, Radar relay, etc.
Military Applications	Multi function RF system, LPI comms, UAV comms and sensing, Passive radar, etc.

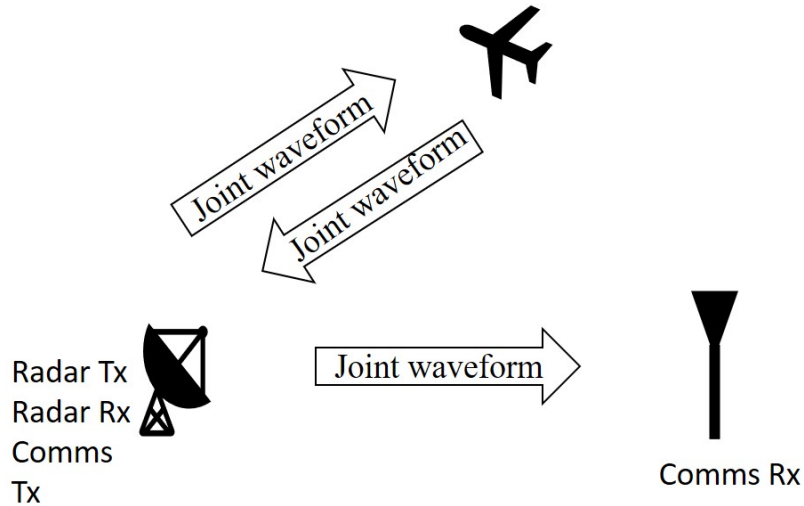


Fig. 4.1. An example of joint radar and communication system.

and military perspectives are listed. The CRSS has originally been motivated by the need for the coexistence of radar and commercial wireless systems. The examples of coexisting systems in various bands are following:

- *L-band* ($1 - 2 \text{ GHz}$): This band is primarily used for long-range air-surveillance radars, such as Air Traffic Control (ATC) radar, which transmits high power pulses with broad bandwidth. The same band, however, is also used by 5G NR and FDD-LTE cellular systems as well as the Global Navigation Satellite System (GNSS) both in their downlink and uplink [142].
- *S-band* ($2 - 4 \text{ GHz}$): This band is typically used for air-borne early warning radars at considerably higher transmit power [108]. Some long-range weather radar also operate in this band due to moderate weather effects in heavy precipitation [47]. Communication systems present in this band include 802.11b/g/n/ax/y WLAN networks, 3.5 GHz TDD-LTE and 5G NR [54].
- *C-band* ($4 - 8 \text{ GHz}$): This band is very sensitive to weather patterns. Therefore, it is assigned to most types of weather radars for locating

light/medium rain [47]. Wireless systems in this band mainly include WLAN networks, such as 802.11a/h/j/n/p/ac/ax.

- *mmWave band (30 – 300 GHz)*: This band is conventionally used by automotive radars for collision detection and avoidance, as well as by high resolution imaging radars [21]. However, it is bound to become busier, as there is a huge interest raised by the wireless community concerning mmWave communications, which are soon to be finalized as part of the 5G New Radio (NR) standard [116]. Currently, the mmWave band is also exploited by the 802.11ad/ay WLAN protocols

4.2 State of art systems and applications for joint radar and communication systems

Combining radar system and communication functions would provide a hybrid detection and ranging application that would benefit from mutual sharing of information between radar and communication using the same frequency band and hardware resources. Furthermore, using mmWave band will provide high data rate for communication and better accuracy and resolution for radar operations.

The main challenge, in a joint radar and communication system, is developing the suitable waveform design that can be simultaneously employed for information transmission and radar sensing. Classic radar waveform design aims at creating waveform with optimum autocorrelation properties, which guarantees the high dynamic range of the measurements when applying correlation processing in the receiver. While for the communication, the data rate and the BER are the most stringent parameters. In a joint and radar communication system it is necessary that the radar performance is not significantly impacted due to random data information that are embedded in the radar waveform. In an automotive environment a joint radar and communication system is used to simultaneously achieve ultra-low latency and high range of operation, with the advantages of better performance and to meet low-SWaP (Size, Weight and Power) requirements. An early integrated radar and communication subsystem for the Space Shuttle Orbiter (NASA) was introduced in

[14]. While the sub-system had different signal processing components for each functionality, the radar and communication implementations shared a wideband transmitter, a two-channel receiver and an antenna, thus providing for significant savings on weight, physical dimensions, power requirements and overall system complexity.

4.2.1 Spread Spectrum techniques

Radar and communications signals can be combined applying multiplexing techniques. The Frequency Division Multiplexing (FDM) scheme is generally less popular than Code Division Multiplexing (CDM) and the Time Division Multiplexing (TDM) counterparts due to mutual interference caused by the spectrum overlapping [143]. Spread Spectrum (SS) techniques were firstly implemented for vehicular communication and ranging applications in [84]. In that system, a vehicle can know the information of another vehicle, and range distance between two vehicles at the same time. The concept is illustrated in Fig. 4.2, where Vehicle 2 multiplies its own information by Pseudo-Noise (PN) code signal which is transmitted from Vehicle 1, and retransmits to Vehicle 1. Vehicle 1 demodulates the signal from Vehicle 2 by the SS technique with PN code which Vehicle 1 owns. Then it can know the information of Vehicle 2 and range distance between Vehicle 1 and Vehicle 2 at the same time. It is called Boomerang Transmission System, because the PN code sequence is transmitted from Vehicle 1 and return there with the information of Vehicle 2 like a boomerang. Moreover, even when Vehicle 2 does not have this system, Vehicle 1 can range distance between two vehicles with the PN code signal which is transmitted from Vehicle 1 and is reflected at Vehicle 1.

Following that development, the Spread Spectrum (SS) technique was exploited for combining radar and communication function, such as LFM spread spectrum [114], [118],[154], Direct-Sequence Spread Spectrum (DSSS) [146], [123], [60], and time-hopping spread spectrum [76]. The basic idea, of these methods, is to use two signals that should be mutually orthogonal. In [114], [118] an up LFM and a down LFM are used for the communication and radar functionality, respectively. The orthogonality condition is not satisfied when

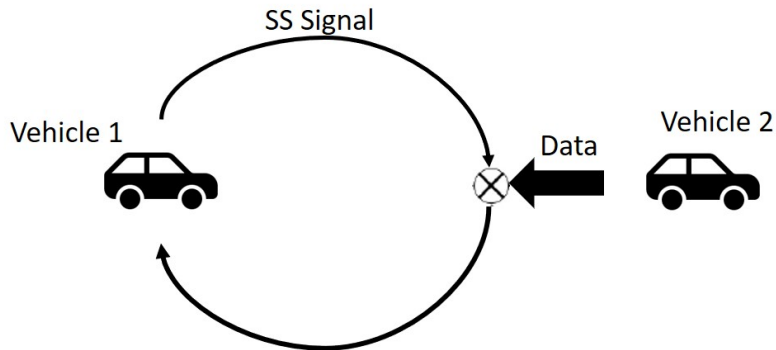


Fig. 4.2. Vehicular communication and ranging applications.

an LFM has a limited time length. In order to overcome this problem, in [154] the orthogonality is obtained by maximizing the ratio of the sidelobe levels (SLLs) of the autocorrelation output to the output of the cross-correlation function.

DSSS codes have a good pseudo-randomness and non-cyclic autocorrelation [61], which meet the requirements of radar-communication integration. DSSS codes are high resolution ranging at the expense of utilizing excessive spectrum resources, SS coding can be exploited for user separation by Code Division Multiple Access (CDMA). This approach provides an inherent support for multi user operation with standard CDMA techniques. In [146] and [123] the integration of radar and communication is based on bipolar PN sequences, namely m -sequence [151]. However, one of the main drawbacks of m -sequences in the radar context is their poor Doppler tolerance [75]. These and related designs such as Barker code sequences are optimized only with respect to the zero Doppler cut of the Ambiguity Function, but produce much higher interference levels in the presence of Doppler shifted waveforms. As for the application to communications, large sets of m -sequences which are used in multiple access channel have typically rather poor cross-correlation properties [151]. While in [60] the integration of these two functions is done on polyphase sequences, such as Opperman sequences that showed to be able to perform well in radar scenarios, but resulted to be very complex to be put in practice. In DSSS schemes redundancy bit reduces the user data rate in proportion to the spreading factor, provided that the symbol rate after the encoder is kept constant. The common ground of spread spectrum techniques is that signal

consist of two orthogonal signals to distinguish radar and communication functions, and then compounded to one waveform to transmit. Thereby, in a receiver, a matched filter is applied to separate the two waveforms and then further processes can be applied, which increases complexity and cost. The TDM is the simplest approach in all solutions for radar and communication integration [69], [149], [126] [152] and [49]. In order to minimize the interference between two functions, these techniques for each time slot use a single function. When communication is in need, it switches to communication mode, while radar functions are completely disabled. In the same way, it switches back to radar signal processor and generator, and radar functions are restored. In [49] for the radar mode, a specially arranged Trapezoidal Frequency Modulation Continuous Wave (TFMCW) modulation is adopted, which combines three time intervals, namely an up LFM, a constant frequency period and a down LFM. Moreover, a constant-frequency period follows the radar cycle in the transmitted signal, which can be encoded with information data using different modulation schemes such as Amplitude Shift Keying (ASK), Frequency Shift Keying (FSK) and Phase Shift Keying (PSK), and some combinations among them. In [85], a radar communication systems was developed with an intended application around dedicated short range communication band where a narrow bandwidth is available. In [85], it was improved to be capable of angle detection besides velocity range estimation with enhanced resolution and accuracy. The major drawback of time-domain integration is the necessity of synchronization. This can be done, by using the timing information of Global Positioning System (GPS) or even techniques such as network time protocol [20]. Additionally, in this scheme it is obvious that the overall communication time proportion cannot be too high in order not to affect radar detection performance. Also, communication state cannot last too long for a single time, or possible object lost may lead to disadvantage in battlefield. Then time-domain approach just fits in situations where only short burst communication is needed, which means it is difficult for this integration approach to replace current communication system completely. However, the advantages of this approach are that this simple design requires no major changes to both hardware and software, and there is no need to re-design radar and communication waveforms.

In [134], an Ultra-WideBand (UWB) noise signal is used as radar waveform, and a segment of the spectrum of this UWB signal is cut for embedding communication signal, then two signals are combined to be transmitted as a unique waveform. This kind of waveform also needs to separate communication signal firstly. In [19] a radar waveform which is compatible with communication was presented. It is generated by modulating LFM signal to carry data by MSK method. The communication receiver demodulated data from the waveform. In this system the receiver does not decide which waveform is for radar or for communication. However, in this technique the zero-Doppler cut depends on the number of bits that are embedded into waveform.

4.2.2 Dual radar communication function based on phased array

In [8] a waveform diversity-based method was reported. In this scheme, to embed a communication signal into radar emission one radar waveform is selected from a dictionary of waveforms, where each waveform represents a communication symbol. The communication receiver deciphers the embedded information by determining which waveform was transmitted. The primary issue with varying the radar waveform during a CPI is the clutter range sidelobe modulation (RMS) [8],[59] that arises, because the pulse compression of different waveforms leads to different sidelobe structures. When Doppler processing is carried out across the CPI of pulsed echoes the presence of RMS induces a partial loss of coherency, the consequence of which is increased residual clutter after cancellation, and thus degrade target visibility. Other systems to get a dual radar communication function use a multi sensor transmit/receiver configurations. The popular techniques include sidelobe Amplitude Modulation (AM) method [35], multi waveform ASK method [50]. The use of time-modulated arrays to realize a dual-function array that enables performing the radar function in mainlobe, while realizing communication in the sidelobe was presented in [35]. The essence of this method is to use time-modulated array techniques to control the instantaneous pattern by

using either a sparse time-modulated array (STMA) or phase-only synthesis time-modulated array (POSTMA). Both STMA and POSTMA offer the ability to introduce variations in the SLL toward a certain spatial direction [35]. STMA is simple to implement by switching the transmit antennas on and off. However, because the number of antennas that need to be switched on is constant, it is not capable of achieving a large number of distinct SLLs. While POSTMA offers enhanced capability to achieve more SLLs, but requires computationally demanding nonlinear optimization. The ability to control the instantaneous pattern sidelobe and to achieve a number of distinct SLLs toward a certain direction has motivated the use of AM to embed information as a secondary communication function to the primary function of the time-modulated array [35].

In [51] the authors presented a PSK-based-method system where the same transmit waveforms are used for both functions. In this scheme, the number of the orthogonal waveforms is given from the communication symbols plus one waveform where it is taken as a common reference to all other waveforms. Each communication symbol is embedded in the phase difference between two signal components associated with each waveform and, then proceeds to estimate and decode the embedded communication symbols. In [2] the information is embedded by sidelobe ASK method and waveform diversity to feed distinct communication streams to multiple communication users located in different sidelobe directions.

4.2.3 Joint radar and communication system based on OFDM

Orthogonal Frequency Division Multiplexing is a frequency multiplexing technique based on the transmission of multiple parallel data streams on orthogonal frequency sub carriers. It is not a modulation, but a multiplexing method based on sub carriers that can be modulated with an arbitrary digital modulator such as PSK.

In the radar community, multi carrier signals recently were attracted interest in the context of frequency agile waveforms, due to their ability to both occupy

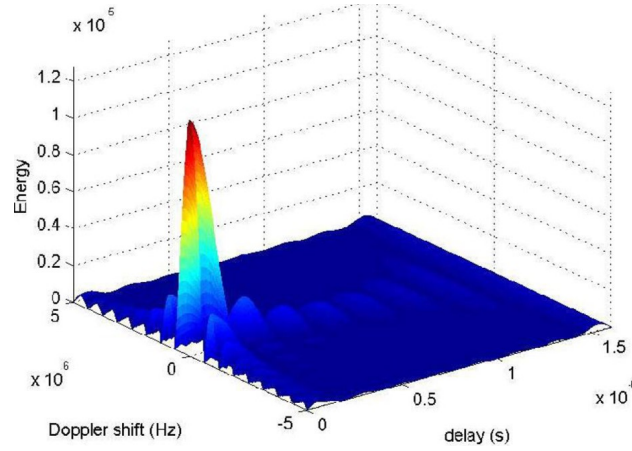


Fig. 4.3. Ambiguity function of a joint radar and communication system based on OFDM [39].

flexibly the available spectral resources and be robust against jammers [31]. Preliminary investigations on the suitability of multi carrier waveforms for radar applications were published in 2000 by Levanon [31], [74]. The idea of introducing information into the multi carrier signal, by phase modulation of the sub carriers and realizing an efficient double use of the spectrum, appears only much later in [33], [131].

Stable performance in multipath fading and relative simple synchronization makes OFDM advantageous for joint radar and communication system [32]. In [30] the system first transmits OFDM sub carriers for radar processing followed by sub carriers enabling radar and communication functionalities. The receiver first estimates the target parameters from the sub carriers dedicated to radar; these parameters then determine the channel for the communication link. The communication data is then extracted, thereby enabling the use of all the carriers for improving the range estimation. The main drawback is that the lack degrees of freedom leading to multiplexing of sub carriers between radar and communications, thus this prevents the full exploiting of all the sub carriers for communication and radar functions.

OFDM based radar has some interesting properties. First, OFDM signals are reported to be advantageous regarding Doppler shift [39]. In Fig. 4.3 the AF given in [39] is reported. As it can be seen that the range-Doppler coupling is not present, which allows for independent and unambiguous range and

Doppler processing. However, in the range profile high sidelobes are present as shown in Fig. 4.4. Additionally, the correlation depends on the data, which makes impossible to guarantee a reliable system performance while transmitting arbitrary information. In order to overcome these disadvantages, in [130] a processing that operates directly on the modulation symbols instead of the baseband was presented. With this processing was demonstrated that two major advantages are achieved. First, the performance of the radar operation is completely independent from the transmitted information. Second, a superior dynamic range compared to the classical correlation based processing is achieved, which is only limited by the sidelobes of the Fourier transform. The range profile shown in Fig. 4.5 is obtained when the processing described in [130] is carried out. Comparing Fig. 4.4 with Fig. 4.5 we can see that sidelobes caused by auto-correlation of the transmitted information do not occur and a windowing function can be applied. In [129] a very similar concept, in the modulation symbol domain, was applied for Doppler estimation. Fig. 4.6 shows the spectrum when two targets are present as we can see two targets are separately. In the FFT processing a Hamming window was applied consequently a high dynamic range is achieved and the sidelobes are well suppressed.

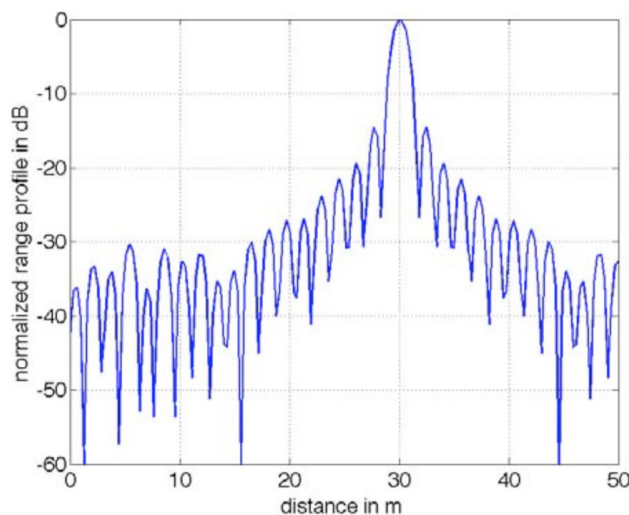


Fig. 4.4. Range profile calculated with the classical correlation based approach [130].

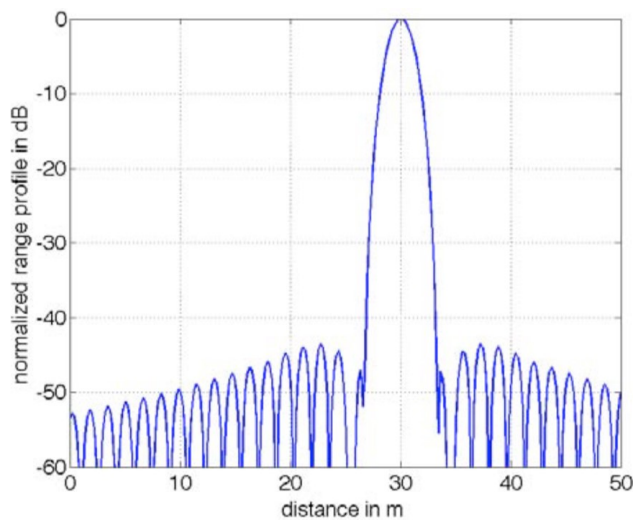


Fig. 4.5. Range profile calculated with the approach proposed in [130].

In [132], it was addressed how both estimation can be combined into a two-dimensional estimation in the modulation symbol domain. The architecture of an OFDM system is shown in Fig. 4.7. As we can see the binary user data is divided into parallel stream, and mapped onto complex valued PSK symbols. By a block-wise inverse FFT and a subsequent parallel-to-serial conversion. In the receiver the same steps are carried out in the inverse order. On the received side a fast Fourier transform is applied and the modulation

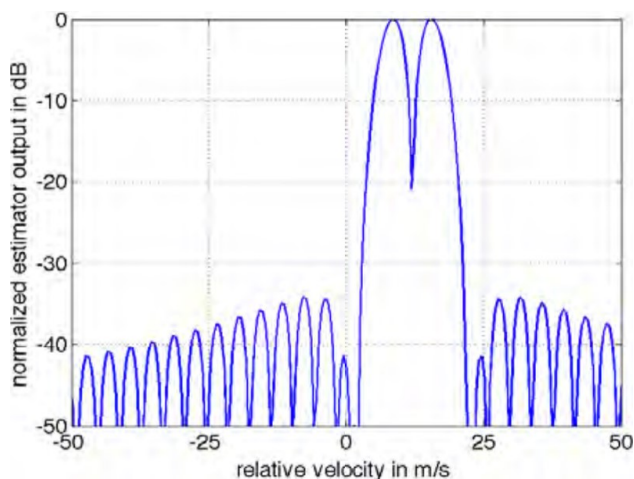


Fig. 4.6. Spectrum when two target at the same distance, but with two different velocities are present [129].

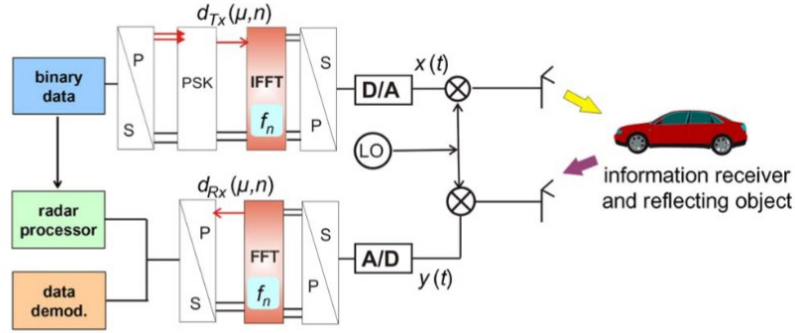


Fig. 4.7. Block scheme of the OFDM system architecture [132].

symbols are recovered. The basis of the algorithm to calculate the range and Doppler is the received modulation symbol matrix \mathbf{D}_{RX} . The complete processing consists of at least three steps. In the first step, the element-wise complex division is performed for all matrix elements. In order to reduce the levels of the sidelobes introduced by the subsequent Fourier transforms a windowing function is applied to \mathbf{D}_{div} . Then, in the second required step, the FFT of every row of \mathbf{D}_{div} is computed. Finally, in the third step, the inverse FFT is calculated for every column of the matrix resulting from the previous step. The resulting matrix represents a range-Doppler map. In the proposed algorithm all steps are linear operation, which guarantees that the same approach will work for an unlimited number of targets with different distance and relative velocities.

Additionally, another major drawback of OFDM is the high Peak-to-Average Power Ratio (PAPR), where it is defined as the ratio of the peak power to the average power of a signal. The reason for high PAPR is due to some signal values of OFDM much higher than the average. The PAPR introduces nonlinear distortions which subsequently creates intermodulation between different carriers with additional interference. These distortions lead to an increase of the communication performance in terms of BER. Several techniques such as clipping, recursive clipping, filtering and windowing were developed to address the PAPR issue [122]. In [29] the mitigation of this issue was achieved through the exploitation of the unused sub carriers and the phase information of pilot tones in the OFDM systems to optimize the signal energy

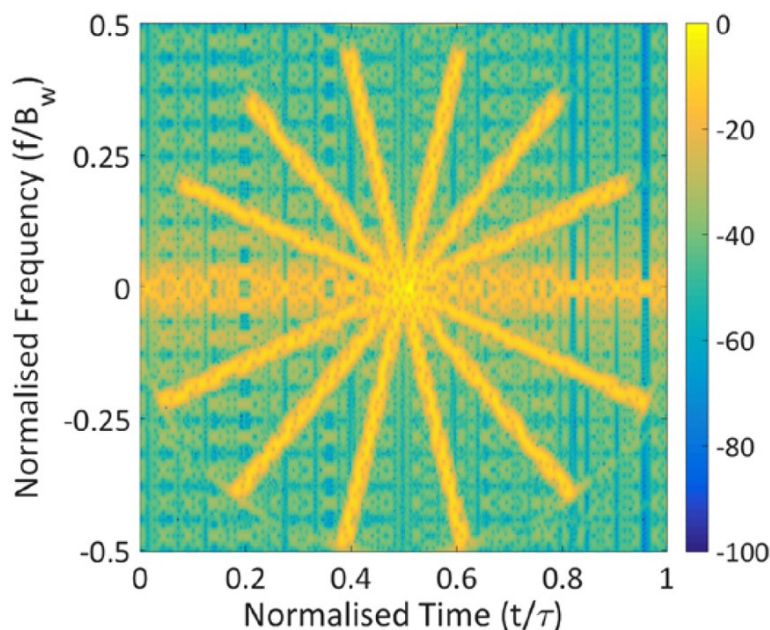


Fig. 4.8. Spectrogram of a FrFT CoRadar waveform with 7 sub carriers [42].

distribution and therefore reduce the high peaks. The proposed approach [29] requires no side information to be transmitted to the receiver and has a lower BER compared with the clipping, recursive clipping, filtering and windowing. The most popular communication signal, for joint radar and communication in automotive environment is OFDM as demonstrated in multiple works based on IEEE 802.11p standard [109]. Other communications waveforms proposed for automotive joint radar and communication system include spread spectrum [138], noise-OFDM [133], multiple encoded waveform [10], and 802.11ad standard [87],[70],[83]. But their performance is limited either by the respective communication protocols, intervehicular synchronization or infeasible hardware implementations. In [110] the OFDM signal based on the standard IEEE 802.11p for V2V communication was used.

4.2.4 Joint radar and communication system based on Orthogonal Time Frequency Space (OTFS)

An Orthogonal Time Frequency Space (OTFS) is proposed to provide significant error performance advantages over OFDM over delay-Doppler channels with a wide range of Doppler frequencies [48],[36], [106]. In [107] authors were shown that OFTS-based radar processing provides benefits for improved radar capability, such as longer range, faster tracking rate, as well as larger Doppler frequency estimation compared to the popular OFDM. In [107] it was also shown that OFTS-based radar result be a promising robust technique to detect the long range and high velocity targets.

4.2.5 Joint radar and communication system based on fractional Fourier transform (FrFT)

A novel concept of joint radar and communication system, called Co-Radar, based on the FrFT was presented in [41]. Similar to the OFDM, the proposed multiplexing scheme embeds data information to be sent into chirp sub carriers with different time-frequency rates. In [41] the authors showed that the proposed system is fully scalable, since it is easily adaptable to the available bandwidth, the length of the pulse, the conditions of the channel. Additionally, in [41] it was demonstrated that the radar performance of the generated waveform are similar to an LFM pulse with same duration and bandwidth. The spectrogram of the proposed FrFT Co-Radar waveform is illustrated in Fig. 4.8. As we can see each sub carriers is rotated by a specific angle, driven by the order of the FrFT, of a phase modulated signal.

In [43], an experimental validation of the FrFT based Co-Radar system was presented. The system was implemented on a Software Define Radio (SDR) device and its performance was demonstrated in a controlled laboratory environment. Communication performance is shown with solid lines in Fig. 4.9, in terms of BER averaged over 10 realisations against $\text{SNR}_{\text{comms}}$. As we can see that as the $\text{SNR}_{\text{comms}}$ increases, the BER decreases. However, when $\text{SNR}_{\text{comms}}$ is greater than 15 dB, the simulated and experimental BER are

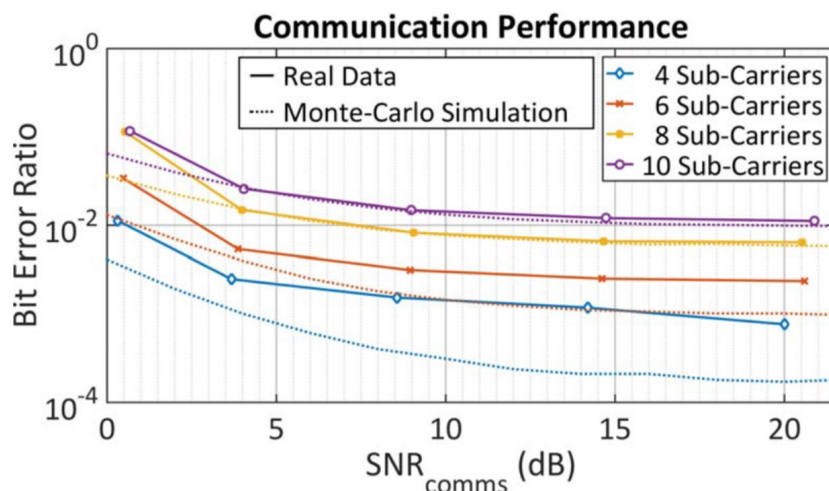


Fig. 4.9. Communication performance on varying $\text{SNR}_{\text{comms}}$ and for different number of chirp sub carriers [43].

very close. The BER was obtained when no error detection and correction techniques was used. Additionally, in Fig. 4.10 the spectrograms when FrFT based Co-Radar pulses with four sub carriers and for two different SNR radar are illustrated. In both cases the Doppler and micro-Doppler (mD) signature of the person walking towards and away from the radar is clearly visible.

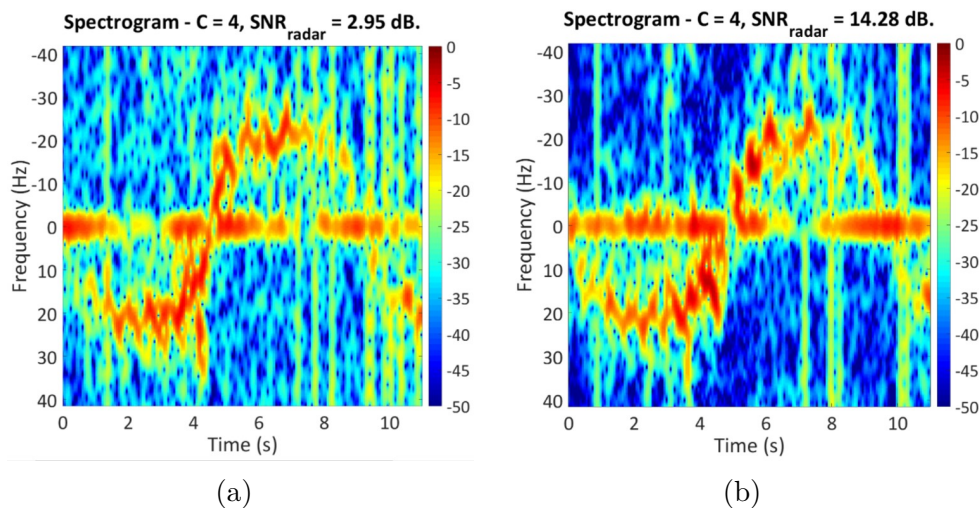


Fig. 4.10. Spectrogram obtained from FrFT based Co-Radar pulses with four sub carriers and different SNR radar, 4.10a SNR is set at 2.95 dB, 2.11b the SNR is set at 14.28 dB [43].

Table 4.2: Radar performance parameters [42]

	FrFT opt.		OFDM opt.		LFM
	FrFT	OFDM	FrFT	OFDM	
Norm ran. res.	1.46	1.01	1.48	1.03	1.01
Norm Dop. res.	$1.3 \cdot 10^{-4}$	$0.9 \cdot 10^{-4}$	$1.31 \cdot 10^{-4}$	$0.9 \cdot 10^{-4}$	$0.89 \cdot 10^{-4}$
Zero-Dop. SLL	-16.6 dB	-4.6 dB	-16.5 dB	-9.9 dB	-13.3 dB
Zero-del. SLL	-16.6 dB	-13.3 dB	-16.5 dB	-13.3 dB	-13.3 dB

Radar performance of the system proposed in [42] was assessed and compared with a joint radar and communication system based on OFDM, that presents a comparable bit rate. The radar performance in terms of resolution and SLL are listed in Table 4.2, showed that the FrFT waveform presents performance closer to an LFM pulse than OFDM waveform. The main advantages of the system presented in [42] are if two chirp signals are completely overlap in time and frequency they can be separable in the FrFT domain, the system is designed by taking into account the radar requirements, such as range and Doppler resolution, and desired SSL, and the possibility to reach data rates while maintaining good radar performance compared to an LFM pulse that occupies the same bandwidth. However the main disadvantage is that at the receiver is necessary to know with precision where the received signal starts, otherwise it is not possible demodulated the data. Additionally the framework proposed in [42] does not fit the standards of automotive radar and communication operation as it employs pulsed waveform meaning that high peak power is needed in order to achieve reasonable detection range.

4.3 Mutual Radar Interference mitigation techniques

In an automotive environment, the widespread use of the radar, where different users may share the same bandwidth at the same time, leads to an increase of mutual interference. Such interference increases the receiver's noise floor and can lead to problems such ghost targets or/and target masking.

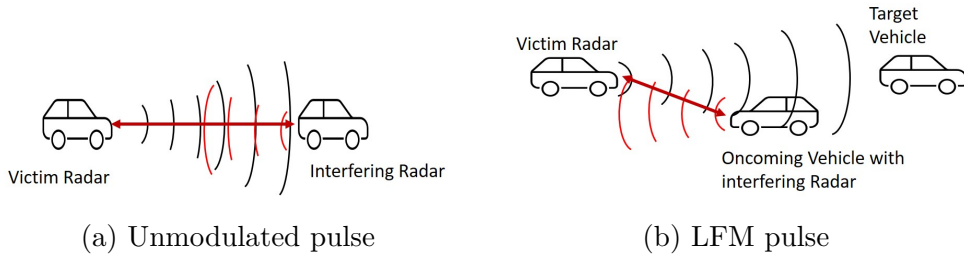


Fig. 4.11. Example interference scenarios for automotive radar.

This is of particular importance for targets with low RCS that cannot be detected reliably. In multi user scenarios, as in an automotive environment, where each user uses a joint radar and communication system both radar and communication performance are degraded. For the radar performance, the communication signal sent from other users is considered as interference, which leads to a degradation of the detection performance. While for the communication performance, the radar signal is considered as interference which leads to a degradation of the BER.

In Fig. 4.11 two scenarios where in each, a vehicle with an interfering radar is creating interference for a victim radar are shown. Fig. 4.11a shows a scenario where the target is also transmitting a radar signal, hence it is a source of interference. While Fig. 4.11b shows a scenario where the target is not transmitting a radar signal, but the interfering radar is represented by another vehicle that is approaching at the main radar.

Different countermeasures were proposed to overcome automotive radar interference. An European funding project, MOre Safety for All by Radar Interference Mitigation (MOSARIM) was conducted to investigate the possible interference mitigation methods for automotive radars [71]. In this project, interference mitigation methods were classified into five domains as followings: Polarization, Time domain, Frequency domain, Space domain, Strategic approach.

- Polarization: In [62], the transmitting antenna was designed in Right Hand Circular Polarized (RHCP) while the receiving antenna was in Left Hand Circular Polarized (LHCP). Thus, interference from aggressor radar's transmitting antenna would be suppressed by the victim radar's

receiving antenna. At the same time, the real target echo was received unhindered due to its polarization change to LHCP on account of the boundary conditions of electromagnetic fields on the surface of the target. Only the direct Line of Sight (LOS) propagation is taken into account and multiple reflection at nearby obstacles are neglected. Reflections on ground surface and other obstacles may turn the polarization of the transmitted wave. So the true cross-polarization interference mitigation effect may be reduced in the presence of obstacle reflection.

- Time domain: the interference signal is processing in time domain. In [90], [139], and [65] the position of interference was found in the time domain, and a window based method was used to remove the interference. In [6] a filter to differentiate the transmitted radar signal from the interference signal was proposed. In this algorithm the received signal is iteratively processed until the desired signal is extracted. The main drawback is that this algorithm is not recommendable in real time scenarios due to its computational complexity. In [140] the interference was removed by using Morphological Component Analysis (MCA). However, this method fails when the slope of the transmitted LFM signal and the slope of the interference are the same.
- Frequency domain: In [7] the interference was avoided by changing the transmitting signal's frequency band after detecting the interference's frequency band. In [89], the SNR was improved by interpolating the beat frequency in the Short Time Fourier Transform (STFT) domain. In [68], [150], and [157] the orthogonality property of random coded LFM sequence leads to inherent interference immunity. The advantages of these methods are very simple implantation and low complexity.
- Space domain: the adaptive beamforming method was presented in In [5], [38], and [103] to mitigate the interference from sidelobes.
- Strategic approach In [67], a control centrer was set-up to receive location/speed information from all the radars, and dispatch waveform parameters to each one to avoid the interference among them.

As we can see, those methods which depend on complicated antenna design, more antenna channels, higher Analog-to-Digital Converter (ADC) sampling rate and a control centre are not attractive for the cost sensitive automotive market.

In [64] an interference mitigation method based on adaptive noise canceller was illustrated. Which takes the positive and negative half of FFT as the input of its primary and reference channel. It works on the current and mostly used LFM radar sensors and does not require costly hardware.

In [4] the interference was estimated and then removed from the received signal. This method works well when the power of the interference signal is less than the power of the desired signal.

Additionally, some machine learning techniques were presented in the context of interference detection and classification in [153]. However, no explicit machine learning approach was presented in the context of interference mitigation. In [115] the Neural Networks (NN) based methods for effective mutual interference mitigation and de-noising in the context of automotive radar was presented. Noteworthy is the used of spectrograms from different steps in the range Doppler signal processing as network inputs their suitability to be preprocessed by Convolutional NNs (CNNs).

4.4 Interference mitigation for communication system

In wireless communication the medium is shared by more than one user, consequently strong interference has arisen leading to a degradation of the Quality of Service (QoS). Reaction to mutual interference is the heart of the shared-spectrum problem, and traditional approaches to combating wireless interference start with channel measurement and/or prediction, followed by an appropriate selection of modulation methods and signal processing algorithms for reliable transmission. The methods used to deal with interference can be loosely grouped into three categories:

- Build a fence

- Use only what you need (efficient modulation power control)
- Grin and bear it (signal processing at the receiver)

Examples of the first item are legion, while examples of the last two items include single-sideband amplitude modulation, frequency modulation with preemphasis at the transmitter and deemphasis at the receiver, power control in cellular wireless systems [148], CDMA coupled to sophisticated signal processing algorithms for interference mitigation at the receiver.

A class of radios that can be programmed to transmit almost arbitrary receiver types is called software radios [121]-[120]. As opposed to traditional radios, which are difficult to modify once a modulation method has been chosen, one can now imagine programming transceivers to use more effective modulation methods. In future, wireless system will be able to choose modulation methods that avoid ambient interference as overpowering it with increased transmission power, or mitigating it with receiver signal processing.

Interference avoidance is the term used for adaptive modulation methods where individual users employ their signal energy in places where interference is weak. Such methods have been shown to optimize shared use. Iterative interference avoidance algorithms yield optimal waveforms that maximize the SINR for all users while maximizing the sum of rates at which all users can reliably transmit information. This concept the first time was introduced in the context of DS-CDMA systems [100] and Minimum Mean-Square Error (MMSE) receivers, but was subsequently developed in a general signal space [52] framework [104] which makes them applicable to a wide variety of communication scenarios. Related methods for transmitter and receiver adaptation have also been used in the CDMA context for asynchronous systems [102].

4.5 Conclusion

In this chapter, the problem of the spectrum sharing between the radar and communication system has been introduced. In literature, different schemes have been introduced allowing both functions to use the same hardware and the same spectrum at the same time. A summary of the different joint radar and communication techniques described in this chapter, is given in Table 4.3.

Table 4.3: Summary of different joint radar and communication systems.

Property	Spread Spectrum techniques	Phased array	OFDM	FrFT
Array of antenna	x	✓	x	x
Orthogonality between radar and communication waveform	✓	x	x	x
Sub-carriers	x	x	✓	✓
Pulse waveform	✓	x	x	✓
Radar performance similar to an LFM waveform	x	x	x	✓

Due to the fact that in an automotive radar environment the LFM waveform is widely used. As we can see from Table 4.3, the radar performance similar to an LFM waveform is obtained using the Co-Radar framework. However, in this framework a pulse radar is transmitted, consequently, it does not fit for an automotive environment.

In a joint radar and communication system based on the Spread Spectrum techniques, the transmitted signal is given compounding the radar and communication signals. Thus means that the transmitter signal is generated by using two different hardware systems. On the received side, two functions can be applied only after two signals are separated. As, we can realise this waveform is generated using a complex hardware. However, in an automotive environment a complex hardware cannot be used, due to the issues of the space, power etc.

In Dual radar communication function the radar signal is transmitted using the main lobe of the antenna, while the data are embedded into the side lobes. In this scenario, the signal is transmitted using an array of the antenna. In an automotive scenario, it is not easy to have more than one antenna.

A joint radar and communication system, widely used in automotive environment, is based on OFDM. As it has been shown, the main advantage is that the range-Doppler coupling is not present, so the range and Doppler frequency can be estimated independently. However, the radar processing has to be applied after that the data information are removed from the received signal. In other words the radar processing has to be applied after the communication receiver. In addition, in this system at each user is assigned a portion of the bandwidth, thus means that in multi user scenarios the bandwidth is split between the different users. As the range resolution depends on the bandwidth, consequently, it depends on the number of the users that shares the same frequency at the same time. In order to avoid this two issues, in literature a joint radar and communication system, called co-Radar, based on the FrFT has been proposed. As the radar performance of the proposed system is similar to an LFM, due to the fact that in this framework a pulse radar is transmitted, it does not fit for an automotive scenario. In the proposed system, in order to increase the bit rate the fractional multiplexing technique has been used. In an automotive environment, the fractional multiplexing techniques will be used to allocate more than one user in the same frequency band at the same time.

In the second part of the chapter, the problem of the interference mitigation has been presented. This problem is evident due to the fact that more than one user needs to share the same channel at the same time. As it has been illustrated the interference can be mitigated transmitting the appropriate signals or applying a processing on the received signal. In a joint radar and communication system the radar is able to recover the data information sent from other users, consequently the interference can be reconstructed and, then, mitigated from the received signal.

In the first part of the chapter, the issue of the separation between radar and communication functions has been presented. In order to solve this issue an overview of the different joint radar and communication system presented in literature has been given. In the previous chapter, we have identified that a FCLFM waveform fits for an automotive environment, due to its capacity to estimate the range and Doppler frequency without ambiguity, even in multi target scenarios. In addition, the radar parameters are estimated ap-

plying the FFT twice. However, the proposed joint radar and communication frameworks do not share the features of an LFM waveform. Owing to it in chapter 5, a new joint radar and communication system based on the FrFT will be presented. The aim of this framework is to generate a waveform that share the LFM feature and at the same time a communication link is also achieved. In order to do it, the FrFT will be used to embed the data information into radar waveform. In addition in the proposed framework the multiplexing fraction technique will be used to allow more users to share the same frequency band at the same time.

In last part of this chapter, the issue of the mutual interference has been presented and described. In a joint radar and communication system, for the radar performance the communication signal is considered as an interference. Due to the fact that in this framework the radar is able to reconstruct the received communication signal and then a subtraction between the received signal and reconstructed one can be carried out. In chapter 7 two new frameworks to mitigate the mutual radar interference will be presented. They will be based on coherent and non-coherent subtraction. Moreover, the issue of how to mitigate the mutual communication interference is not the goal of this thesis.

Chapter 5

Joint Radar and Communication system for automotive environment

In an automotive environment, radar and communication systems are both used to improve pedestrian and driver safety. As described in Section 4.1, the separation of these two systems is a waste of the similar hardware such as antennas, digital signal processing units, transceiver, furthermore, it makes hard to avoid the interference between two systems and to use efficiently the spectrum. This has recently spurred extensive efforts towards devising a coexisting solution for simultaneously operations for radar target illuminations and wireless service using the same bandwidth as described in Section 4.2. In chapter 4 an overview of the different frameworks to allow a joint radar and communication system have been presented. However, there are not waveforms allowing a joint radar and communication system that share an LFM characteristic and at the same time fits for an automotive scenarios. Due to the fact that in an automotive environment an LFM waveform is widely used due to its capacity to estimate range and Doppler simultaneously and in unambiguous manner even in multi target scenarios. The aim of this chapter is to present a new joint radar and communication system based on the FrFT. The FrFT is used to obtain a radar waveform sharing LFM characteristic and at the same time a communication link is also achieved.

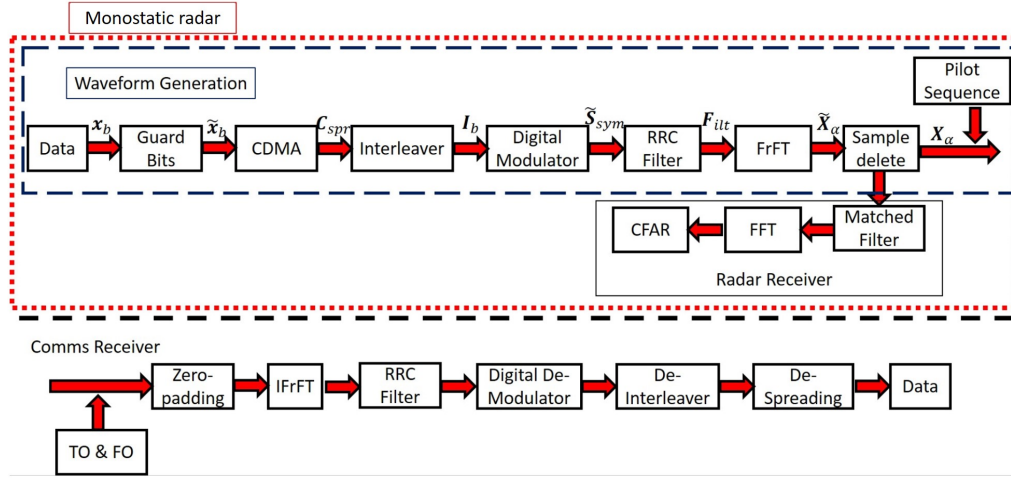


Fig. 5.1. Block diagram of (top) monostatic radar and (bottom) the Communication of the FrFT based on a joint radar communication basic configuration.

Then the analytical model of the proposed waveform, and its PSD are also derived when two encoding schemes as BFSK and BPSK are used. The remainder of the chapter is organized as follows. In Section 5.1 the proposed FrFT joint radar and communication framework is introduced. Section 5.1.2 derives the mathematical model of the proposed automotive radar waveform for the cases in which a BFSK or a BPSK encoding is used. To complete the characterisation the Power Spectral Density formulation of the two family of waveforms is derived.

5.1 Proposed framework design

In this Section, the monostatic radar for the proposed joint radar and communication system based on FrFT for automotive applications is presented. The waveform generation process is illustrated at the top of Fig. 5.1. Starting from the data to be transmitted, let \mathbf{x}_b be a vector that contains data information, which can be written as

$$\mathbf{x}_b = [x(0), x(1), \dots, x(N_b - 1)] \quad (5.1)$$

where $x(n) \in \{0, 1\}$ and N_b is the number of bits. In the Guard Bits block, G_g random bits are added at the end of the information bits in order to compensate the group of the delay introduction from the Root Raised Cosine (RRC) filter [80]. The resulting sequence is

$$\tilde{\mathbf{x}}_b = \mathbf{x}_b \hat{\ } \tilde{\mathbf{x}}_g \quad (5.2)$$

where $\tilde{\mathbf{x}}_g$ contains G_g random bits generated by Guard Bits block, while $(\cdot) \hat{\ } (\cdot)$ indicates the concatenation operation. Then, a CDMA is proposed to ensure low level of mutual interference between different users accessing at the same channel. When a CDMA is applied the raw data are spread by pseudorandom (PR) code sequence. In the proposed system, a Pseudo Noise sequence is selected. In this stage, each user spreads its raw data with a specific sequence by L_p bits, the resulting sequence is

$$\begin{aligned} \mathbf{C}_{spr} &= \tilde{\mathbf{x}}_b \mathbf{P} = (\mathbf{x}_b \mathbf{P}) \hat{\ } (\tilde{\mathbf{x}}_g \mathbf{P}) \\ &= (\mathbf{x}_{bL_p}) \hat{\ } (\tilde{\mathbf{x}}_{gL_p}) \end{aligned} \quad (5.3)$$

where $\mathbf{P} = [P(0), P(1), \dots, P(L_p - 1)]$ is the PN vector given by L_p bits. The resulting vector \mathbf{C}_{spr} is given by $(N_b + G_g)L_p$ bits. In multi user scenarios, each user modulates its data with different PN sequence that are orthogonal with each other. The Interleaver block is applied to spread a burst of errors across the entire sequence. It is applied only on the data information vector \mathbf{x}_{bL_p} . The main function of the interleaver in transmission is to alter the order of the input bits sequence. Consequently, the sequence obtained after the interleaver, $\tilde{\mathbf{x}}_{bL_p}$ has all the elements of \mathbf{x}_{bL_p} , but in a different order. The sequence at the output of the interleaver block is:

$$\mathbf{I}_b = (\tilde{\mathbf{x}}_{bL_p}) \hat{\ } (\mathbf{x}_{gL_p}) \quad (5.4)$$

At this point, the output of the interleaver is given as input to the Digital Modulation, where the bits are mapped in symbols. In the proposed framework, two encoding schemes as BFSK or BPSK are proposed.

A BFSK encoding scheme is the simplest form of the Frequency-Shift Keying encoding. FSK scheme is the frequency encoding in which digital information

$x(n)$ is transmitted through the discrete frequency change of a carrier wave. BFSK uses two discrete frequencies to transmit binary information. With this scheme, the “1” is called the mark frequency, f_M , and the “0” is called the space frequency, f_S . The sequence of symbols is:

$$\tilde{S}_{sym_{BFSK}}(t) = \sum_{n=1}^{(N_b+G_g)L_p} e^{(j2\pi f_{\mathbf{I}_{b,n}} t)} \hat{s}(t_n) \quad (5.5)$$

where:

$$f_{\mathbf{I}_{b,n}} = \begin{cases} f_S & \text{if } \mathbf{I}_{b,n} = 0 \quad n \in [1, N_b L_p] \\ f_M & \text{if } \mathbf{I}_{b,n} = 1 \quad n \in [1, N_b L_p] \end{cases} \quad (5.6)$$

and $\hat{s}(t_n)$ is a square pulse centred in t_n defined as:

$$\hat{s}(t_n) = \begin{cases} 1 & t_n \left(\frac{2n-1}{2}\right) \leq t \leq t_n \left(\frac{2n+1}{2}\right) \quad n \in [1, N_b L_p] \\ 0 & \text{otherwise} \end{cases} \quad (5.7)$$

On the other hand, BPSK encoding scheme is the simplest form of PSK. It uses two phases which are separated by π . The sequence of symbols obtained after the BPSK encoding scheme is expressed as:

$$\tilde{S}_{sym_{BPSK}}(t) = \sum_{n=1}^{(N_b+G_g)L_p} e^{(j2\pi \mathbf{I}_{b,n})} \hat{s}(t_n) \quad (5.8)$$

where

$$e^{(j2\pi \mathbf{I}_{b,n})} = \begin{cases} 1 & \text{if } \mathbf{I}_{b,n} = 0 \quad n \in [1, N_b L_p] \\ 0 & \text{if } \mathbf{I}_{b,n} = 1 \quad n \in [1, N_b L_p] \end{cases} \quad (5.9)$$

while $\hat{s}(t_n)$ is given by (5.7). After digital modulation the RRC filter is applied. The filter is used to minimise the Inter-Symbol Interference (ISI) that may be caused by the channel. The RRC filter is characterised by the following parameters: Roll off Factor β which determines the bandwidth of the spectrum and Filter Span in Symbol which truncates the impulse response to a S value. For efficiency reasons, it is implemented as a multirate filter that up-samples the output by a factor R_s . The sequence obtained after that

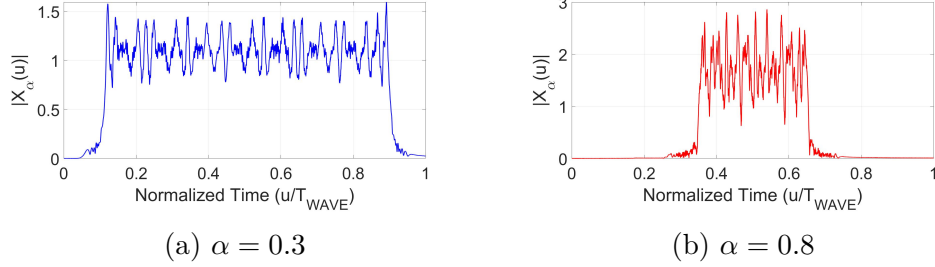


Fig. 5.2. Envelope of the signal with two different orders of the FrFT and when a BFSK encoding is used, in 5.2a α is set at 0.3 while in 5.2b the order of the FrFT is set at 0.8.

the RRC filter has been applied on the modulation symbols is

$$\mathbf{F}_{ilt}(t) = \tilde{S}_{sym}(t) \circ \mathbf{h}_{RRC}(t) \quad (5.10)$$

where $\mathbf{h}_{RRC}(t)$ is the time response of the RRC filter [137].

The length of the sequence depends on the encoding scheme that has been used: for the BFSK the length is $U_{BFSK} = (N_b + G_g)L_p N_s R_s$ where N_s is the number of samples per symbol, while the number of samples when the BPSK is used is then $U_{BPSK} = (N_b + G_g)L_p R_s/2$.

As we can see the baseband signal \mathbf{F}_{ilt} has been obtained by applying only typical communication operations.

The FrFT with a specific order α is then applied on the baseband signal, the resulting waveform is

$$\tilde{\mathbf{X}}_\alpha(u) = \tilde{\mathfrak{F}}^\alpha(\mathbf{F}_{ilt}(t)) \quad (5.11)$$

where $\tilde{\mathfrak{F}}^\alpha(\cdot)$ denotes the fast discrete approximation of FrFT (see Section 3.9) with a fractional order α . In this step, the signal is mapped into a pulse in the time-frequency domain. In this framework, the fractional order division multiple access can be implemented assigning a specific order of the FrFT to each user. The time duration of the waveform after the FrFT is

$$\begin{aligned} \tilde{T}_{WAVE_{BFSK}} &= U_{BFSK}/f_s \\ \tilde{T}_{WAVE_{BPSK}} &= U_{BPSK}/f_s \end{aligned} \quad (5.12)$$

In Fig. 5.2 two envelopes obtained applying the FrFT on BFSK encoding

scheme are illustrated. These two envelopes are obtained when on the same baseband signal \mathbf{F}_{ilt} two different orders of the FrFT are applied. In Fig. 5.2a the envelope obtained when the order of the FrFT is set at 0.3 is shown, while the envelope when α is set at 0.8 is illustrated in Fig. 5.2b. Comparing Fig. 5.2a with Fig. 5.2b, it can be seen that when α moves from 0 to 1 the energy of the signal is concentrated in the middle of the waveform $u = \tilde{T}_{WAVE}/2$, and very low intensity samples appear at the beginning and end of the pulse. This is due to the fact that when the order of the FrFT moves from 0 to 1 the time duration decreases while the bandwidth increases. As we can see from Fig. 5.2 after that the FrFT is applied a pulse waveform is obtained. In order to allow continuous operations in the Sample Delete stage the threshold is applied to remove the low energy samples that appear at the beginning and the end of the pulse. The threshold is calculated as

$$T_{FrFT} = \max(0.1|\tilde{\mathbf{X}}_{\alpha}|^2) \quad (5.13)$$

and it is applied on the vector $|\tilde{\mathbf{X}}_{\alpha}|^2$. To better understand of this process, the vector $\tilde{\mathbf{X}}_{\alpha}$ obtained after the FrFT is given by U_{FrFT} samples. As we can see from Fig. 5.2 the intensity of the first $U_{FrFT,beg}$ and last $U_{FrFT,las}$ samples is very low and the information are not embedded in that samples, consequently, they can be removed. Thus, the number of the samples obtained after the samples removal is given by

$$U_{\alpha} = U_{FrFT} - (U_{FrFT,beg} + U_{FrFT,las}) \quad (5.14)$$

The time duration of the waveform is $T_{WAVE} = U_{\alpha}/f_s$. The signal obtained after the sample delete is indicated with \mathbf{X}_{α} . When $U_{BFSK,BPSK}$ is fixed, the number of the samples after the delete process U_{α} depends only on the order of the FrFT that has been used to embed data information into radar waveform. In multi user scenarios, the time duration of the CPI changes from user to user. On the receiver side, in order to apply the communication function is necessary to know the duration of the CPI. This issue is solved, because after the synchronization the receiver knows the order of the FrFT that was used by the transmitter and consequently the duration of the CPI is known as well.

The time-frequency profile of a CPI comprising five consecutive waveforms obtained with the proposed framework is shown in Fig. 5.3. As it can be seen the CPI has a time-frequency profile similar to the one of a FCLFM waveform presented in Section 2.2.10. Compared to FCLFM waveforms, however in the proposed waveform, data information are also embedded allowing joint radar and communication operations. A representation in time domain of absolute value of the signal is given in Fig. 5.4.

In order to enhance the radar performance, on the radar receiver side a coherent integration of N_{wave} waveforms is carried out. This means that in every CPI the same bits of information are embedded, and the data change from CPI to CPI.

On the receiver side, in order to perform the IFrFT is necessary to know

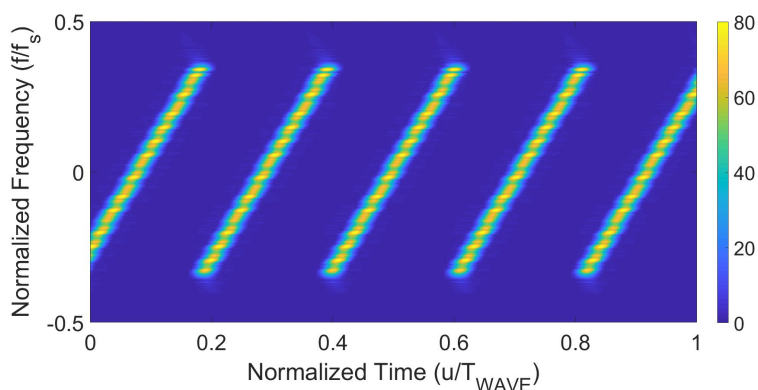


Fig. 5.3. Spectrograms of a Coherent Processing Interval.

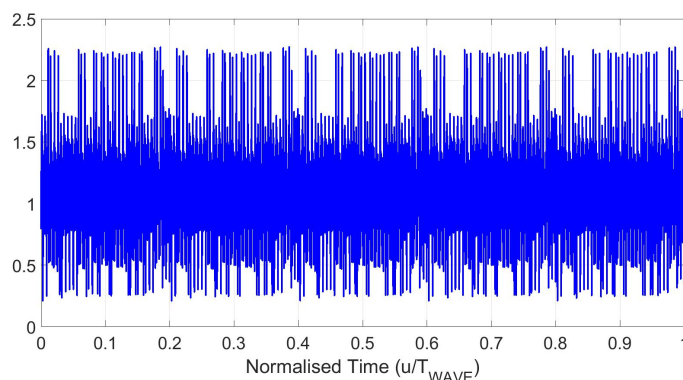


Fig. 5.4. Representation of the waveform in time domain.

with exactly precision the delay of the received waveform. In order to solve this issue, a pilot sequence is also transmitted. The pilot sequence is obtained by applying on baseband signal, with amplitude equal to one and zero phase, two orders of the FrFT, α and $-\alpha$, and then sum the two signals. Such pilots can be used by the communication receiver to estimate the time and frequency offset of the received signal as described in [156]. This sequence is placed at beginning of the CPI and it is transmitted every χ consecutive CPI. In multi user scenarios, for the communication receiver, it is also necessary to discriminate the data sent from different users. To achieve this, each user generates a pilot sequence with the same order α used to map the data information into the radar waveform.

For the radar part, following matched filter and Doppler processing, standard detection techniques, such as Cell-averaging CFAR (CA-CFAR) [113], can be applied to detect the targets. As illustrated in Fig. 5.1 the radar processing is applied after that the pilot sequence has been removed.

5.1.1 Communication Receiver

The block diagram of the communication receiver is illustrated at the bottom of Fig. 5.1. The synchronization is performed by applying on the pilot sequence two FrFTs of order $Q_1 = 1 - \alpha$ and $Q_2 = -(1 - \alpha)$. In multi user scenarios, when the appropriate α is used the frequency offset and time offset can be estimated using the FrFT outputs as described in [156]. While when there is an order mismatch the output will appear flat, similar to the noise. Thus the synchronization is not performed. As the radar processing cannot be applied on the part of the signal occupied by the pilot, the pilot sequence should not be repeated in every CPI. On the other hand, good synchronization cannot be achieved if the pilot is not transmitted regularly enough. Consequently, the χ has to be chosen taking into account these two considerations.

After the synchronization the order of the FrFT used to rotate the signal in time frequency domain is known, consequently the duration of the CPI is known as well. Thus, after the synchronization the received signal can be rotated to baseband and the waveform can be demodulated. The length of

the input signal to the IFrFT must be equal to the length of the signal after the FrFT in transmission. For this reason, a zero-padding is applied at the beginning and the end of the received signal. The number of the zeros to add at the beginning and the end of the pulse depends only on the order of the FrFT used in transmission. So after the synchronisation the number of zeros that need to added are known. After the zero padding, the IFrFT is performed with the same order of the FrFT that was used in transmission. The sequence is then passed through an RRC filter, which also down-samples the waveform by a factor of R_s . The digital demodulator translates the symbol in a sequence $N_b L_p$ bits, according to the employed coding. At this point, the de-interleaver performs the inverse of the interleaver. A despreading is applied to the received signal, using exactly the same code that was used in transmission and adds up all the values over each bit period. Due to the fact that at each order of the FrFT is associated a different PN code sequence. Thus, when the order of the FrFT is known, the PN code used in transmission is known as well. After this process the integrated functions $M_{IF}(n)$ are obtained. Finally, the decision rules used are

$$\begin{aligned} \tilde{m}(n) &= 1 \quad \text{if} \quad M_{IF} > 0 \\ \tilde{m}(n) &= -1 \quad \text{if} \quad M_{IF} < 0 \end{aligned} \quad (5.15)$$

Then -1 is coded as zero. Thus, the N_b bits are recovered.

5.1.2 Frequency domain representation

The analytical model of the proposed waveform, and its PSD are derived considering a BFSK and BPSK encoding scheme. In order to obtain a simple mathematical model, the FrFT is applied directly on the symbol sequence obtained from the encoding block. Hence in this analysis, the RRC filter is not applied, consequently, the G_g guard bits are not added. In this consideration (5.5) and (5.8) become, respectively

$$\tilde{S}_{sym_{BFSK}}(t) = \sum_{n=1}^{N_b L_p} e^{j2\pi f_{\hat{x}_n} t} \hat{s}(t_n) \quad (5.16)$$

Table 5.1: Further Properties of the FrFT [94].

Signal	FrFT with angle ϕ
$x(t - \tau)$	$e^{i\pi\tau^2 \sin\phi \cos\phi} e^{-i2\pi u\tau \sin\phi} S_\alpha(u - \tau \cos\phi)$
$e^{j2\pi\xi t} x(t)$	$e^{-i\pi\xi^2 \sin\phi \cos\phi} e^{i2\pi u\xi \cos\phi} S_\alpha(u - \xi \sin\phi)$
$x(-t)$	$S_\alpha(-u)$

$$\tilde{S}_{sym_{BPSK}}(t) = \sum_{n=1}^{N_b L_p} e^{j\pi\hat{x}_n} \hat{s}(t_n) \quad (5.17)$$

where $\hat{x}_n = \tilde{x}_{bL_p, n}$, while $\hat{s}(t_n)$ is given by 5.7, and $f_{\hat{x}_n}$, and $e^{j\pi\hat{x}_n}$ are:

$$f_{\hat{x}_n} = \begin{cases} f_S & \text{if } \hat{x}_n = 0 \quad n \in [1, N_b L_p] \\ f_M & \text{if } \hat{x}_n = 1 \quad n \in [1, N_b L_p] \end{cases} \quad (5.18)$$

$$e^{j\pi\hat{x}_n} = \begin{cases} 1 & \text{if } \hat{x}_n = 0 \quad n \in [1, N_b L_p] \\ -1 & \text{if } \hat{x}_n = 1 \quad n \in [1, N_b L_p] \end{cases} \quad (5.19)$$

The analytical models, and its PSD, for both encoding schemes, are derived using the properties of the FrFT listed in 5.1.

PSD for the BFSK case

The FrFT of (5.16) is calculated applying the linearity property of the FrFT

$$\mathbf{X}_\alpha = \mathfrak{F}^\alpha \left\{ \sum_{n=1}^{N_b L_p} e^{(j2\pi f_{\hat{x}_n} t)} \hat{s}(t_n) \right\} = \sum_{n=1}^{N_b L_p} \mathfrak{F}^\alpha \left\{ e^{(j2\pi f_{\hat{x}_n} t)} \hat{s}(t_n) \right\} \quad (5.20)$$

Using the time shifting property in Table 5.1 the FrFT of a square pulse centred in \tilde{t}_n is given by

$$\mathfrak{F}^\alpha \{ \hat{s}(t_n) \} = e^{j\pi\tilde{t}_n^2 \sin\phi \cos\phi} e^{-j2\pi u\tilde{t}_n \sin\phi} S_\alpha(u - \tilde{t}_n \cos\phi) \quad (5.21)$$

where $S_\alpha(u - \tilde{t}_n \cos \phi)$ is the FrFT of a square pulse centered at $\tilde{t}_n \cos \phi$. The FrFT of a square pulse centred at zero $s(t)$ is defined as, [15]:

$$S_\alpha(u) = D_\alpha e^{-j\pi u^2/B_\alpha} \{ [C(\tilde{u}_+) - C(\tilde{u}_-)] + j \operatorname{sgn}(B_\alpha) [S(\tilde{u}_+) - S(\tilde{u}_-)] \} \quad (5.22)$$

where $D_\alpha = \frac{A_\alpha}{\sqrt{2|B_\alpha|}}$, while $C(x) + jS(x) = \int_0^x e^{j(\pi/2)y^2} dy$ is the Fresnel integral with real part $C(x)$ and imaginary part $S(x)$, and \tilde{u}_\pm is given by:

$$\tilde{u}_\pm = \pm \sqrt{(|B_\alpha|/2)} - \operatorname{sgn}(B_\alpha) \sqrt{2/|B_\alpha|} C_\alpha u \quad (5.23)$$

with A_α , B_α and C_α are defined in Section 3.7, respectively. At this point, $S_\alpha(u - \tilde{t}_n \cos \phi)$ is given by substituting $(u - \tilde{t}_n \cos \phi)$ in (5.22):

$$S_\alpha(u - \tilde{t}_n \cos \phi) = D_\alpha e^{-j\pi(u - \tilde{t}_n \cos \phi)^2/B_\alpha} \{ [C(\hat{u}_+) - C(\hat{u}_-)] + j \operatorname{sgn}(B_\alpha) [S(\hat{u}_+) - S(\hat{u}_-)] \} \quad (5.24)$$

where \hat{u} is:

$$\hat{u}_\pm = \pm \sqrt{(|B_\alpha|/2)} - \operatorname{sgn}(B_\alpha) \sqrt{2/|B_\alpha|} C_\alpha (u - \tilde{t}_n \cos \phi) \quad (5.25)$$

Substituting (5.24) in (5.21), $\mathfrak{F}^\alpha \{ \hat{s}(\tilde{t}_n) \}$ can be rewritten as:

$$\mathfrak{F}^\alpha \{ \hat{s}(t_n) \} = D_\alpha e^{j\pi \tilde{t}_n^2 \sin \phi \cos \phi} e^{-j2\pi u \tilde{t}_n \sin \phi} e^{-j\pi(u - \tilde{t}_n \cos \phi)^2/B_\alpha} \{ [C(\hat{u}_+) - C(\hat{u}_-)] + j \operatorname{sgn}(B_\alpha) [S(\hat{u}_+) - S(\hat{u}_-)] \} \quad (5.26)$$

In order to calculate the FrFT by (5.20), the linearity property of the FrFT is applied:

$$\mathfrak{F}^\alpha \{ \tilde{\mathbf{S}}_{sym_{BFSK}}(t) \} = \mathfrak{F}^\alpha \left\{ \sum_{n=1}^{N_b L_p} e^{(j2\pi f_{\hat{x}_n} u)} \hat{s}(u_n) \right\} = \sum_{n=1}^{N_b L} \mathfrak{F}^\alpha \left\{ e^{(j2\pi f_{\hat{x}_n} u)} \hat{s}(u_n) \right\} \quad (5.27)$$

For simplicity, it is evaluated for a fixed bit:

$$\mathfrak{F}^\alpha \{ \tilde{\mathbf{S}}_{sym_{BFSK}}(t_n) \} = \mathfrak{F}^\alpha \left\{ e^{(j2\pi f_{\hat{x}_n} t)} \hat{s}(t_n) \right\} \quad (5.28)$$

$\mathfrak{F}^\alpha \{\tilde{\mathbf{S}}_{sym_{BFSK}}(t_n)\}$ can be derived using the second property listed in Table 5.1, it is:

$$\mathfrak{F}^\alpha \{\tilde{\mathbf{S}}_{sym_{BFSK}}(t_n)\} = e^{-j\pi f_{\hat{x}_n}^2 \sin \phi \cos \phi} e^{j2\pi u f_{\hat{x}_n} \cos \phi} \bar{S}_\alpha(u - f_n \sin \phi) \quad (5.29)$$

where $\bar{S}_\alpha(u - f_{\hat{x}_n} \sin \phi)$ is given by substituting $(u - f_{\hat{x}_n} \sin \phi)$ in (5.26), becomes:

$$\begin{aligned} \bar{S}_\alpha(u - f_{\hat{x}_n} \sin \phi) = & D_\alpha e^{j\pi \tilde{t}_n^2 \sin \phi \cos \phi} \\ & e^{-j2\pi(u - f_{\hat{x}_n} \sin \phi) \tilde{t}_n \sin \phi} e^{-j\pi(u - f_{\hat{x}_n} \sin \phi - \tilde{t}_n \cos \phi)^2 / B_\alpha} \\ & \{[C(\bar{u}_{+,n}) - C(\bar{u}_{-,n})] + j \operatorname{sgn}(B_\alpha) [S(\bar{u}_{+,n}) - S(\bar{u}_{-,n})]\} \end{aligned} \quad (5.30)$$

where \bar{u}_\pm is:

$$\bar{u}_{\pm,n} = \pm \sqrt{(|B_\alpha|/2) - \operatorname{sgn}(B_\alpha) \sqrt{2/|B_\alpha|} C_\alpha(u - \tilde{t}_n \cos \phi - f_n \sin \phi)} \quad (5.31)$$

For simplicity, we define $u_1 = (u - f_{\hat{x}_n} \sin \phi - \tilde{t}_n \cos \phi)$ and (5.30) can be rewritten as:

$$\begin{aligned} \bar{S}_\alpha(u_n - f_{\hat{x}_n}) = & D_\alpha e^{j\pi \tilde{t}_n^2 \sin \phi \cos \phi} e^{-j2\pi(u - f_{\hat{x}_n} \sin \phi) \tilde{t}_n \sin \phi} e^{-j\pi u_1^2 / B_\alpha} \\ & \{[C(\bar{u}_{+,n}) - C(\bar{u}_{-,n})] + j \operatorname{sgn}(B_\alpha) [S(\bar{u}_{+,n}) - S(\bar{u}_{-,n})]\} \end{aligned} \quad (5.32)$$

Substituting (5.32) in (5.29), we obtained that the FrFT of (5.28) is:

$$\begin{aligned} \mathfrak{F}^\alpha \{\tilde{\mathbf{S}}_{sym_{BFSK}}(t_n)\} = & D_\alpha e^{-j\pi f_{\hat{x}_n}^2 \sin \phi \cos \phi} e^{j\pi \tilde{t}_n^2 \sin \phi \cos \phi} e^{j2\pi u f_{\hat{x}_n} \cos \phi} \\ & e^{-j2\pi(u - f_{\hat{x}_n} \sin \phi) \tilde{t}_n \sin \phi} e^{-j\pi u_{1,n}^2 / B_\alpha} \\ & \{[C(\bar{u}_+) - C(\bar{u}_-)] + j \operatorname{sgn}(B_\alpha) [S(\bar{u}_+) - S(\bar{u}_-)]\} \end{aligned} \quad (5.33)$$

Substituting (5.33) in (5.27) follows

$$\begin{aligned} \mathfrak{F}^\alpha \{ \tilde{\mathbf{S}}_{sym_{BFSK}}(t_n) \} = \sum_{n=1}^N \left\{ D_\alpha e^{-j\pi f_{\hat{x}_n}^2 \sin \phi \cos \phi} e^{j\pi \tilde{t}_n^2 \sin \phi \cos \phi} e^{j2\pi f_{\hat{x}_n} u \cos \phi} \right. \\ \left. e^{-j2\pi(u - f_{\hat{x}_n} \sin \phi) \tilde{t}_n \sin \phi} e^{-j\pi u_1^2 / B_\alpha} \right. \\ \left. \{ [C(\bar{u}_{+,n}) - C(\bar{u}_{-,n})] + j \operatorname{sgn}(B_\alpha) [S(\bar{u}_{+,n}) - S(\bar{u}_{-,n})] \} \right\} \end{aligned} \quad (5.34)$$

The first and the second exponential are two phase shifts, where for a fixed angle they depend on the frequency associated with a bit information and on its position in the bit sequence. The third and fourth terms are two exponentials with two different tones at $f_{\hat{x}_n} \cos \phi$ and $\tilde{t}_n \sin \phi$, respectively. The last terms take into account the FrFT of a square pulse shifted at $\tilde{t}_n \sin \phi + f_{\hat{x}_n} \cos \phi$.

In order to validate the analytical model the Mean Square Error (MSE) of the amplitude and phase are evaluated. The MSE of the amplitude and phase are illustrated in 5.5a and 5.5b, they are defined as:

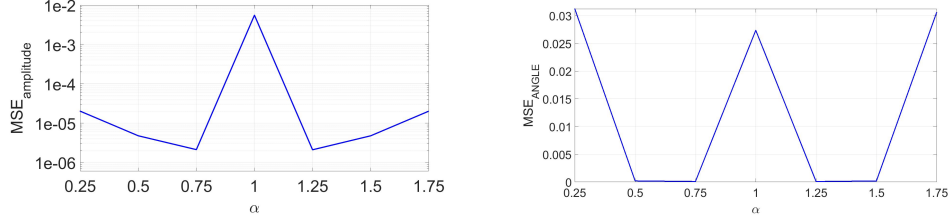
$$MSE_{AMPLITUDE} = \frac{1}{N} \sum_{i=1}^N (Y_i - \tilde{Y}_i)^2 \quad (5.35)$$

$$MSE_{ANGLE} = \frac{1}{N} \sum_{i=1}^N (An_i - \tilde{An}_i)^2 \quad (5.36)$$

where Y and An are the amplitude and phase obtained when the mathematical model is obtained by (5.34), while \tilde{Y} and \tilde{An} are the amplitude and phase obtained when the signal is numerically computed applying the DFrFT (see Section 3.9). The both MSEs are computed considering $\alpha \in [0.25, 1.25]$. Fig. 5.5a shows that in terms of the amplitude the two signals are very similar, as we can see the MSE moves from 10^{-2} to 10^{-6} . Moreover, the MSE of the phase, 5.5b, shows that a large difference between the two signal is present. This difference is due to the approximations that have been done to obtain the analytical model of the square pulse, [15].

The PSD, $S_{xx}(u)$, is calculated as the squared magnitude of the FT of (5.34). The FT can be derived from the FrFT with an angle $\phi = \pi/2$, meaning that $\alpha = 1$. The FT of (5.34) can be written as $\mathfrak{F}^{\alpha=1}(\mathfrak{F}^\alpha(\tilde{\mathbf{S}}_{sym_{BFSK}}(t_n)))$, which by

Chapter 5. Joint Radar and Communication system for automotive environment



(a) MSE of the amplitude when the BFSK is used. (b) MSE of the phase when the BFSK is used.

Fig. 5.5. Mean Square Error (MSE) of the amplitude 5.5a and phase 5.5b when the BFSK encoding scheme is used.

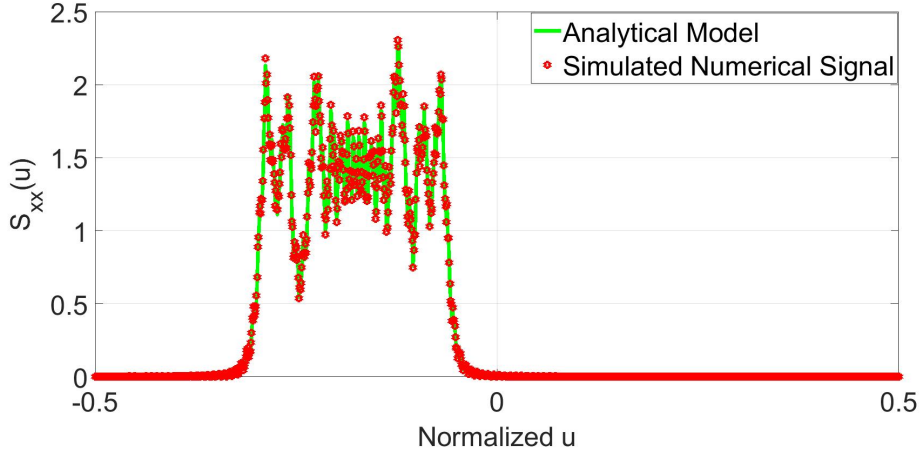


Fig. 5.6. Analytical and simulated PSDs when the BFSK modulation is used.

using the additivity property it becomes $\mathfrak{F}^{\alpha+1}(\tilde{\mathbf{S}}_{sym_{BFSK}}(t_n))$:

$$\mathfrak{F}^{\alpha+1}\{\tilde{\mathbf{S}}_{sym_{BFSK}}(t_n)\} = \sum_{n=1}^N \left\{ D_{\alpha+1} e^{-j\pi f_{\hat{x}_n}^2 \sin \theta \cos \theta} e^{j\pi \tilde{t}_n^2 \sin \theta \cos \theta} e^{j2\pi f_{\hat{x}_n} u \cos \theta} e^{-j2\pi(u - f_{\hat{x}_n} \sin \theta) \tilde{t}_n \sin \theta} e^{-j\pi \tilde{u}_{1,n}^2 / B_{\alpha+1}} \right. \\ \left. \{ [C(U_{+,n}) - C(U_{-,n})] + j \operatorname{sgn}(B_{\alpha+1}) [S(U_{+,n}) - S(U_{-,n})] \} \right\} \quad (5.37)$$

Fig. 5.6 shows the PSD obtained by (5.37) and that obtained when the PSD is numerically computed with the Matlab function provided in [93] applied to the FrFT of a BFSK encoding sequence. The PSDs are derived with four bits

and when the order of the FrFT is at 0.5. Fig. 5.6 shows that the analytical PSD is in agreement to that generated using the Matlab function.

PSD for the BPSK case

In a similar process as the one done for the BFSK, it is possible to derive the analytical model for the PSD of the BPSK, (5.17). In order to calculate the FrFT of (5.17), the linearity property of the FrFT is applied:

$$\mathfrak{F}^\alpha \{\tilde{\mathbf{S}}_{sym_{BPSK}}(t_n)\} = \mathfrak{F}^\alpha \left\{ \sum_{n=1}^{N_b L_p} e^{j\pi\tilde{x}_n} \hat{s}(u_n) \right\} = \sum_{n=1}^{N_b L} \mathfrak{F}^\alpha \left(e^{j\pi\tilde{x}_n} \hat{s}(u_n) \right) \quad (5.38)$$

where $e^{j\pi\tilde{x}_n}$ does not depend on t , so it can be taken off from the FrFT, consequently (5.38) it can be rewritten as:

$$\mathfrak{F}^\alpha \left\{ \tilde{\mathbf{S}}_{sym_{BFSK}}(t_n) \right\} = \sum_{n=1}^{N_b L_p} e^{j\pi\tilde{x}_n} \mathfrak{F}^\alpha \{ \hat{s}(t_n) \} \quad (5.39)$$

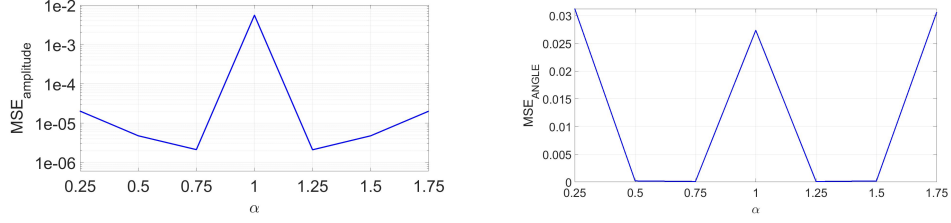
$\mathfrak{F}^\alpha \{ \hat{s}(t_n) \}$ is given by (5.26), consequently (5.39) becomes:

$$\begin{aligned} \mathfrak{F}^\alpha \{ \hat{s}(t_n) \} = & \sum_{n=1}^N e^{j\pi\tilde{x}_n} D_\alpha e^{j\pi\tilde{t}_n^2 \sin \phi \cos \phi} e^{-j2\pi u \tilde{t}_n \sin \phi} e^{-j\pi(u - \tilde{t}_n \cos \phi)^2 / B_\alpha} \\ & \{ [C(\hat{u}_{+,n}) - C(\hat{u}_{-,n})] + j \operatorname{sgn}(B_\alpha) [S(\hat{u}_{+,n}) - S(\hat{u}_{-,n})] \} \end{aligned} \quad (5.40)$$

In order to evaluate the analytical model when the BPSK encoding scheme is used the MSE of the amplitude and phase are computed as when the BFSK encoding scheme is used. Comparing Fig. 5.7 with Fig. 5.5, we can see that the two figures are perfectly the same. So also when the BPSK encoding scheme is used the amplitude of the analytical signal and numerical one is very close, while a large difference is present when the MSE is computed taking into account the phase of the two signals.

The FT of (5.40) can be written as:

Chapter 5. Joint Radar and Communication system for automotive environment



(a) MSE of the amplitude when the BFSK encoding scheme is used. (b) MSE of the phase when the BFSK encoding scheme is used.

Fig. 5.7. Mean Square Error (MSE) of the amplitude 5.7a and phase 5.7b when the BFSK encoding scheme is used.

$$\begin{aligned} \mathfrak{F}^{\alpha+1}\{\hat{s}(t_n)\} &= \sum_{n=1}^{N_b L} e^{j\pi\tilde{x}_n} D_{\alpha+1} e^{j\pi\tilde{t}_n^2 \sin\theta \cos\theta} e^{-j2\pi\tilde{u}_n \sin\theta} e^{-j\pi(u_n - \tilde{t}_n \cos\theta)^2 / B_{\alpha+1}} \\ &\{[C(\tilde{u}_{+,n}) - C(\tilde{u}_{-,n})] + j \operatorname{sgn}(B_{\alpha+1}) [S(\tilde{u}_{+,n}) - S(\tilde{u}_{-,n})]\} \end{aligned} \quad (5.41)$$

where

$$\tilde{u}_{\pm,n} = \pm\sqrt{(|B_{\alpha}|/2) - \operatorname{sgn}(B_{\alpha})\sqrt{2/|B_{\alpha}|}C_{\alpha}(u - \tau_n \cos\theta)} \quad (5.42)$$

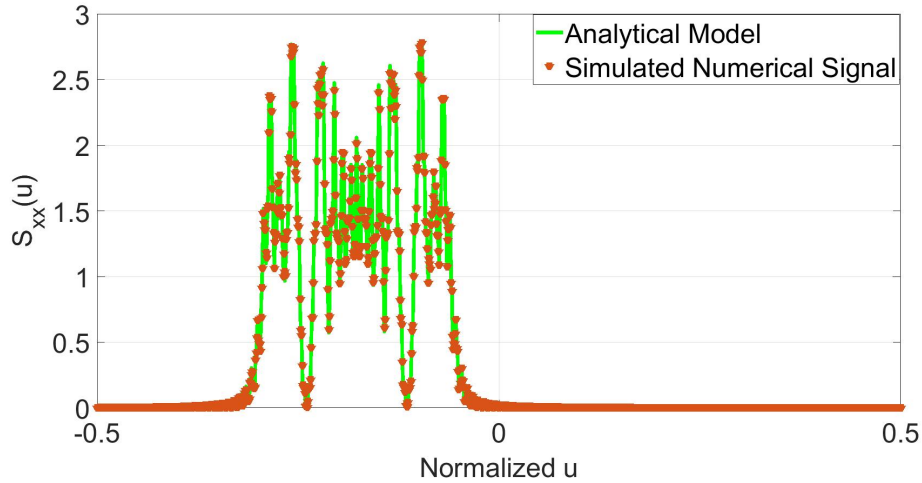


Fig. 5.8. Analytical and simulated PSDs when the BFSK modulation is used.

$$S_{xx}(u) = \left| \sum_{n=1}^N e^{j\pi\tilde{x}_n} D_\alpha e^{j\pi\tilde{t}_n^2 \sin\theta \cos\theta} e^{-j2\pi u\tilde{t}_n \sin\theta} e^{-j\pi(u_n - \tilde{t}_n \cos\theta)^2 / B_{\alpha+1}} \right. \\ \left. \{[C(\hat{u}_{+,n}) - C(\hat{u}_{-,n})] + j \operatorname{sgn}(B_{\alpha+1}) [S(\hat{u}_{+,n}) - S(\hat{u}_{-,n})]\} \right|^2 \quad (5.43)$$

In order to validate the analytical model derived in (5.43), the analytical PSD and the PSD obtained when the FrFT of BPSK is derived using the Matlab function in [93], are plotted in Fig. 5.8. These are obtained by considering the same bits used in Section 5.1.2 and with $\alpha = 0.5$. Comparing both PSDs, we can see that PSD of the analytical model fits that obtained from the Matlab function.

5.2 Conclusion

In this chapter, a novel joint radar and communication system based on the FrFT for automotive applications has been presented. So considering its related framework, the FrFT has been used to embed, directly, data information into a radar waveform allowing a joint radar and communication system. In addition, the analytical model of the proposed waveform and its PSD have been derived considering both encoding schemes.

In the following a comparison between the proposed system with that described in chapter 4 is given. In the proposed framework the data information are embedded in the radar waveform, so a single waveform is generated rather than to generate two different waveforms and then combined as described in Section 4.2.1. In addition, in the proposed framework the radar and communication processing are applied directly on the received signal, while in frameworks proposed in Section 4.2.1 at the receiver side, it is necessary to separate the two waveforms, and then the radar and communication processing can be applied.

The dual radar and communication systems presented in Section 4.2.2 requires an array of the antenna. In these frameworks, the radar function is performed using the main lobe of the antenna, while the communication function is carried out considering the side lobe of the same antenna. In the proposed system both functions are carried out using a single antenna. Comparing the proposed framework with those presented in Section 4.2.1 and Section 4.2.2

we can see that proposed waveform can be generated using a simple hardware. In OFDM at each user is assigned more than one sub-carrier (see Section 4.2.3) rather than a single sub-carrier as in the proposed waveform, consequently, in OFDM a high bit rate is achieved. However, in multi user scenarios, in OFDM the bandwidth is split between all users, this means that the range resolution depends on the number of the users that shares the same bandwidth at the same time. In the proposed framework this issue is not present, because at each user a single order of the FrFT is assigned, consequently, the range resolution depends on the order of the FrFT and no on the number of the users that share the same frequency band at the same time. In addition, in the proposed system the radar processing is applied directly on the received radar signal, while in OFDM the radar processing is applied after that the data information are removed from the received radar signal.

In the proposed framework the FrFT has been used to generate a chirp-like waveform embedding information in the time-frequency domain and thus enabling communication functions in a manner similar to the one proposed in Section 4.2.5. The main differences are: rather than exploiting the fractional order to improve data transition, in the proposed framework multi user operations are allowed by assigning a specific order of the FrFT to each user. Additionally, to allow CW operation a sample deletion and a CPI operation have been proposed. Finally, the pilot sequence is placed at the beginning of the CPI instead of each pulse.

The drawbacks of the proposed framework are the following: a low bit rate is achieved, synchronisation between the transmitter and receiver and due to the fact that this system uses the FrFT, so on the communication side it is necessary to estimate the time where the received signal starts. The drawback related to the low bit rate is presented due to the following aspects. The first aspect, it is that on the radar side, a coherent processing has been applied. So this means that in a single CPI the same data information have to be embedded. The second aspect, it is that at each user a single sub-carrier is assigned. The drawback related of the synchronisation has been solved transmitting a pilot sequence. However, when the pilot sequence is not transmitted a new user cannot demodulate the received data. In other words, this means that when a new user share the channel it cannot demodulate the

received information, but it can transmit the data information to other users. Last drawback of the proposed system is related to the FrFT. As mentioned in the previous chapter the IFrFT can be applied in a correct way only, if the time where the received signal start is, exactly, know with. In this framework, this issue has been solved selected an opportunity pilot sequence, but in real scenario it is not easy to estimate parameters without some errors.

In last part of the chapter, the analytical model of the proposed waveform has been presented and compared in terms of MSE with that obtained when a fast FrFT has been used. The MSE has been computed considering the amplitude and the phase of the two signals. The results have been shown that the amplitude of the two signals is very similar. While there is a difference of the phase.

To conclude in this chapter, a new joint radar and communication system has been presented. In this framework, the FrFT has been used to embed the data information into radar waveform allowing a communication link. In the proposed framework, the waveforms are transmitted in manner similar to FCLFM. In last part of the chapter, the analytical model for BFSK and BPSK encoding schemes has been derived.

The main objective of the proposed framework is to obtain a radar system that shares the same characteristic of an LFM waveform, but allowing a communication link between the users. In next chapter, the radar performance of the proposed waveform will be computed considering both encoding schemes and compared with that obtained when an LFM waveform is transmitted. Moreover, in order to show the capability of the proposed system to share data information with other users, the communication performance will be presented. While the analytical model will be used to compute the performance while the reconstructed signal is obtained using the analytical model rather than the algorithm to generate a discrete fast FrFT.

Chapter 6

Performance of the proposed joint radar and communication system

A joint radar communication system treats radar as primary and communication as secondary function, the secondary function should not disturb the primary function of the joint system, but it should take full advantage of the offered frequency and space allocations. In addition, in a joint radar and communication system the data information are embedded into the transmitted radar signal, consequently, the transmitted radar waveform depends on the data to be sent, and thus, it changes with time. However, the transmitted radar waveform of a joint radar and communication system should be able to perform radar function with arbitrary transmitted data and the radar performance should not be affected too much by the data.

The main of this chapter is to evaluate the radar performance of the joint radar and communication system presented in Section 5.1, and to compare this performance with that obtained when an FCLFM waveform is transmitted. In addition, in order to show the capability of the proposed system to achieve a communication link, the communication performance is evaluated considering different types of channels.

The main of the radar performance is to evaluate how the proposed waveform depends on the transmitted data, in order to do it, the AF and its properties

are analysed when bits information are mapped in symbols using a BFSK or BPSK encoding scheme. In this analysis, the performance of the proposed waveform is compared with that obtained when an LFM waveform with the same bandwidth is transmitted. Additionally, in the proposed joint radar and communication system in order to allocate more than one user in the same frequency band a fractional order division multiplexing is implemented. However, when the difference between two consecutive orders of the FrFT decreases a high mutual radar interference can arise. This interference leads to a degradation of the detection performance. The probability of the false alarm increase, because a ghost target caused by the interference is detected. While the probability of the detection decreases, because a real target is masking by a ghost one. For this reason, it makes sense to assess the detection performance of the proposed system in the presence of two users that are in close proximity to each other and operate in the same frequency band. The detection performance is assessed considering a worst case scenario where the two users transmit the same data and use the same PN sequence, but they are uniquely identified by two different orders of the FrFT. When the two orthogonality orders are used the mutual radar interference does not arise, but in this case only two users can be allocated in the same channel at the same time. In multi user scenarios, the difference between the two orders of the FrFT is not equal to one, consequently, when the difference, α_{diff} , between two orders of the FrFT decreases there will be an increase of mutual interference.

The multi target detection capability of the proposed joint radar and communication system is also demonstrated. In particular, to meet the requirements for automotive applications, a radar sensor must be capable of measuring a target's range and Doppler frequency simultaneously and unambiguously even in multi target situations. Additionally, the detection performance is evaluated in multi user scenarios where the targets transmit a radar communication signal. In this scenario, the signal from other user is seen as interference signal as it causes a radar performance degradation.

The main of the communication performance is to show that in the proposed system a communication link is achieved. The performance is evaluated in terms of BER considering different communication channels. This perfor-

mance is carried out considering two scenarios. In the first scenario, the BER is evaluated against different values of $\text{SNR}_{\text{comms}}$, while in the second scenario, the BER is evaluated when more than one user transmits its information on the same channel at the same time.

The remainder of the chapter is organized as follows. In Section 6.1 the radar performance is evaluated in terms of waveform's Ambiguity Functions when two different schemes of encoding BFSK and BPSK are used, and then this performance is compared with that obtained considering an LFM waveform. In Section 6.2 the ability of the proposed system to discriminate different users that share the same frequency band at the same time is illustrated. Section 6.3 shows a range-Doppler detection when more than one target is present. While a range-Doppler detection when the targets transmit also a communication signal is illustrated in Section 6.4. In Section 6.5 the detection performance in terms of Receiving Operative Characteristics (ROC) curves is derived for different values of $\text{SINR}_{\text{radar}}$. In Section 6.6 the simulated communication performance is evaluated considering different types of channels as Additive white Gaussian noise (AWGN), Rice, Rayleigh and Log Normal. In Section 6.6.1 and Section 6.6.3 the performance is evaluated against different $\text{SNR}_{\text{comms}}$ and $\text{SINR}_{\text{comms}}$, respectively.

6.1 Radar performance

In this Section, the radar performance of the proposed joint radar and communication system is evaluated in terms of the waveform's AF when two different schemes of encoding, BFSK and BPSK are used. In addition, the radar performance of both encoding schemes is compared with that obtained when an LFM waveform is transmitted. Particularly the Doppler and delay cuts of the AF and their SLLs are considered. To evaluate and compare the radar performance obtained the analysis is carried out with fixed time-bandwidth product. Since the transmitted radar depends on the data to be sent. As the bit sequence to be transmitted changes with time, it is expected that also the waveform transmitted by the system changes and, thus, also the properties (i.e. AF) change. The system parameters used in this analysis are reported in Table 6.1. This parameters are chosen in order to obtain a

Table 6.1: System Parameter

Parameters	Description	Values
f_c	Operating Frequency.	77 GHz
N_b	Number of bits.	7
G_g	Random bits.	1
N_s	Number of samples per symbols.	4
f_s	Sampling Frequency.	150 MHz
β	Roll off factor.	0.95
S	Filter Span in Symbols.	24
R_s	Output Samples per Symbols.	13
L_p	Length of PN Sequence.	7
PN sequence	Primitive Polynomial.	z^3+z^2+1
N_{wave}	Number of the waveform in a CPI.	90
P_t	Transmit Power.	20 dBm
G_t	Transmit Antenna Gain.	30 dB
G_r	Receive Antenna Gain.	30 dB
σ_{radar}	Radar Cross Section.	1

low computational cost.

The AF and its two main cuts, for both encoding schemes, are computed over a Monte Carlo simulation with 100 iterations and for four values of $\alpha = [0.2, 0.4, 0.5, 0.8]$. The mean AFs, for BFSK and BPSK are shown Fig. 6.1 and Fig. 6.2, respectively. Fig. 6.1 shows that when the BFSK encoding is used, the AF is similar to that of an LFM one, Section 3.3, meaning that it shares with it positive and negative aspects, such as bulk compression, and lack of Doppler tolerance. On the other hand, when a BPSK encoding scheme is used, see Fig. 6.2, the AF has a much flatter shape and the range-Doppler coupling is not present.

The zero-Doppler and zero-delay cuts of AF for four different orders and for both encoding schemes are illustrated Fig. 6.3 and Fig. 6.4. respectively. Both zero cuts are compared with those obtained when an LFM waveform is transmitted; its has the same time-bandwidth product of the proposed waveform. As it can be seen, the range and Doppler resolution obtained considering the two encoding schemes are similar to that an LFM waveform. It is due to the fact that the resolution depends on the bandwidth rather than

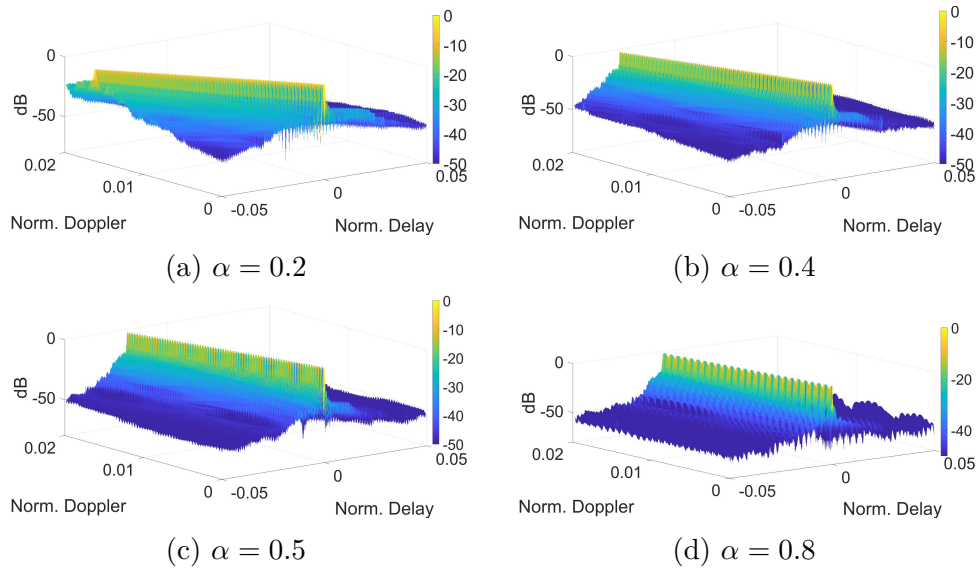


Fig. 6.1. Ambiguity Function when the BFSK modulation is used.

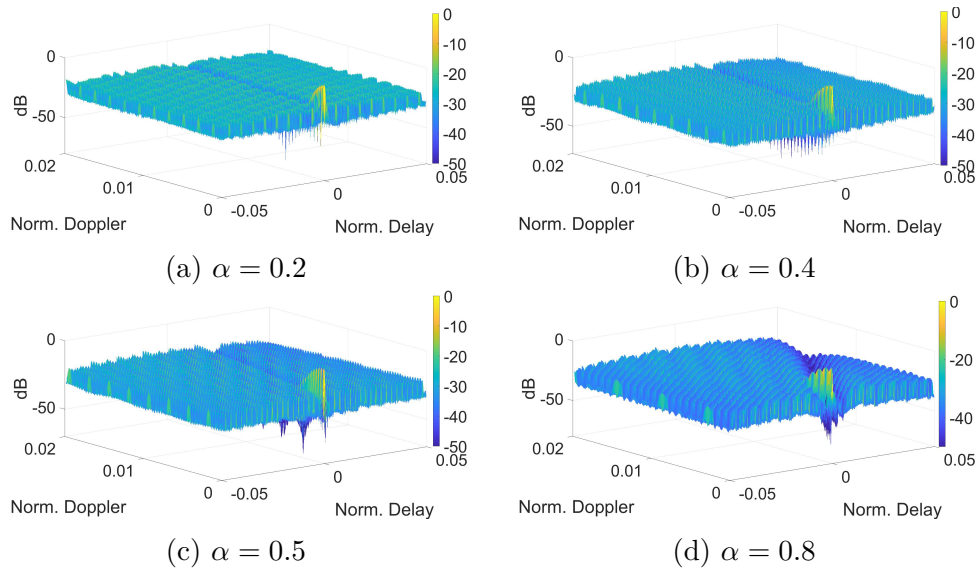


Fig. 6.2. Ambiguity Function when the BPSK modulation is used.

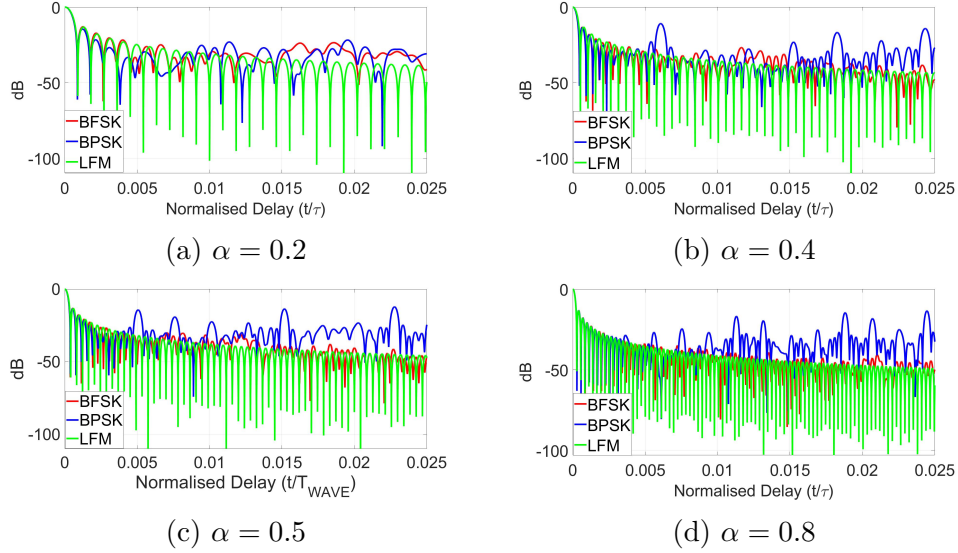


Fig. 6.3. Zero-Doppler cut of the BFSK, BPSK, and LFM waveforms AF.

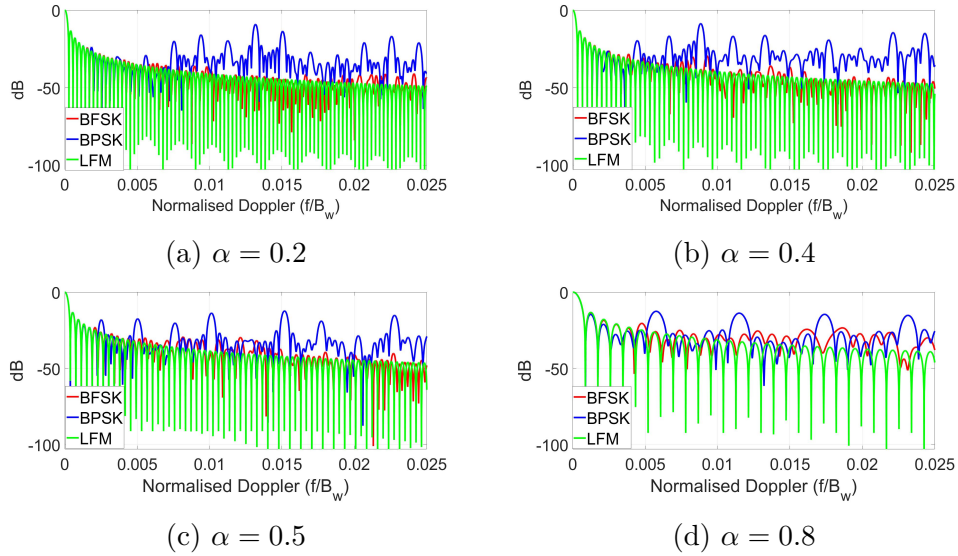
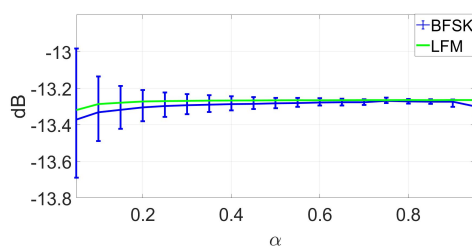


Fig. 6.4. Zero-delay cut of the BFSK and BPSK waveforms AF.

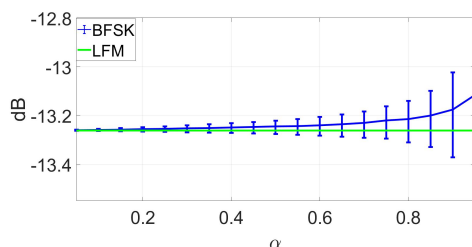
the encoding used. Fig. 6.3 shows that when the order of the FrFT increases the range resolution decreases. It is due to the fact that when the order of the FrFT moves from 0 to 1 the bandwidth of the signal increases. The two cuts show that the range and Doppler resolution of the both encoding schemes are similar to an LFM waveform.

Fig. 6.3a shows that when α is 0.2 the zero-Doppler cut obtained by using both encoding schemes is similar to the case in which an LFM waveform is transmitted; for $\alpha = [0.4, 0.5, 0.8]$, see Figs. 6.3b-6.3d, the zero-Doppler cut obtained using a BFSK encoding scheme is similar to that obtained considering an LFM waveform. While when a BPSK encoding scheme is used, it presents higher sidelobes than an LFM waveform. In Fig. 6.4, it is shown that the sidelobes at zero-delay cut of the BPSK are higher than the BFSK. When the BPSK is used the peaks are at -20 dB below the maximum value. Comparing the sidelobes for both cuts obtained by using BFSK and BPSK encoding schemes, it can be seen that for both cuts the BPSK has higher peaks than the BFSK. The high peaks obtained when the BPSK is used are due to phase jumps between 0 and π . In addition, in both cuts the sidelobe obtained considering an BFSK encoding are similar to an LFM waveform.

The peaks SLLs obtained considering the proposed waveform and LFM one are calculated through 100 Monte Carlo runs, for values of $\alpha \in (0, 1)$ while for each iteration different data information are embedded in the radar waveform. The time-bandwidth of the LFM waveform is the same at that of the proposed waveform. Fig. 6.5 shows for each value of α the mean value



(a) zero-Doppler cut

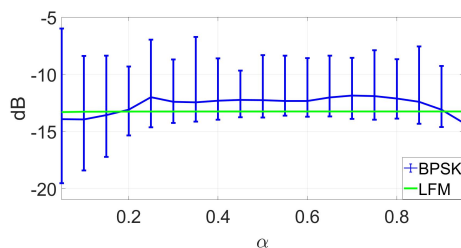


(b) zero-delay cut

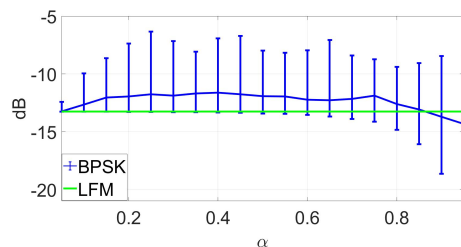
Fig. 6.5. SLL when the BFSK encoding scheme and LFM waveform are used.

and the interval between the minimum and maximum values of the SLL when the BFSK is used. From Fig. 6.5a it can be seen that the mean value of SLL at zero-Doppler cut is very close to the sidelobe level of an LFM waveform. Additionally, for $\alpha \in (0, 0.4]$ the difference between the maximum and minimum moves from 0.7 dB to 0.15 dB while when α is bigger than 0.4 the maximum and minimum are very close to the LFM value. As seen in Fig. 6.5b, for $\alpha \in (0.1, 0.8]$ the difference is bigger than 0.3 dB and also for this cut the SLL of the proposed waveform is very close to an LFM waveform. Comparing the SLL at zero-Doppler cut with the SLL at zero-delay cut, it can be seen that in Fig. 6.5a the SLL decreases while in Fig. 6.5b increases with the values of α .

In Fig. 6.6 the mean value and the interval between the minimum and maximum values of the SLL for each values of $\alpha \in [0, 1]$ are shown when the BPSK encoding is applied, and they are compared with that obtained transmitting an LFM waveform. Fig. 6.6a shows that the mean value of the SLLs at zero-Doppler cut is not constant and a large difference between the maximum and minimum is present. While in Fig. 6.6b is shown that the mean values of the SLL at zero delay cut it close to mean values, however, in



(a) zero-Doppler cut



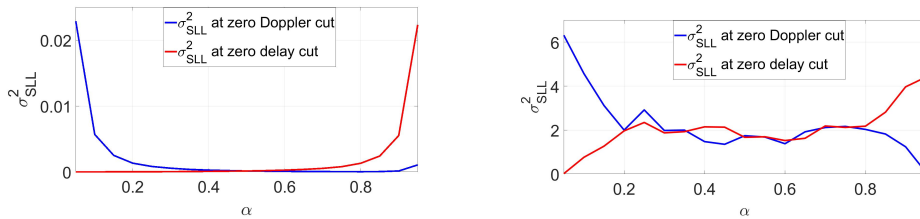
(b) zero-delay cut

Fig. 6.6. SLL when the BPSK encoding and LFM are used.

this cases the maximum values do not exhibit a clear trend. In both cuts, the mean value of the SLL is bigger than to that obtained considering an LFM waveform. Comparing Fig. 6.5 with Fig. 6.6, it can be seen that when BPSK encoding is used the SLL depends more on encoding and less on the FrFT order. While when a BFSK is used the radar performance is similar to that obtained considering an LFM waveform, thus the radar performance depends less on the data information and more on the order of the FrFT.

In order to further motivate these results the variance of the mean values σ_{SLLs}^2 is also calculated for both cuts by using the same values of α and the same number of iterations. Fig. 6.7a and Fig. 6.7b show the variance of the SLL at zero-Doppler and zero-delay cuts when a BFSK and BPSK are used, respectively. Fig. 6.7a shows that the variance of SLL at zero-Doppler cut moves from 0.0025 to 0 while the variance of SLL at zero-delay cut moves from 0 to 0.025. When a BFSK encoding is used the values of the SLL obtained for different orders of the FrFT are spread close to their average value. While Fig. 6.7b shows that when a BPSK scheme is used the SLLs diverge from their average values.

This analysis highlights that for both encoding strategies the SLLs diverge from their average value when the fractional order used is < 0.2 and > 0.8 . Meaning that values of $\alpha \in [0.3, 0.8]$ represent a more suitable range mitigating the side-lobe modulation effect. The results obtained considering the AF and its two main cuts have been shown that when the BFSK encoding scheme is used the radar performance of the proposed joint radar and communication system does not depend highly on the data information and it is similar to than of an LFM waveform. As mentioned in chapter 2.3 the energy of the



(a) Variance when the BFSK is used. (b) Variance when the BPSK is used.

Fig. 6.7. Variance when the BFSK and BPSK encoding scheme are used.

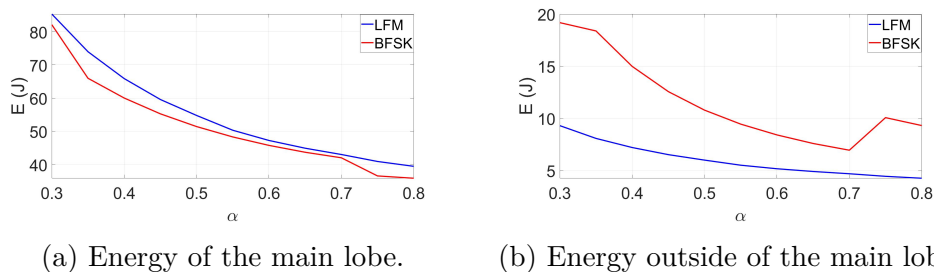


Fig. 6.8. Energy for different zero-Doppler cuts when the FrFT is applied on BFSK encoding scheme and when an LFM waveform is transmitted.

AF can go somewhere else. So it is interesting to compute the energy of the AF for different zero-Doppler cuts. So the energy of the main lobe and outside it, for the different zero-Doppler cuts, of the proposed waveform when the FrFT is applied on the BFSK encoding scheme are illustrated in 6.8a and 6.8b, respectively. Both energy is computed when α moves from 0.3 to 0.8 and for each value of alpha 100 Monte Carlo simulations are carried out. Where in each iteration different data information are embedded in the radar waveform. The both energies are compared with those obtained when an LFM waveform is transmitted. The analysis is carried out considering the same time-bandwidth product. Comparing Fig. 6.8a with Fig. 6.8b we can see that for both waveform the energy of the main lobe is bigger than outside of it. In addition, looking at 6.8b we can see that the energy outside of the main lobe when the proposed waveform is transmitted is bigger than when an LFM waveform is considered. This means that when the proposed waveform is transmitted ghost target can arise leading to a degradation of the detection performance. However, as we can see the difference between the two energy outside the main lobe is less than 10 Joule. Consequently, in the rest of the chapter, the performance of the proposed joint radar and communication system is evaluated considering only the BFSK encoding scheme. While the same parameters reported in Table 6.1 are used.

6.2 User discrimination

In the proposed joint radar and communication system, multi user operations are allowed by assigning a specific order of the FrFT to each user. When the number of users increase, consequently, the difference between the orders of the FrFT decreases leading to detection performance drop due to the rise of ghost targets.

In this Section, the ability of proposed joint radar and communication system to discriminate different users is analysed. The analysis is carried out when two users share the same channel at the same time and they are uniquely identified by two different orders of the FrFT.

The performance is assessed considering the cross-correlation function and the ROC curves for different values of α_{diff} . Where α_{diff} is the difference between the order assigned at each user. Due to the fact that in this Section we want to show how the interference arises for different values of α_{diff} , the performance is carried out considering a worst case scenario. This means that the two users transmit the same data, they use the same PN sequence code to spread their data, and the values of the power at which the respectively signals are received by the radar are not take into account. The analysis is carried out in cross-range domain, hence on the received radar signal after the matched filter a Square Law Detector (SLD) is applied. Then to perform the detection the magnitude of each waveform is compared with a CA-CFAR detector [113].

The ROC curves show in Fig. 6.9 are created by plotting the Probability of Detection (P_D) against the Desired Probabilities of False Alarm (DP_{FA}). While the Probabilities of False Alarm (P_{FA}) vs DP_{FA} is illustrated in Fig. 6.10. The curves shown in Fig. 6.9 and Fig. 6.10 are obtained at various threshold setting and for a specific SNR_{radar} . The CA-CFAR detector is used to set the threshold. In this analysis the SNR_{radar} is set at -8 dB. As the main scope of this analysis is to show how the interference is arisen when the α_{diff} decreases, the SNR_{radar} is a symbolic value. The P_{FA} is calculated based on the number of false alarms and the number of trials, while P_D is given from the number of detection on the number of trials. The number of Monte Carlo simulations used to obtain the results shown in Fig. 6.9 and in Fig. 6.10 is

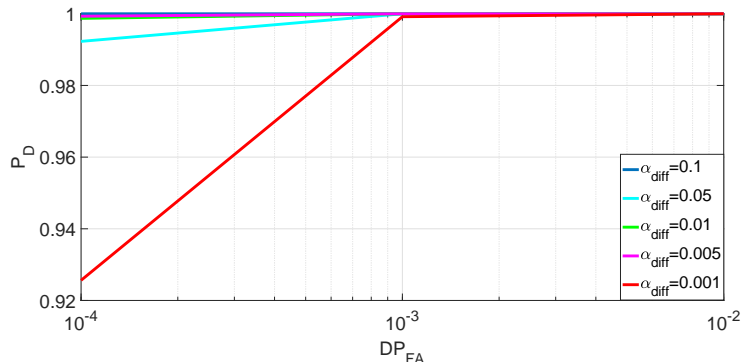


Fig. 6.9. Receiver Operating Characteristic curves between P_D and design DP_{FA} .

given from:

$$N_{trials} = \frac{100}{DP_{FA}} \quad (6.1)$$

where N_{trials} is the number of Monte Carlo runs that they are needed to obtain a DP_{FA} . The performance is evaluated for values of $DP_{FA} = 10^{-4}, 10^{-3}, 10^{-2}$. The cross-correlation is a comparison between two waveforms and it measures the orthogonality of one waveform relative to the other. Due to this, the cross-correlation is used to justify the results shown in Fig. 6.9 and Fig. 6.10. The cross-correlation function is obtained by calculating the mean value of 100 Monte Carlo runs for each α_{diff} . Fig. 6.11 shows that as α_{diff} moves from 0.1 to 0.001 there is an intensity increase in the cross-correlation. Consequently, high cross-correlation values can lead to problems such as ghost targets

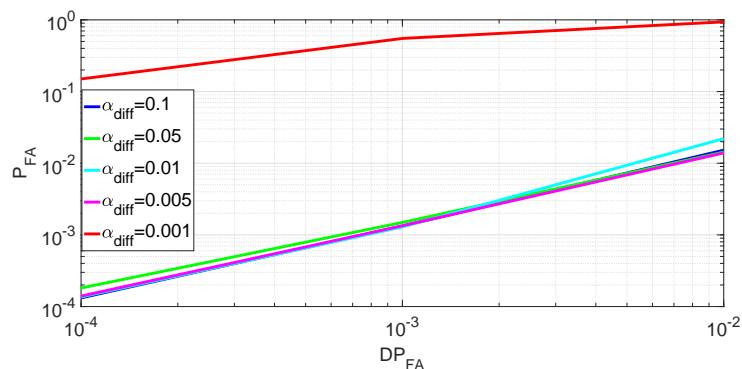


Fig. 6.10. P_{FA} values versus design DP_{FA} .

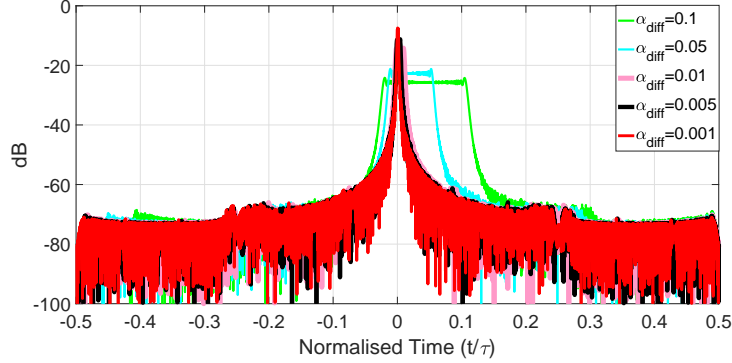


Fig. 6.11. Cross-Correlation between the main and interference users for different values of α_{diff} .

which will increase the number of false alarms and in undesirable losses of sensitivity for detection radar targets. This behaviour is more evident by taking a close look at the curves shown in Fig. 6.9 and Fig. 6.10. In Fig. 6.10, it can be seen that for $\alpha_{\text{diff}} \in [0.1, 0.005]$ the P_{FA} is equal to DP_{FA} while for $\alpha_{\text{diff}} = 0.001$ the P_{FA} is not equal to DP_{FA} . In Fig. 6.9 it can be seen that for $\alpha_{\text{diff}} \in [0.1, 0.0001]$ the P_{D} moves from 0.92 to 1. As we can see, when α_{diff} is less than 0.001 the maximum value of the cross-correlation is less than the maximum value of the SLLs and the radar performance is preserved. While when α_{diff} is equal to 0.001 the maximum value of the cross-correlation is close to the maximum value of the SLLs, consequently the detection performance is degraded. The P_{FA} increases because a ghost target is detected. While the P_{D} decreases, because the real target is not detected due to the presence of the false target generated by the secondary user. In summary, the simulation analysis shows that by applying a fraction order division multiplexing, it is possible to allocate more than one users in the same frequency band and at the same time without degrading the detection performance. The minimum difference between two orders of the FrFT preventing the detection performance to be degraded, can be obtained through the maximum value of the cross-correlation between two waveforms, that is equal to the maximum value of the SLLs.

6.3 Multi target scenarios

In an automotive environment where more than one target is present, a radar sensor must be able to distinguish the different targets and to measure the range and velocity simultaneously and unambiguously. In this Section, the capability of the proposed waveform to distinguish different targets in the range-Doppler map is evaluated. The simulated parameters for the targets used in this analysis are reported in Table 6.2. For the simplicity, in this analysis, a order of the FrFT by 0.5 is used and the T_{WAVE} is set at 0.013 millisecond. In Section 6.1, it has been shown that when the FrFT is applied on the BFSK encoding scheme and for values of the order of the FrFT that moves from 0.3 to 0.8 the radar performance of the proposed waveform is similar to that obtained when an LFM waveform is transmitted, consequently, this results can be obtained also using different orders of the FrFT.

The received radar signal can be written as:

$$\mathfrak{s}_{rx}(u) = \sum_{i=1}^{N_T} \mathcal{A}_i X_\alpha(u - \tau_i) e^{j2\pi f_{D,i} u} \quad (6.2)$$

where N_T is the number of the targets present in the scene, \mathcal{A}_i is the amplitude received from i -th target, X_α is the transmitted radar signal with order α , τ_i is the delay from i -th target and $f_{D,i}$ is the Doppler frequency of the i -th target.

An example of ideal range-Doppler map considering four targets is illustrated in Fig. 6.12. As we can see the echoes are received at the radar with different levels of the power due to different range, R , according to (2.3). In multi target scenarios, a weaker target may be masked by the sidelobes associated to a stronger target. In order to solve this issue a windowing process is applied

Table 6.2: Location of the targets

R (m)	f_D (Hz)	P_{radar} (dB)
2	1425.9	-26.4
5	6415.7	-58.24
5	9981.5	-58.24
7	-1426	-70

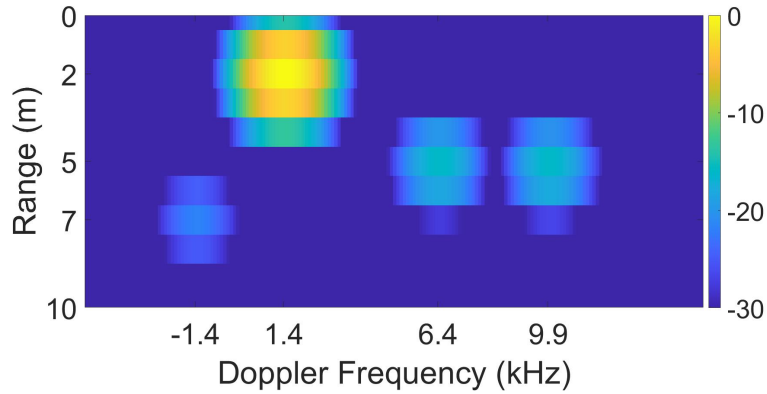


Fig. 6.12. Multi target environment, when 4 targets are present.

[113]. In this analysis, a Blackman Harris windows has been applied to reduce the SLLs at both range and Doppler domain.

The range-Doppler detection shown in Fig. 6.13 is obtained applying the CA-CFAR on the range-Doppler map, Fig. 6.12. The range-Doppler detection is obtained with a (DP_{FA}) by 10^{-4} , while the number of guard and training cells are set at 50 and 20, respectively.

Comparing Fig. 6.13 with the actual locations of the targets in Table 6.2, it can be seen that multiple targets can be separated even if they are located at the same distances or have different distance and Doppler frequencies. The main goal of this Section has been to illustrate that using the proposed

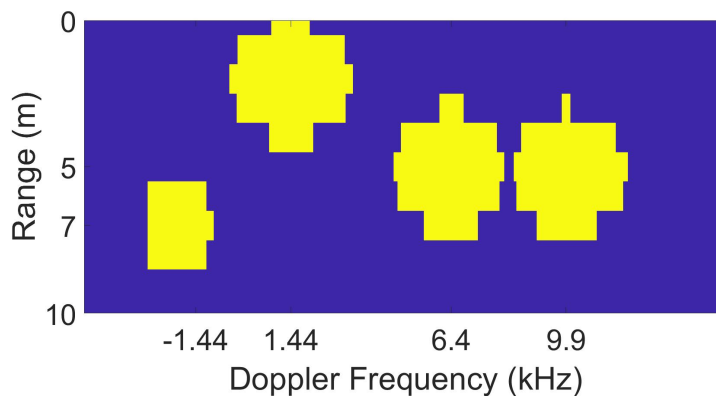


Fig. 6.13. Range-Doppler detection when 4 targets are present.

system the range and Doppler frequency of the targets can be estimated. Consequently the proposed waveform fits for an automotive environment.

6.4 Multi User scenario

In an automotive environment, the targets may also transmit a radar signal. Hence, in this environment mutual radar interference can arise leading to a degradation of the radar performance. In multi user scenarios, the received radar signal can be written as:

$$\mathfrak{R}(u) = \mathfrak{s}_{rx}(u) + \mathfrak{J}_{rx}(u) \quad (6.3)$$

where $\mathfrak{s}_{rx}(u)$ is the radar signal calculated from (6.2) and $\mathfrak{J}_{rx}(u)$ is direct signal received from the other users, it is given by:

$$\mathfrak{J}_{rx}(u) = \sum_{k=1}^{N_I} \mathcal{C}_k X_{\alpha_k}(u - \tilde{\tau}_k) e^{j2\pi \tilde{f}_{D_k} u} \quad (6.4)$$

where N_I is the number of interfering users, which in this analysis is equal to the number of the target, see Section 6.3, \mathcal{C}_k is the amplitude of the k -th interference signal received from the radar, and $\tilde{\tau}_k$ is the one way propagation delay between radar and k -th target, and \tilde{f}_{D_k} is the Doppler frequency calculated on single path between radar and k -th user. In order to take into account the lack of synchronisation between the radar and each user, the delay, $\tilde{\tau}$, is modelled as a uniform distribution while the Doppler is deterministic. The interference power received at the radar from k -th user is given by Friis equation, [40], which can be written as:

$$P_{\text{Int},k} = P_t G_t G_r \left(\frac{\lambda}{4\pi} \right)^2 \left(\frac{1}{R_{\text{Int}_k}} \right)^2 \quad (6.5)$$

where R_{Int_k} is the distance from the interfering user to the radar.

In this analysis, the targets are also the source of interference, hence R_{Int} is equal to R . The performance is evaluated considering a worst case scenario where the radar receives both radar and interference signal in its

Table 6.3: Interference power

User	α	Initial Conditions	P_{Inter} (dB)	T_{WAVE} millisecond
1	0.5	001		0.013
2	0.6	101	-8	0.011
3	0.4	110	-8	0.015
4	0.7	010	7.6	0.008
5	0.8	111	-20	0.005

mainlobe. The order α , the initial conditions of the PN sequence, the power of interference, and the time duration of each waveform is given in Table 6.3. Comparing the received power scattered by a target Table 6.2 with the received power from an interference user Table 6.3, we can see that the interference signal is almost higher than the reflected radar signal and hence appears as noise in the range-Doppler map. Fig. 6.14 shows the range-Doppler map when the targets are also the source of interference. Comparing Fig. 6.14 with the range-Doppler map illustrated in Section 6.3 we can see that in multi user scenario strong interference is present.

The range-Doppler detection obtained applying the CA-CFAR on range-Doppler map shown in Fig. 6.14 is illustrated in Fig. 6.15. The parameters of the CA-CFAR are the same used in Section 6.3. Comparing Fig. 6.15 with Fig. 6.13 we can see that the target at 7 meters is not detected. This is due to the fact that the maximum power value of interference signal is -20 dB while

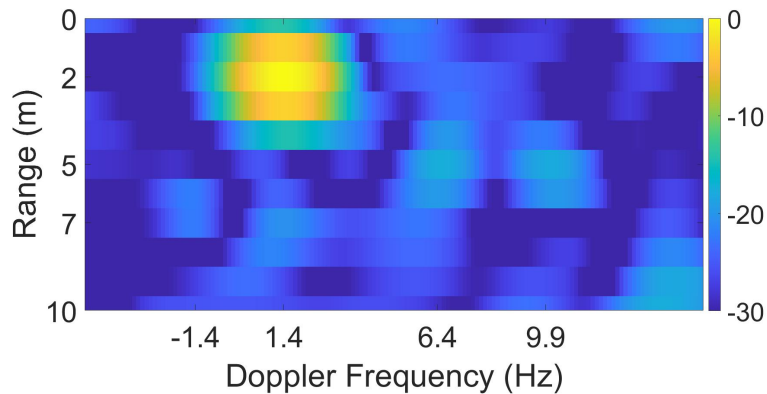


Fig. 6.14. Range-Doppler map in multi user scenarios.

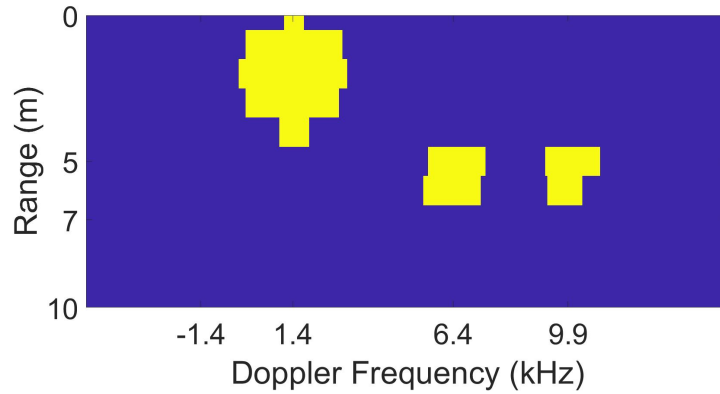


Fig. 6.15. Range-Doppler detection in multi user scenarios.

the power value of the real target at 7 meters is -21.34 dB. Consequently this small difference leads to masking of the target with low intensity.

Additionally, Fig. 6.16 shows the range-Doppler map when each user transmits a FCLFM waveform. The bandwidth, time duration and windowing are the same to the ones used to obtain the range-Doppler map shown in Fig. 6.14. As it can be seen even when the radar transmits a LFMF waveform strong interference is present. Comparing Fig. 6.16 with Fig. 6.14, we can see that in both cases the interference is present. Thus, it is due to the fact that the waveforms are not orthogonal and the power of the interfering signal is higher than the useful radar signal rather than the data information. In this analysis using a simple CA-CFAR detector the target at 7 meters is

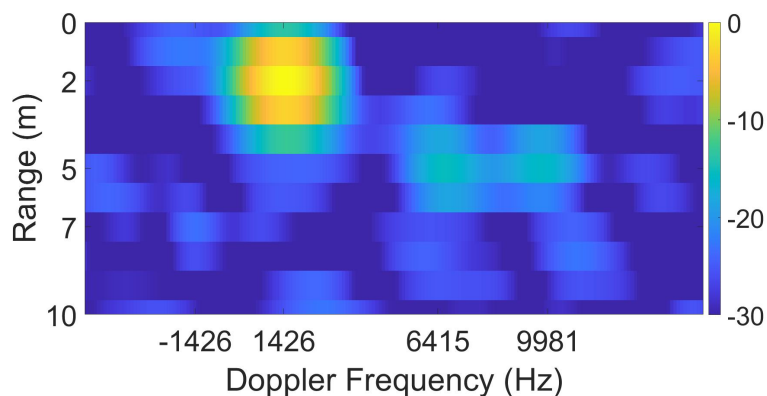


Fig. 6.16. Range-Doppler map, with LFMF waveform.

not detected, however using a different CFAR techniques this target may be detected. A simple CA-CFAR has been used to demonstrate that the mutual radar interference caused by other users that use the same channel at the same time leads to a degradation of the detection performance.

6.5 Detection Performance versus SINR

In this Section, the ROC curves are derived to assess the detection performance for different values of $\text{SINR}_{\text{radar}}$.

As we are considering both noise and interference we must revise the signal model used so far, thus we write the received radar signal as:

$$y(u) = \mathfrak{R}(u) + n(u) \quad (6.6)$$

where $\mathfrak{R}(u)$ is given by (6.3) while $n(u)$ is the noise modelled as AWGN. The analysis is carried out considering a worst case scenario where the radar receives both radar and interference signals in its mainlobe.

The SINR at the receive radar can be written as

$$\text{SINR} = \frac{\sum_{i=1}^{N_T} P_{\text{Radar},i}}{\sum_{k=1}^{N_I} P_{\text{Int},k} + P_{\text{noise}}} \quad (6.7)$$

where $P_{\text{Radar},i}$ and $P_{\text{Int},k}$ are given by (2.3) and (6.5), respectively, while P_{noise} is the power of background noise.

The detection performance is derived by considering a simple scenario in which a user and a target/user are present. For this scenario, the SINR given by (6.7) becomes:

$$\text{SINR} = \frac{P_{\text{Radar}}}{\sum_{k=1}^2 P_{\text{Int},k} + P_{\text{noise}}} \quad (6.8)$$

In this framework the users are uniquely identified from different orders of the FrFT and they use different PN codes of the same length to spread the raw data, these parameters are listed in Table 6.4. The ROC curves are derived considering three values of SINR -49 dB, -69 dB and -83.3 dB, these values correspond to different automotive scenarios. The first value corresponds to a scenario where the target and user/interference are at 3

Table 6.4: Simulated Users Parameter

User	α	Initial Conditions
Main	0.5	001
1	0.4	110
2	0.6	101

meters from the radar, while the second and the third value correspond to a scenario where the user is at 3 meters from the radar and the target/user is placed 6 and 9 meters from the radar, respectively. These SINR values are calculated before of the processing gains, i.e matched filter and coherent processing. This means that after the processing a gain is introduced. We consider zero mean noise with variance $\sigma_n^2 = 1.02$. Also this value of the noise is symbolic, because we want to show that the interference leads to a degradation of the detection performance.

The ROC curves shown in Fig. 6.17 are obtained with 10^4 iterations and for each iteration different data information are embedded in the radar waveform. The ROC curves are derived at various threshold settings based on a CA-CFAR detector and for three values of desired false alarm rate $DP_{FA} 10^{-4}, 10^{-3}$ and 10^{-2} .

From Fig. 6.17, it can be appreciated that when the SINR is -49 dB the target is detected with a P_D approaching 1 even when DP_{FA} is 10^{-4} . While in order to obtain a P_D of 0.9 when the SINR is -69 dB it is necessary to decrease the false alarm rate at 10^{-2} . In an automotive environment, the radar sensors are key components for comfort and safety functions. This means that a low DP_{FA} is required. For a more reasonable value of $DP_{FA} = 10^{-3}$ the detection probability is less than 0.4. In an automotive environment where the number of the users that share the same channel at the same time is continuously growing, high mutual radar interference is expected. As shown in Fig. 6.17 high values of interference leads to a degradation of the detection performance. In order to solve this problem additional strategies to mitigate the interference are required and will be introduced in chapter 7.

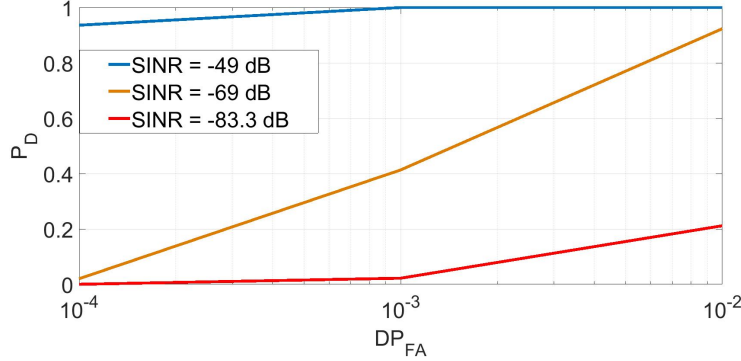


Fig. 6.17. ROC curves in multi user scenarios.

6.6 Communication performance

In previous Sections, it has been shown that the radar performance of the proposed joint radar and communication system using a BFSK encoding scheme does not depend highly on the data information embedded in the radar waveform. In this Section, the capability of the proposed system to achieve also a communication link is demonstrated. In order to evaluate the communication performance, the signal is assumed to experience a slow-flat fading channel [128], therefore a time-invariant narrowband channel model is considered. Let be \mathbf{s}_{tx} the vector which contains the transmitted signal samples. The received signal can be written as:

$$\mathbf{y} = \mathbf{h} \circ \mathbf{s}_{tx} + \mathbf{n} \quad (6.9)$$

where \mathbf{h} is the vector that contains the channel coefficients, \mathbf{n} is the white Gaussian noise, and the operator (\circ) indicates the Hadamard, or entry-wise, product.

The complex elements of the vector \mathbf{h} are drawn from a statistical distribution whose parameters depend on the propagation path [105]. In addition to the AWGN, the only scenario for which $\mathbf{h} = 1$, three other cases are considered. For cases of which the LOS path is present, the channel is modelled as Rician with a Rice factor of 4 dB. Conversely, when no LOS path exists, the channel coefficients \mathbf{h} are draw from a Rayleigh distribution with scale parameter $\sqrt{2}/2$. Finally, in order to take into account shadowing and diffraction that

can occur in urban environment, a combination of Rice and Lognormal is considered [27]. In this case, the channel coefficients are obtained as the product of a Rice process normalised in power and a Lognormal variable, whose associated Gaussian variable has a standard derivation of 4.

The communication performance is evaluated only when the BFSK encoding is used as it resulted to be the approach that affect less the radar performance (see Section 6.1). In this Section the performance is evaluated considering two scenarios. In the first scenario, the performance is evaluated for different values of $\text{SNR}_{\text{comms}}$ in terms of BER. While in the second scenario, the BER is carried out considering different $\text{SINR}_{\text{comms}}$ values. The BER is defined as the ratio between the number of bits wrongly decoded and the total number of bits sent. Additionally, the first scenario corresponds at a scenario where only single user is present and the $\text{SNR}_{\text{comms}}$ is calculated after the synchronization step. In the second scenario more than one user transmits the signal on the same channel and at the same time, in this scenario the $\text{SINR}_{\text{comms}}$ is calculated after the RRC filter.

6.6.1 Single User scenarios

In a single user scenario, where only one user transmits the data on the channel, hence the interference is not present and the received communication signal is given by (6.9). The BER versus $\text{SNR}_{\text{comms}}$ for four different channel models as: AWGN, Rice, Rayleigh and Lognormal is illustrated in Fig. 6.18. The BER for each channel is obtained via 10^7 Monte Carlo runs order $\alpha = 0.5$ and with $\text{SNR}_{\text{comms}}$ from -20 to 20 dB. In this analysis, the communication performance is evaluated considering a single order of the FrFT, because the main goal is to illustrate that using the proposed system a communication link is also achieved.

In rural environment where the main component is LOS and the channel is modelled as a Rice, a $\text{BER} = 10^{-4}$ is obtained with an $\text{SNR}_{\text{comms}}$ of 15 dB. In urban environment the signal is subject to diffraction and shadowing hence the channel is modelled as a Lognormal to ensure a BER of 10^{-4} it is required to have $\text{SNR}_{\text{comms}}$ of some dBs more than in rural environment. Furthermore,

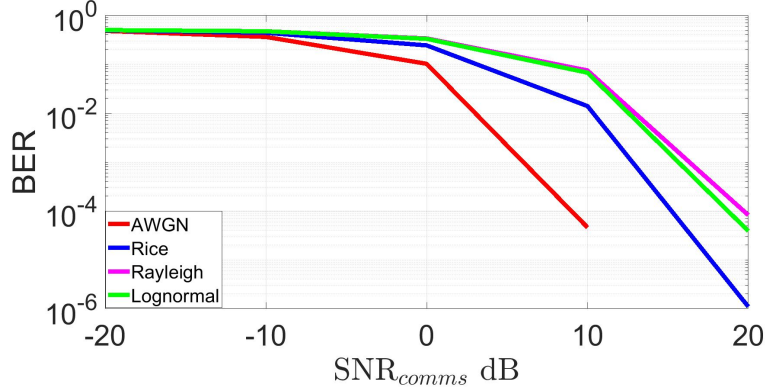


Fig. 6.18. Bit Error Rate versus $\text{SNR}_{\text{comm}_s}$ when the BFSK encoding is used.

where the LOS is not present and the channel is modelled as Rayleigh, a $\text{BER} = 10^{-4}$ is obtained with an $\text{SNR}_{\text{comm}_s}$ of 20 dB.

6.6.2 Link Budget

In the following, the link budget and radar equation for the communication and radar applications are calculated. The SNR is chosen depending on the desired radar and communication performance. Typical system parameters and requirements are summarised in Table 6.5. The maximum radar range, R_{max} and the maximum radar-communication receiver distance, $R_{\text{Int,max}}$ are obtained. For this specific analysis, the radar link budget is obtained by rearranging the radar range equation, 2.6 as follows:

Table 6.5: Link budget parameters

Parameters	Description	Values
P_t	Transmit Power.	20 dBm
G_t	Transmit Antenna Gain.	30 dB
$G_{r,comm}$	Communication receiver antenna gain.	7 dB
σ_{radar}	Radar Cross Section.	1
λ	Wavelength	0.389 cm
k	Boltzmann's constant	1.38×10^{-23} J/K
T_O	Noise reference temperature	290 K
F	Radar and communication noise figure	5 dB
B_w	Bandwidth	150 MHz

$$R_{max} = \sqrt[4]{\frac{P_t G_t G_r \lambda^2 \sigma_{radar}}{(4\pi)^3 F k T_0 B_w \text{SNR}_{radar}}} \quad (6.10)$$

while the radar-communication receiver distance $R_{\text{Int},max}$ is obtained by rearranging (6.5)

$$R_{\text{Int},max} = \sqrt[4]{\frac{P_t G_t G_r \lambda^2}{(4\pi)^2 F k T_0 B_w \text{SNR}_{comms}}} \quad (6.11)$$

For the communication, in an urban environment a $\text{SNR}_{comms} = 20$ dB secures a $\text{BER} = 10^{-4}$. At the same time, a data stream of 0.7 Mb/s can be directed to a communication receiver placed at a distance of 400 km. For the radar when $\text{SNR}_{radar} = 8$ dB, a target with Radar Cross Section of 1 m^2 can be detected at a maximum range of 79.72 m. Typically, in an automotive environment, multiple users shall be able to communicate with each other. In cases where the users are in close proximity, different fractional orders can be allocated in each user, while those fractional orders can be reused in cases where the users are at higher distance $R_{\text{Int},max}$.

6.6.3 Multi User scenarios

In a scenario where more than one user transmits its data on a channel that it also shared from other user, the received signal, \mathbf{s}_{rx} can be written as:

$$\mathbf{s}_{rx} = \sum_{i=1}^{N_T} \mathbf{s}_{\text{Radar},i} + \sum_{k=1}^{N_I} \mathbf{s}_{\text{Com},i} \quad (6.12)$$

where $\mathbf{s}_{\text{Radar},i}$ and $\mathbf{s}_{\text{Com},i}$ contains the scattered signal samples from the i -th target and transmitted signal samples from k -th user.

Table 6.6: Simulated Users Parameter

User	α	Initial Conditions
Main	0.5	001
1	0.4	110
2	0.6	101

The $\text{SINR}_{\text{comms}}$ can be written as:

$$\text{SINR}_{\text{comms}} = \frac{P_{\text{Com},M}}{\sum_{k=2}^{N_I} P_{\text{Com},k} + \sum_{i=1}^{N_T} P_{\text{Ra},i} + P_n} \quad (6.13)$$

where $P_{\text{comms},M}$ and $P_{\text{comms},k}$ are the power of the communication signal sent by the main user and k -th user respectively. The signal sent by the k -th user is seen as interference signal. While $P_{\text{Ra},i}$ is the power radar scattered by the i -th target. The power of communication signal is given by (6.5) while the power radar scattered is given by (2.3).

In this analysis, the noise is modelled as AWGN with zero mean and variance $\sigma_n^2 = 1.02$. The communication performance is evaluated considering a scenario where a user/target and interference user are present. For this scenario, the SINR given by (6.13) becomes:

$$\text{SINR}_{\text{comms}} = \frac{P_{\text{comms},M}}{P_{\text{comms},1} + P_{\text{radar},M} + P_n} \quad (6.14)$$

The FrFT orders α and the initial conditions to generate different PN codes used in this analysis are listed in Table 6.6. The BER curves are obtained considering four values of $\text{SINR}_{\text{comms}}$, which are 27 dB, 33 dB, 42 dB, and 49 dB. The curves shown in Fig. 6.19 are obtained with 10^5 Monte Carlo runs. In rural environment when the $\text{SINR}_{\text{comms}}$ moves from 27 dB to 49 dB the BER moves from 10^{-1} to 10^{-3} . In urban environments where the signal is subject to diffraction a BER 1.410^{-3} is obtained when $\text{SINR}_{\text{comms}}$ is 49 dB. In the same scenario to ensure a BER less than 10^{-2} the $\text{SINR}_{\text{comms}}$ has to be higher than 44 dB. Therefore to obtain the same BER in urban environments as in rural environments the $\text{SINR}_{\text{comms}}$ has to be 10 dB higher. Furthermore, where the LOS is not present, a with $\text{SINR}_{\text{comms}}$ of 49 dB the BER is 3.410^{-2} . Additionally, when the channel is modelled as AWGN the BER is zero. The communication performance has shown that in order to obtain a high value of the BER a high values of $\text{SNR}_{\text{comms}}$ and $\text{SINR}_{\text{comms}}$ are required.

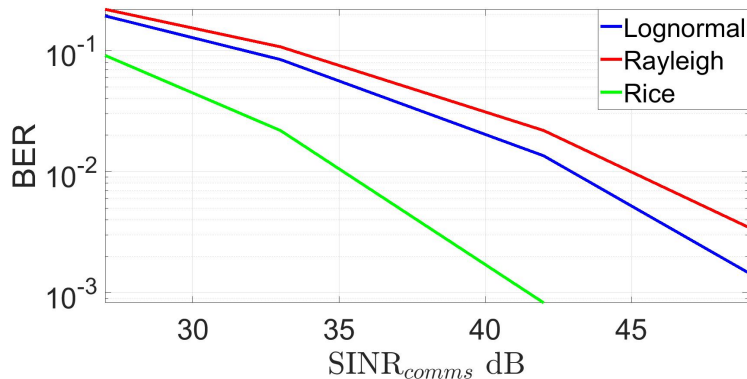


Fig. 6.19. Bit Error Rate versus $\text{SINR}_{\text{comms}}$ when the BFSK encoding is used.

6.7 Conclusion

In this chapter the radar and communication performance of the proposed joint radar and communication system have been computed. The goal of this chapter has been to show that the radar performance is similar to that obtained when an LFM waveform is transmitted, and at the same time a communication link is also achieved. The results have shown using the same waveform it is possible to do radar and communication function at the same time and in the same frequency. Thus, on the receiver side both functions can be applied without to separate the two waveforms as it carried out in the Spread Spectrum techniques (see Section 4.2.1). In addition, due to the fact that the data information are embedded directly in the radar waveform a diversity antenna patten is not achieved as it is proposed, Section 4.2.2, in Dual radar and communication function.

The results have shown that when a BFSK encoding scheme is used the radar performance is similar to an LFM waveform. Thus means, that on receive radar side the standard radar processing can be applied directly on the received signal and its performance does not depend highly on the data information. However, in a joint radar and communication system based on OFDM, the radar parameters can be estimated only after those data information are removed by the received radar signal. In addition, the results have shown that by employing a multiplexing fractional it is possible to allocate more than one user in the same frequency band. So that preserving the radar

performance and the range resolution will only depend on the order of the FrFT rather than OFDM, where in multi user scenarios the range resolution depends on the number of the users sharing the same bandwidth at the same time. In an OFDM system at each user more than one sub-carrier are assigned. Thus means that a high bit rate is achieved than in the proposed system, where a single sub-carrier is assigned at each user. In addition, in OFDM the communication performance is better than the proposed framework. It is due to the fact that a BPSK encoding scheme has been applied. So, in terms of the radar performance the proposed system is favoured than the OFDM, due to the fact that the radar processing can be applied directly on the received radar signal without to demodulate the signal and the range resolution does not change than the number of users. On the other hand, for the communication performance the OFDM is favoured, due to the fact that a high bit rate can be achieved and the BER is better than that obtained when the proposed system has been used.

The Co-Radar and the proposed system use the FrFT to embed data information into radar waveform. As mentioned in the previous chapter the main differences are that in Co-Radar system the multiplexing fractional order has been used to embed more than one sub-carriers in the same pulse thus leads to increase the bit rate. On the other hand, in the proposed system the multiplexing fractional order has been adopted to allocate more than one user. So, in order to transmit the data in the proposed system a single user can adopt a single sub-carrier instead of more than one as in Co-Radar system. In addition, in the proposed system the waveforms have been transmitted in a consecutive manner. The results have shown that the proposed system fits for an automotive environment, due to its capacity to estimate range and Doppler frequency in unambiguous manner, even in multi target situations. In this chapter, it has been shown that in this system the radar function can be carried out with arbitrary transmitted data and the radar performance is not affected too much by the data information. However, a low bit rate and a poor BER are achieved. In addition, the results have been shown that in multi user scenarios, due to the fact the users transmit also a communication signal strong mutual radar interference has arisen leading to a degradation

Chapter 6. Performance of the proposed joint radar and communication system

of the radar performance. In order to solve this issue in next chapter two interference mitigation framework will be presented.

Chapter 7

Interference Mitigation Strategies for the proposed system

In an automotive environment, where multiple users are in close proximity to each other and moreover these operate in the same frequency band mutual radar interference may arise as shown in Section 6.4. The mutual radar interference leads to a degradation of the detection performance as illustrated in Section 6.5. In the second part of chapter 4 different strategies to mitigate the mutual radar interference have been presented. In a joint radar communication system due to the capacity of the radar to reconstruct the received interference signal. So this interference can be reconstructed and then mitigated. In this chapter two interference mitigation approaches for the proposed joint radar and communication system are introduced. The successful waveform reconstruction depends on accurate estimation of some key parameters such as delay $\tilde{\tau}$, Doppler frequency \tilde{f}_D , and the amplitude \mathcal{C} of received interfering signals.

In the first framework, the interference is mitigated in a coherent manner. While in the second framework, the interference is alleviated in a non-coherent manner.

The performance of the coherent framework is evaluated in terms of Signal Interference Ratio obtained when the interference has been mitigated, SIR_{out} ,

against different offset values such as Doppler frequency and received amplitude of the interfering signal. This performance is evaluated when the received and reconstructed are obtained by applying the framework illustrated in Section 5.1, and when the received signal is generated applying the Matlab function while the interference signal is reconstructed by using the mathematical model presented in Section 5.1.2. These performances are compared with those obtained when the non-coherent framework is applied considering the same scenario.

In order to improve the detection performance shown in Section 6.5 the non-coherent framework is applied. In addition, the performance of the non-coherent framework is also evaluated by considering three scenarios: in the first two scenarios the radar transmitter is switched off, so the radar receives only the signal from the interference user. In the first scenario, the performance is evaluated on simulated signal without noise, while in the second scenario, the interference mitigation is applied on real data acquired using a SDR device. Finally, in the third scenario the radar transmitter is on and a target is present.

The remainder of the chapter is organized as follows. The coherent framework interference is presented in Section 7.1. In Section 7.2 the non-coherent framework is described. In Section 7.3 the performance of these two frameworks are evaluated in terms of SIR_{out} against different offset values of Doppler frequency and received amplitude of the interference signal. The improvement of the detection performance using the non-coherent framework is illustrated in Section 7.4. In Section 7.5 the non-coherent framework is analysed by means of simulated interference signals when the radar transmitter is switched off, consequently, only the interference signal is received. Finally, in Section 7.6 the performance is evaluated using the real data.

7.1 Coherent Interference Framework

The coherent interference mitigation framework is illustrated in Fig. 7.1. In order to reconstruct the interference on the received signal two stages are applied. In the first stage, the communication operations are applied to recover the bits sent by other users. When the bits are recovered, the interference

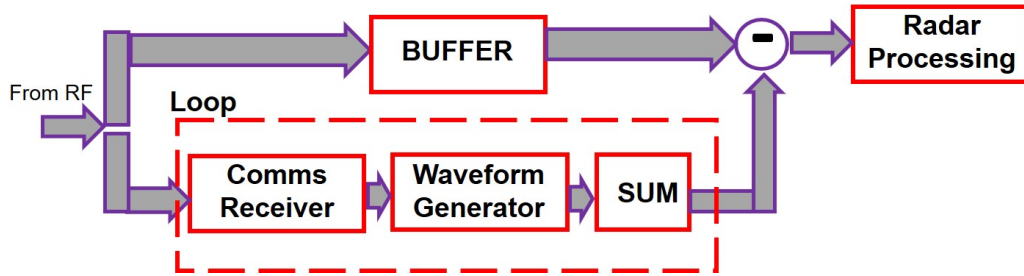


Fig. 7.1. Interference mitigation framework where the subtraction is carried out in coherent manner.

signal can be reconstructed using the waveform generator, Section 5.1, or the mathematical model presented in Section 5.1.2. After these two stages, the interference is rebuilt. The sum is carried out by taking into account the estimated time delay of the interfering signals. After these operations, the reconstructed interfering signal is coherently subtracted from the received radar signal. At this stage, the residual signal can be processed with the standard radar processing tools. The estimation of the amplitude of the received interference is obtained by applying a matched filter between the received and reconstructed interference. The buffer is used to store the received signal until the interference signal has been reconstructed.

7.2 Non-coherent Interference Mitigation Framework

In Section 7.1 a coherent interference framework has been presented. When the subtraction is carried out in a coherent manner a small error on the estimation of the Doppler frequency may lead to a lack of the synchronization. Consequently, the subtraction will not be performed in a correct way and further interference components may be introduced. In order to improve the performance even in scenario where the Doppler frequency of the interfering user is not perfectly estimated a non-coherent interference mitigation framework is introduced. The block diagram of the proposed framework is represented in Fig. 7.2. In this framework, the subtraction is carried out

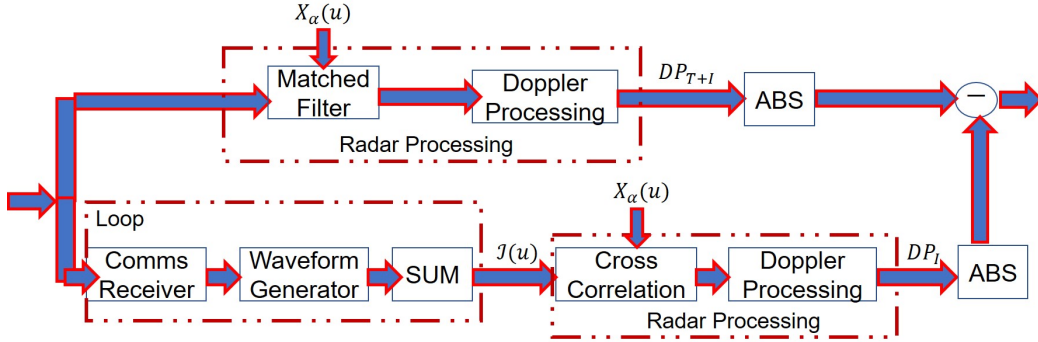


Fig. 7.2. Interference mitigation framework where the subtraction is carried out in non-coherent manner.

between the absolute values of the radar plus interference parameters DP_{T+I} and the interference parameters DP_I . In other words, the subtraction is applied between the range-Doppler map or (i.e range profile, spectrograms) when the targets and interference are present and the range-Doppler map or (i.e. range profile, spectrograms) obtained by the reconstructed interference signal. Given the loss of phase information, further processing that would need interference free inputs would need to be intensity based only (i.e. detection and target recognition), however the Doppler information can be obtained from the interference free range-Doppler map or from the spectrogram obtained at the end of the interference removal process.

As it is shown in Fig. 7.2 on the received signal, two parallel processes are carried out. In the first, the standard radar processing tool is applied, the output of this process is indicated with DP_{T+I} . The parameters obtained at this point are influenced by both target and interference components. Moreover, in order to recover the bits sent by the interference users the demodulation functions are applied. After this step, the interference signal can be reconstructed by applying the waveform generator as described in Section 5.1 or by using the signal model as described in Section 5.1.2. These operations are repeated for each interfering user present in the received signal, and then a sum between all reconstructed signal is carried out. After the loop the following signal is obtained:

$$\mathfrak{J}(u) = \sum_{k=1}^{N_I} \hat{\mathcal{C}}_k \hat{I}_{k\alpha_I,k}(u - \hat{\tau}_{I,k}) e^{j2\pi \hat{f}_{D,k} u} \quad (7.1)$$

In order to obtain the interference parameters, the signal $\mathfrak{J}(u)$ is organized into a fast-time/slow-time data matrix. At the end of this stage, a correlation between the signal obtained after the loop, (7.1), and the radar signal, $X_\alpha(u)$, in fast-time is carried out, while a Doppler processing is applied in slow-time. At the end of these stages DP_I is obtained. In order to mitigate the interference by the targets plus interference parameters, a subtraction between the absolute value of DP_{T+I} and DP_I is carried out. After this process, the absolute value of the residual intensity is shown.

7.3 Performance of the proposed frameworks

In this Section, the performance of the coherent framework is evaluated when the Doppler frequency and the received amplitude of the interference signal are not perfectly estimated and then this performance is compared with that obtained when the interference is mitigated using the non-coherent framework. The analysis is performed in terms of the SIR_{out} obtained after the interference mitigation and for different offset values such as Doppler frequency, $\delta_{\hat{f}_D}$ and amplitude δ_C .

When the interference is mitigated using the coherent framework the SIR_{out} is calculated as:

$$SIR_{out} = \frac{P_{Radar}}{P_{Int}} \quad (7.2)$$

While when the subtraction is performed in a non-coherent manner the SIR_{out} is calculated as the ratio of the power associated to DP_T and DP_I . Where DP_T indicates the parameters contained only target.

The analysis is carried out when the Doppler frequency and the amplitude of the received interference signal are set at 1 kHz and 0.85, respectively.

Interference frameworks based on waveform generation

In this analysis, the bits are mapped though the BFSK encoding and the values of each parameter are reported in Table 6.1. The SIR_{out} versus offset

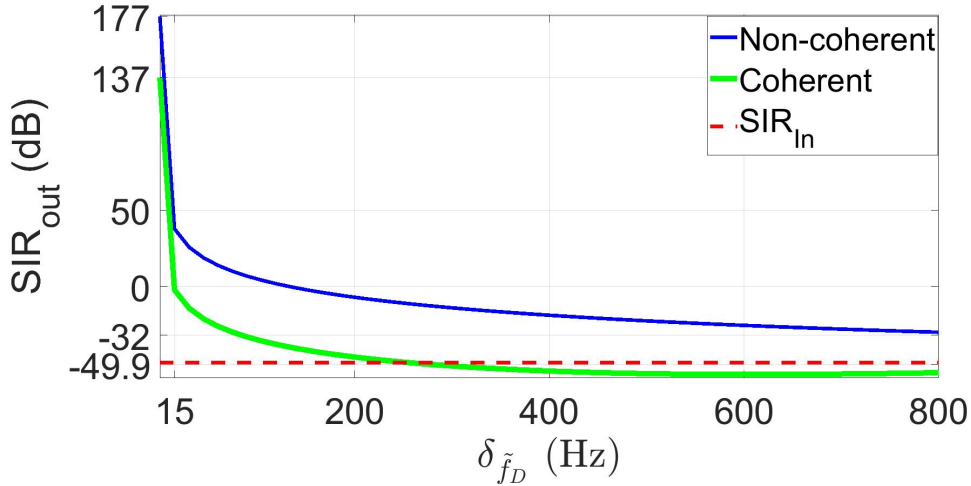


Fig. 7.3. SIR_{out} obtained when both frameworks are applied against the offset frequency $\delta_{\tilde{f}_D}$.

frequency is illustrated in Fig. 7.3. The two curves are obtained when the interference is mitigated by using the coherent and non-coherent framework, respectively. Fig. 7.3 shows that when $\delta_{\tilde{f}_D} \in [0.005, 800]$ Hz the SIR_{out} obtained using the coherent framework moves from 137 dB to -53 dB. As it can be seen when $\delta_{\tilde{f}_D}$ is at 15 Hz a SIR_{out} by 0 dB is obtained. When $\delta_{\tilde{f}_D} \in [0.05, 15]$ Hz the SIR_{out} obtained applying the coherent framework moves from 137 dB to 0 dB. Thus, an error by 15 Hz of the Doppler frequency leads to a drop of the SIR_{out} by 137 dB. Comparing SIR_{out} with SIR before the interference mitigation, $SIR_{In} = 49.9$ dB, we can see that when $\delta_{\tilde{f}_D}$ is bigger than 200 Hz the SIR_{out} of the coherent framework is bigger than SIR_{In} , consequently, the interference is not mitigated. On the other hand, when the interference is mitigated by using the non-coherent framework, we can see that for the same values of $\delta_{\tilde{f}_D}$ the SIR_{out} moves from 177 dB to -32 dB. Comparing the two curves shown in Fig. 7.3, it can be seen that the performance of the non-coherent framework does not depend highly on the estimation of the Doppler frequency of the interfering user.

In Fig. 7.4 the SIR_{out} against different δ_C values obtained by using the two frameworks is illustrated. When δ_C moves from 0 to 0.85 the SIR_{out} obtained by the two frameworks moves from 105 dB to SIR_{In} . The SIR_{out} is equal to

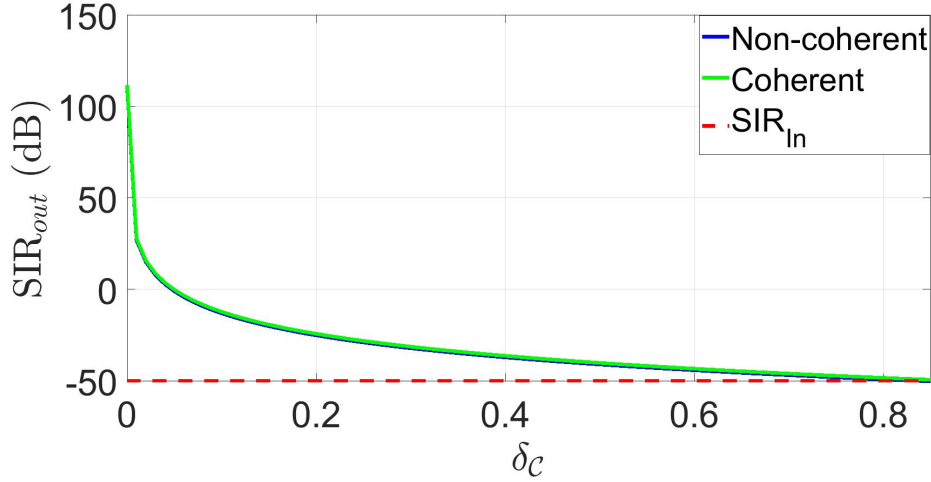


Fig. 7.4. SIR_{out} obtained when both frameworks are applied against the offset amplitude δ_C .

SIR_{In} only when the δ_C is set at the same value of the received amplitude. These curves show that the performance of these two frameworks depends on the estimation amplitude in the same manner.

When the delay is not perfectly estimated the two frameworks cannot be applied. This is due to the fact that in order to apply the IFrFT a perfectly time synchronisation is required. This is the main limitation of the proposed joint radar and communication system has been described in chapter 5.

Interference frameworks based on signal model

In this analysis, the received signal are generated by using the Matlab function while the signal is reconstructed by using the signal model derived in Section 5.1.2. The analysis is carried out considering the same values by $\delta_{\tilde{f}_D}$ and δ_C used in Section 7.3. In Fig. 7.5 the SIR_{out} against the $\delta_{\tilde{f}_D}$ is shown. The two curves shown that a small value of $\delta_{\tilde{f}_D}$ leads to a low SIR_{out} . However, comparing the two curves we can see that the performance of the non-coherent framework is better than those obtained when the coherent subtraction is carried out.

The SIR_{out} versus different values by δ_C is illustrated in Fig. 7.6. The SIR_{out} of the non-coherent framework moves from 1.5 dB to $SIR_{In} = 49.9$ dB, while

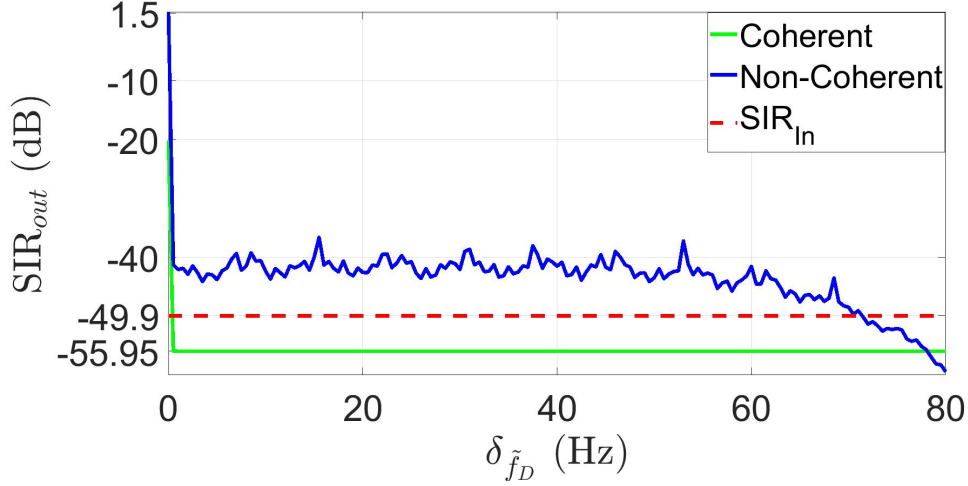


Fig. 7.5. SIR_{out} obtained when both frameworks are applied against the offset frequency $\delta_{\tilde{f}_D}$ considering that the interference signal is reconstructed using the analytical model of the proposed joint radar and communication system.

when the subtraction is carried out in a coherent manner the SIR_{out} moves from -49.9 dB to -20 dB. Comparing Fig. 7.3 and Fig. 7.4 with Fig. 7.5 and Fig. 7.6 we can see that in both cases the performance of the non-coherent

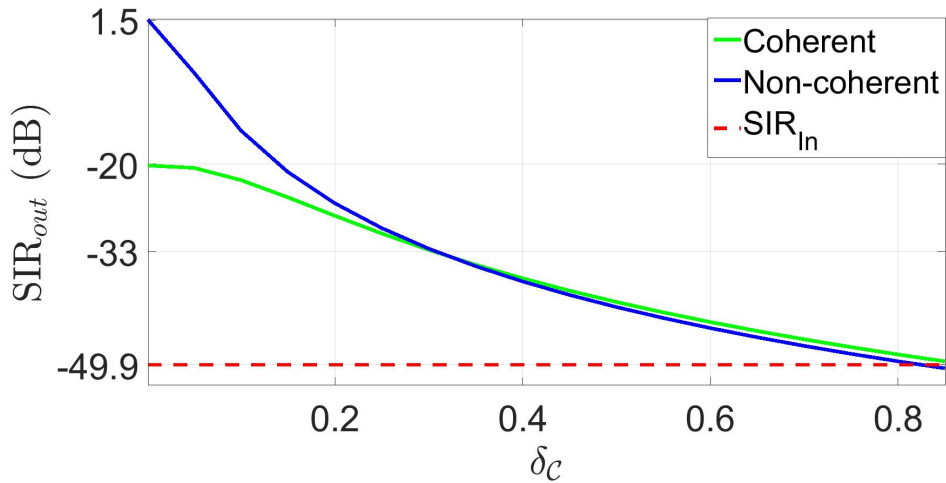


Fig. 7.6. SIR_{out} obtained when both frameworks are applied against the offset amplitude δ_c considering that the interference signal is reconstructed using the analytical model of the proposed joint radar and communication system.

framework is better than to that obtained when the subtraction is carried out in a coherent manner. Additionally, when the interference signal is reconstructed by using the analytical model a drop of the performance is achieved. It is due to the fact that as illustrated in Section 5.1.2, the Mean Square Error of the phase between the two signals is very high.

Finally, comparing the two frameworks we can see that after the coherent framework the phase of the signal is preserved and the framework can work in cases where the interference will saturate the receiver. However, in this Section has been shown that the performance depends highly on the estimated of the Doppler frequency of the interference signal. On the other hand, the non-coherent framework can work even in scenario where the \hat{f}_D is not perfectly estimated. However, this framework can be fail in cases where the interference will saturate the receiver.

In the rest of the chapter the analysis is carried out considering only the non-coherent framework.

7.4 Assessment of non-coherent interference mitigation

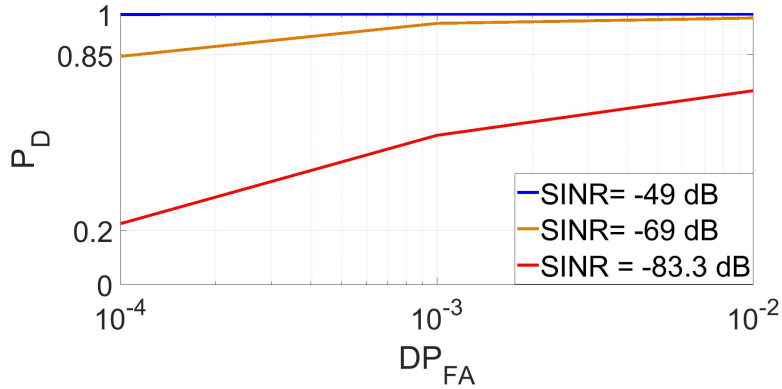
In this Section, in order to assess the interference mitigation impact, the detection performance in terms of ROC curves held in Section 6.5 is repeated when interference is mitigated applying the non-coherent framework. The ROC curves shown in Fig. 7.7 are obtained following two scenarios: when the parameters are estimated and when each parameter is perfectly estimated. The ROC curves obtained from these two scenarios are illustrated in Fig. 7.7a and Fig. 7.7b, respectively.

In Fig. 7.7a is shown that when $\text{SINR}_{\text{radar}}$ moves from -49 dB to -69 dB the detection probabilities move from 0.9 to 1. While when $\text{SINR}_{\text{radar}}$ is -83.3 dB the maximum value of detection probabilities is 0.6 and it is obtained when DP_{FA} is 10^{-2} . These results are obtained in scenario where I_I and $\tilde{\tau}$ are perfectly estimated while $\delta_{\hat{f}_D}$ and δ_C are 143 Hz and 0.002, respectively.

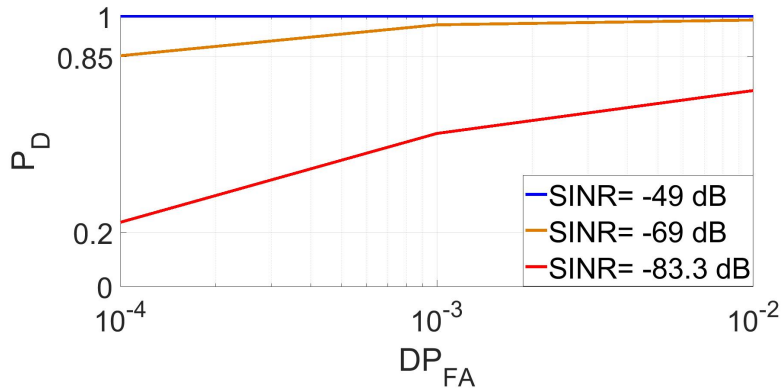
Comparing the ROC curves obtained after interference mitigation, Fig. 7.7a, with those obtained when the interference is present, see Section 6.5, we can

see that $\text{SINR}_{\text{radar}} \in (0, -69)$ before interference mitigation results to $P_D \in (0.1, 1)$ while when the interference has been mitigated P_D moves from 0.9 to 1, while for $\text{SINR}_{\text{radar}} \in (-69, -83.3)$ the P_D before interference mitigation moves from 0 to 0.2 while after interference processing $P_D \in (0.4, 0.7)$. These results shown that when a non-coherent framework is applied an improvement of the detection performance is obtained.

Finally, comparing Fig. 7.7a with Fig. 7.7b we can see that the detection performance obtained when the parameters are estimated is the same to that when the parameters are known.



(a) Using the estimated parameters.



(b) Parameters are perfectly estimated.

Fig. 7.7. ROC curves obtained after interference mitigation, where in 7.7a each parameter is estimated, while in 7.7b the parameters are perfectly estimated

7.5 Non-Coherent Interference Mitigation On Simulated Signal

In this Section, the performance is assessed by means of simulated interference signals. The analysis is carried out by considering PSD and spectrogram representation. The performance is quantified by considering that the radar receives only the signal sent from the interference user meaning that the received signal contains no target information, but only the interference signal. The system parameters are listed in Table 7.1. These parameters are detailed in Section 5.1. Where $G_{ch_{Radar}}$ and $G_{ch_{Int}}$ are the gains of the radar and interference channel respectively, while $G_{ch_{Receive}}$ is the gain of the receive channel. The length of the radar waveform, X_α is 0.39 ms while the CPI is 0.0786 s, the order α of the FrFT is 0.5 and a BFSK encoding is used. These parameters have been chosen to obtain a low computational cost. A carrier frequency of 2 GHz is chosen to provide comparison with the experimental results in Sections 7.6. The received radar signal is

$$\mathfrak{J}_{rx}(u) = I_{\alpha_I}(u - \tilde{\tau})e^{j2\pi\tilde{f}_D u} \quad (7.3)$$

Table 7.1: System Parameters for a low computational cost

Parameters	Description	Values
f_c	Operating Frequency.	2 GHz
N_b	Number of bits.	9
G_g	Random bits.	1
N_s	Number of samples per symbols.	4
F_s	Sampling Frequency.	1 MHz
β	Roll off factor.	0.95
S	Filter Span in Symbols.	24
R_s	Output Samples per Symbols.	13
L_p	Length of PN Sequence.	7
f_{sep}	Frequency separation.	8 KHz
PN sequence	Primitive Polynomial.	z^3+z^2+1
$G_{ch_{Radar}}$	Radar Transmit Gain Value.	10 dB
$G_{ch_{Inter}}$	Interference Transmit Gain Value.	55 dB
$G_{ch_{Receive}}$	Receive Gain Value	30 dB

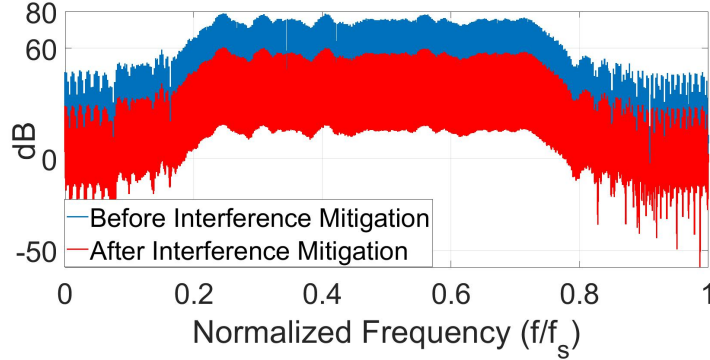


Fig. 7.8. Power Spectral Density of the simulated signal before and after interference mitigation.

where I_{α_I} is interference signal with order $\alpha_I = 0.4$, $\tilde{\tau}$ is set at zero, and \tilde{f}_D is set at 100 Hz. The reconstructed signal is

$$\hat{\mathcal{J}}_{rec}(u) = \hat{I}_{\alpha_I}(u - \hat{\tau})e^{j2\pi\hat{f}_D u} \quad (7.4)$$

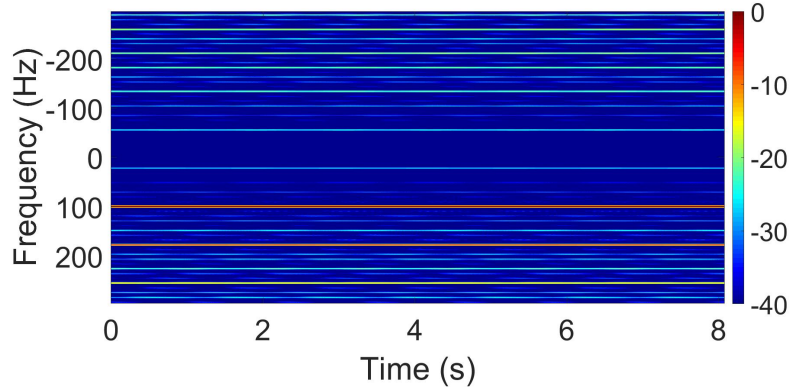
The time delay and amplitude are perfectly estimated while \hat{f}_D is 100.12 Hz. The PSDs of (7.3) and (7.4) are

$$S_{rr}(f) = |\mathfrak{F}(\mathcal{J}_{rx}(u))|^2 \quad (7.5)$$

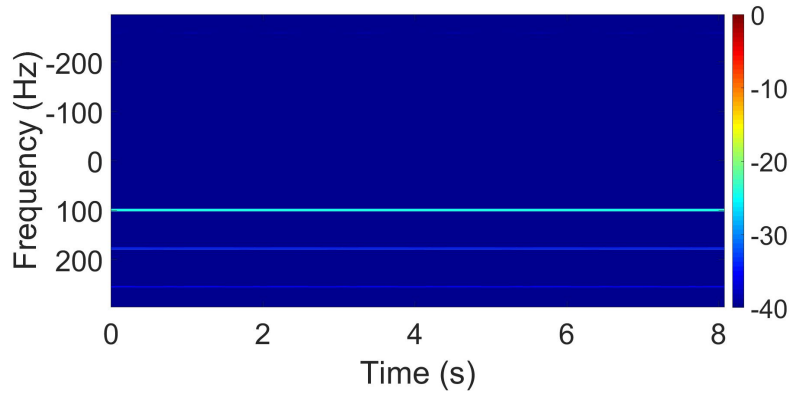
$$\tilde{S}_{rr}(f) = |\mathfrak{F}(\hat{\mathcal{J}}_{rec}(u))|^2 \quad (7.6)$$

In Fig. 7.8 the PSDs obtained before and after interference mitigation are illustrated. The PSD before interference mitigation is obtained by (7.5) where the maximum and mean values are 79 dB and 50.31 dB, respectively. In order to decrease these values the non-coherent interference framework is applied. In other word, a subtraction between (7.5) and (7.6) is carried out. After this process, the interference has been mitigated and the maximum and minimum values are 61 dB and 34.31 dB, respectively. Comparing the two plots shown in Fig. 7.8 it can be seen that the maximum value has been decreased by 18 dB and the mean by 16 dB.

The spectrograms shown in Fig.7.9 are obtained by following these process: the range bins are summed and then a STFT is applied in slow-time. The



(a) $\alpha = 0.2$



(b) $\alpha = 0.4$

Fig. 7.9. Spectrograms of the received signal 7.9a before and 7.9b after interference mitigation. The figures are normalized with the respect to the maximum values obtained by 7.9a.

range bins are obtained by filtering the interference signal, (7.3), with a filter matched to the radar signal $X_\alpha(u)$. The spectrograms are generated by using a Hamming window of length 0.742 seconds and 99% overlap.

The spectrogram obtained applying the STFT on the received signal is shown in Fig. 7.9a, where a strong frequency component, see at 100 Hz, is present due to the interfering signal. While the spectrogram shown in Fig. 7.9b is obtained when the interference is mitigated. The maximum value of the spectrogram after the interference mitigation is 22.6 dB below the maximum value obtained before that the interference is mitigated.

In this Section, it has been shown that after the interference mitigation the

mean power has significantly reduced, see Fig. 7.8. This means, that in multi user scenarios, interference mitigation leads to an improvement in terms of estimation radar parameters. Additionally, in Fig. 7.9 it is also demonstrated that the same processing can be applied to obtain an improvement on time frequency analysis. In an automotive environment, where more than one user wants to use the same channel at the same time, the proposed interference mitigation framework leads to an improvement in terms of estimation radar performance, as range, Doppler frequency, and time frequency analysis.

7.6 Non-Coherent Interference Mitigation on Real Signal

In this Section, the performance of the non-coherent framework is evaluated on real data. The real data are acquired in a controlled laboratory environment and the acquisition geometry is illustrated in Fig. 7.10. The monostatic radar is placed at bottom left, the interference users at the top right and the orange area indicates where a person is walking towards and away from the radar to generate a Doppler signal. The distance R_{Int} is 1.80 m. The analysis is performed following three scenarios. In the first scenario, the

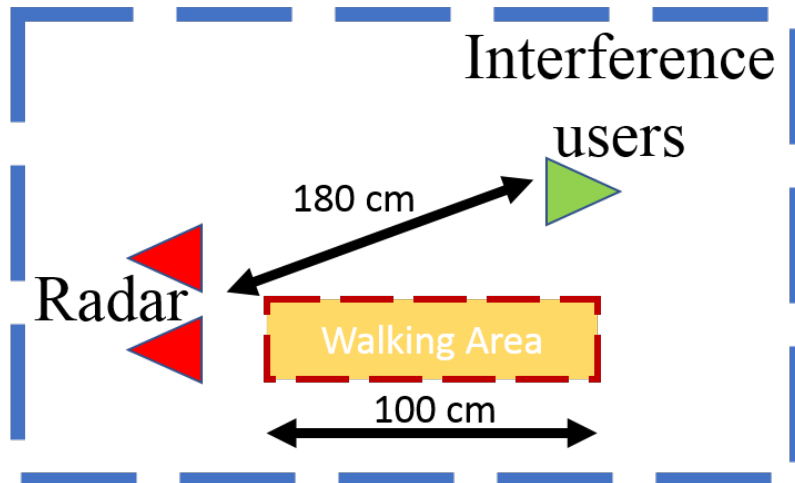


Fig. 7.10. Acquisition geometry of the laboratory-based experimental campaign.

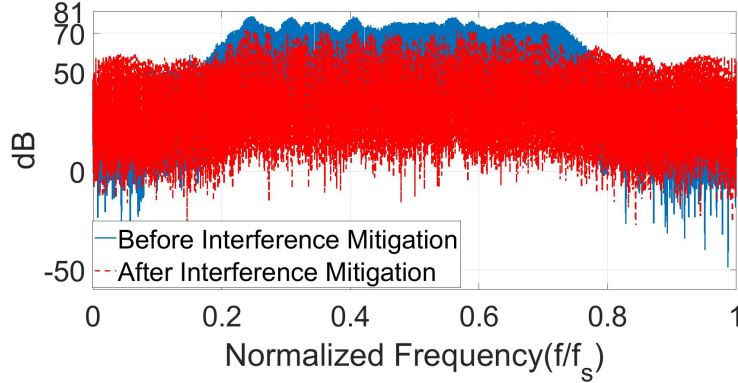


Fig. 7.11. Power Spectral Density of the real signal before and after interference mitigation.

transmitter of the radar is switched off, while in the second scenario and third scenarios the transmitter is switched on and one and two interference users are present, respectively. In this experimental the same parameters presented in Section 7.5 are used.

A single interfering user

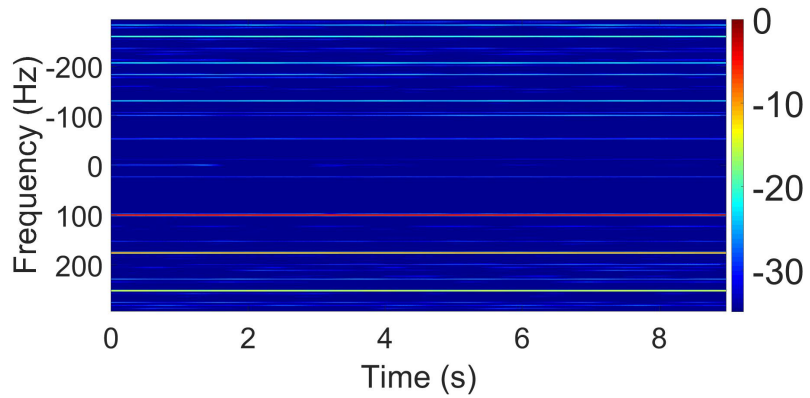
When the transmitter is switched off, the received signal interference is

$$y(u) = \mathfrak{J}_{rx}(u) + n(u) \quad (7.7)$$

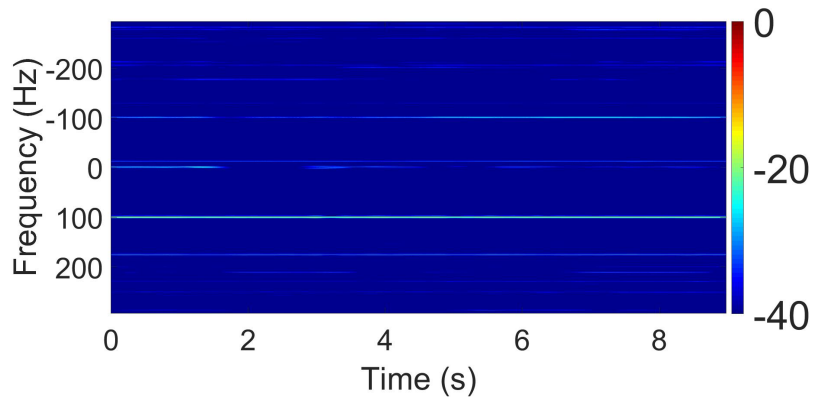
where $\mathfrak{J}_{rx}(u)$ is obtained by (7.3) while $n(u)$ is the noise, where the mean value is -40 dB. In this analysis, δ_c and $\delta_{\tilde{f}_D}$ are 0.007 and 0.12 Hz, respectively, while the delay is perfectly estimated.

The PSD obtained from the received signal (7.7) and that obtained after interference mitigation are shown in Fig. 7.11. The maximum and mean values of the PSD obtained before interference mitigation are 78.89 dB and 49.89 dB respectively. While when the interference has been alleviated the maximum values is decreased by 7 dB and the mean by 8 dB.

The spectrograms shown in Fig. 7.12 are obtained when the target is not present and the same processing and parameters as described in Section 7.5 are applied. Comparing Fig.7.12a with Fig. 7.12b we can see that the intensity at 100 Hz is decreased by 20.9 dB.



(a) $\alpha = 0.2$



(b) $\alpha = 0.4$

Fig. 7.12. Spectrograms of the received signal 7.12a before and 7.12b after interference mitigation. The figures are normalized with the respect to the maximum values obtained by 7.12a.

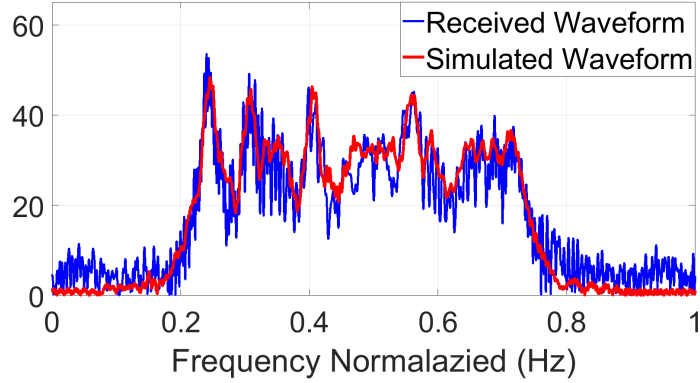


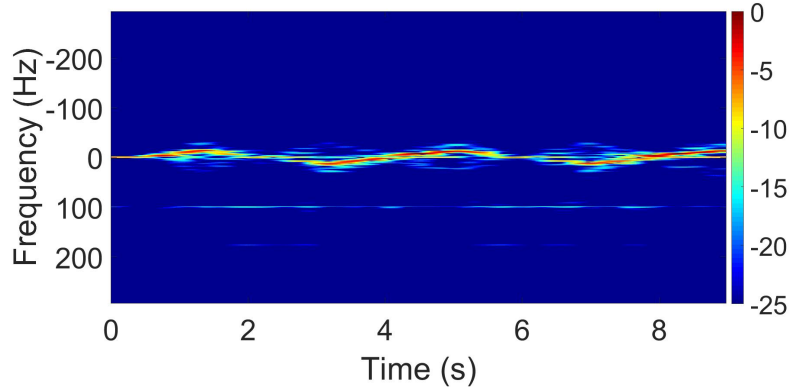
Fig. 7.13. Spectrum of the received and simulated signal.

Comparing the results from the laboratory data with those from the simulated signal (see Section 7.5 and Section 7.6), it can be seen that lower interference reduction is achieved. Particularly, comparing the PSD in Fig. 7.8 and Fig. 7.11 it is noted that for the simulation signal the mean and maximum of the interference is reduced by 16 dB and 18 dB while for the real signal a reduction of 7 dB and 8 dB is obtained, respectively. Furthermore, comparing the spectrograms in the maximum reduction of the interference in the simulated signal is 22.6 dB, while for the real signal the same value is 20.9 dB.

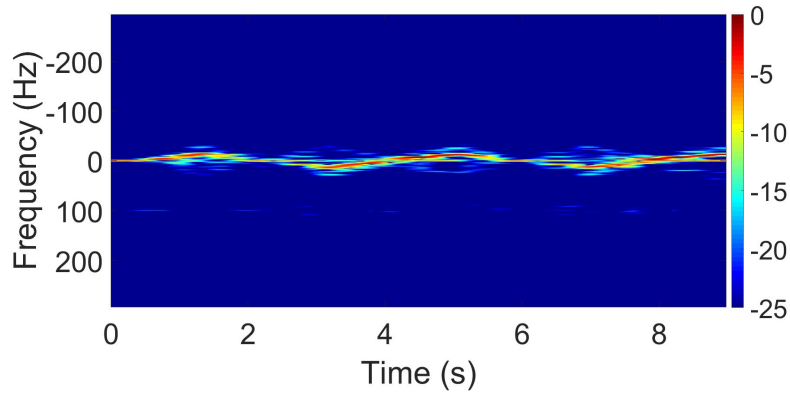
In order to justify this drop in performance, the spectrum of the received and simulated signal are examined in Fig. 7.13. Comparing these two plots we can see that the spectra of the two signals are not the same. The difference is due to hardware impurities and non linearities. In order to increase the performance it is necessary to solve the mismatch between the real and reconstructed signal. A possible solution would be that to determinate the impulse response of the hardware and then pass the reconstructed signal from a filter with the same impulse response to account for the non linearities and make it more similar to the received signal.

Target plus a single interfering user

In this analysis, the non-coherent framework is applied when the transmitter radar is on and a person is walking towards the radar. The spectrograms



(a) $\alpha = 0.2$



(b) $\alpha = 0.4$

Fig. 7.14. Spectrograms of the signal scattered by a person 7.14a before and 7.14b after interference mitigation. The figures are normalized with the respect to the maximum values obtained by 7.14a.

obtained in this scenario are shown in Fig. 7.14. The spectrograms are obtained as described in Section 7.5. In Fig. 7.14a the Doppler due to the interference user (see 100 Hz) and mD signature are present. While the spectrogram obtained after the interference mitigation is shown in Fig. 7.14b. Comparing Fig. 7.14a with Fig. 7.14b we can see that the mD signature of the target remains unchanged while the contribution from the interference user has been decreased by 4 dB.

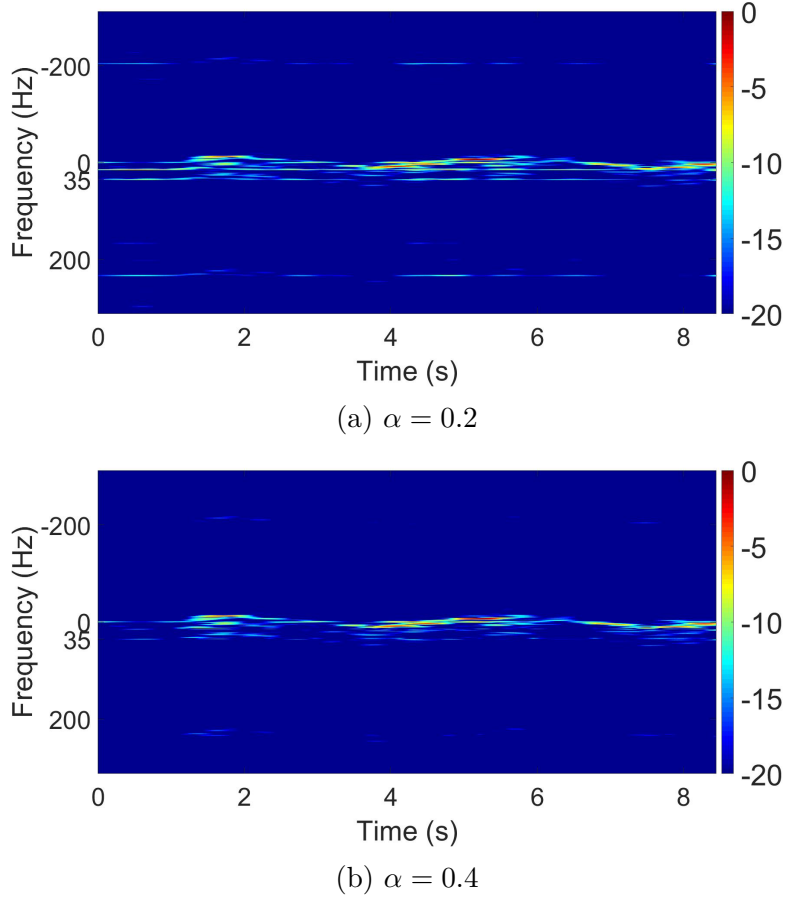


Fig. 7.15. Spectrograms of the signal scattered by a person 7.15a before and 7.15b after interference mitigation. The figures are normalized with the respect to the maximum values obtained by 7.15a.

Target plus two interfering users

In this analysis, the non-coherent framework is applied on received radar signal which is given by the echoes scattered by a person plus two interference signals and noise. The interference signals plus noise can be written as:

$$\mathcal{J}_{rx}(u) = \mathcal{C}_1 I_{1,\alpha_1}(u - \tilde{\tau}_1) e^{j2\pi \tilde{f}_{D,1} u} + \mathcal{C}_2 I_{2,\alpha_2}(u - \tilde{\tau}_2) e^{j2\pi \tilde{f}_{D,2} u} + n(u) \quad (7.8)$$

where I_{1,α_1} and I_{2,α_2} are the interference signal with two different orders, $\alpha_1 = 0.5$ and $\alpha_2 = 0.6$, while $f_{D,1}$ and $f_{D,2}$ are setting at 15 Hz and 35.5 Hz, while the noise is the same to that presents in Section 7.6. The delay is

Table 7.2: Maximum values before interference mitigation

Frequencies (Hz)	Values (dB)
15	-5
35.5	-8

Table 7.3: Maximum values after interference mitigation

Frequencies (Hz)	Values (dB)
15	-15
35.5	-16

perfectly estimated while the $\delta_{\hat{f}_D}$ are -0.18 Hz -0.63 Hz.

The spectrograms shown in Fig. 7.15 are generated by using the same parameters used in Section 7.5. The spectrogram obtained from the received signal is shown in Fig. 7.15b where Doppler due to the interference users (see 15 Hz and 35.5 Hz) and mD signature are present. While the spectrogram shown in Fig. 7.15a is obtained when the interference is alleviated. Comparing the two spectrograms shown in Fig. 7.15 we can see that the mD signature of the target remains unchanged and strong interference are decreased. The maximum values before and after interference mitigation are given in Table 7.2 and Table 7.3, respectively. Comparing Table 7.2 with Table 7.3 we can see that the maximum values of interference are decreased by 10 dB and 7 dB. In order to increase the performance it is necessary to solve the problem of the hardware impurities presented.

7.7 Conclusion

In this chapter two novel FrFT based interference mitigation methods for automotive environment have been presented. In these two frameworks, the interference is reconstructed and then mitigated by the return radar signal. In the first framework, the interference is mitigated applying a coherent subtraction between the received signal and reconstruct interference signal. In the second framework, the subtraction is carried out in a non-coherent manner. The performance of these two frameworks has been evaluated in

terms of SIR_{out} against different values of offset frequency and amplitude. The results have shown that when the coherent subtraction is carried out the performance is highly depend on the estimation of the Doppler frequency. For an offset value by 15 Hz a drop by 132 dB has been obtained. On the other hand, the results have shown that when the subtraction is carried out in a non-coherent manner, the performance is not highly depend on the estimation of the Doppler frequency. Additionally, the SIR_{out} obtained for different values of offset amplitude when the coherent framework has been applied is very similar to that obtained when the non-coherent framework has been applied. Moreover, the performance of the two frameworks is evaluated even when the interference has been reconstructed using the analytical model. Those results have showed that for a small value of offset a drop by SIR_{out} has been achieved. Consequently, the non-coherent framework works even in scenario where the Doppler frequency of the interference signal is not perfectly estimated.

The non-coherent framework has been successfully validated using an SDR device, and its performance has been evaluated in the absence and presence of the return radar signal. In the first cases, the performance is evaluated by considering a simulated and real signal, where the real signal is acquired in a controlled laboratory environment. In both cases, the offset frequency is 0.12 Hz, the separation between two order of the FrFT is 0.1 and has been shown that the interference is decreased. Finally, the framework is analysed considering two scenarios. In the first the target and one interference user are present, while in the second scenario, a target and two interference users are present. In both scenarios, it has been shown that the interference is decreased while the mD signature does not change. The non-coherent framework can be fail in cases where the interference will saturate the receiver.

The main advantage of these two frameworks is the capability to mitigate the mutual radar interference reconstructed the received radar signal. This means that on the transmitter side, no additional processing is required. These two frameworks are two main disadvantages. The first disadvantage is that the capability to mitigate the interference depends on the accuracy of the estimated parameters. While the second is due to the fact that the radar processing is applied only after the interference has been alleviated. This

Chapter 7. Interference Mitigation Strategies for the proposed system

means that a target close to the radar cannot be detected very fast and it is most dangerous. In order to avoid this issue, the idea should be to apply the radar processing twice. In the first time, the targets close to the main can be detected, and then the interference can be mitigated to detect the target that are fairway to the radar.

To conclude in this chapter two interference frameworks have been introduced and their performance have been evaluated. As the results have shown the non-coherent frameworks fits better for an automotive scenarios due to its capability that the performance was not depend highly on the estimation of the Doppler frequency.

Chapter 8

Conclusion and Future work

In this thesis, a new joint radar and communication system, based on the fractional Fourier transform (FrFT) for automotive applications, was presented. So considering its related framework, the FrFT was used to embed data information into a radar waveform allowing a joint radar communication system, where the radar performance does not depend highly on the transmitted data. In order to allow more than one user in the same frequency band a fractional order division multiplexing was proposed. In multi user scenarios, mutual radar interference, caused by other users that share the same frequency band at the same time, can be prevented only if each users has to transmit waveforms that are uncorrelated with those of other users. Due to spectrum limitations, when the number of users increase the uncorrelated property cannot be satisfied even by using fractional order division multiplexing. So it can lead to a degradation of the radar and communication performance and, in order to alleviate such an interference, two frameworks for interference mitigation were presented and described.

In chapter 2 an extensive research review was presented, dedicated to a number of very important aspects of the modern radar systems. Key areas, such as basic radar concepts and advanced radar techniques were discussed, mainly, focused on the radar waveform and pulse compression through signal processing techniques. In addition, the design automotive radar waveform was introduced and illustrated. The importance of the radar waveform for automotive environment was discussed and different types of waveforms were

presented.

In chapter 3 the basic concepts of time-frequency (T-F) analysis were discussed in connection with the commonly used tools associated with it. Moreover, the importance of the Ambiguity Function (AF) for radar signal processing was discussed by highlighting its significant properties. In particular the AF of an LFM was presented. In addition, the definition of the Short-Time-Frequency-Transforming (STFT) and Power Spectral Density (PSD) were given. In last part of the chapter, the FrFT was extensively presented. The notion of fractional domain and the FrFT were discussed included the FrFT properties, implementations (i.e. discrete and fast approximation) and application in signal and communication processing.

In chapter 4 a review of joint radar and communication system was presented. The reviewed frameworks are grouped in five different groups. The common base of these different frameworks was that everyone has been used to provide radar and communication functions, to run simultaneously using the same hardware and sharing the same spectrum. As in multi users scenarios where more than one user is located in the same frequency band, the issue of mutual radar interference may arise leading to a degradation of the detection and communication performance. Thus, in last part of the chapter a review of the frameworks to alleviate the mutual interference for radar and communication system was presented.

In chapter 5, a novel joint radar and communication system based on the FrFT for automotive environment was presented. The proposed waveform was transmitted similar to an FCLFM as presented in chapter 2. The core of the transmitter waveform was the FrFT. It was used to embed data information, directly, in the radar waveform allowing to radar and communication functions to run simultaneously using the same hardware and both functions share the same frequency. The standard radar processing was applied on the signal scattered by the targets. This processing was not applied on the pilot sequence which was only used to perform the synchronisation. On the other side, the core of the communication receiver was the Inverse FrFT (IFrFT), which was used to rotate the received signal in baseband and then the inverse communication functions were applied to recover the data information that was embedded in the received signal. However, the IFrFT could be applied

profitably only when the time signal start was estimated correctly. In order to do this, a synchronisation process was presented. In the proposed system a fractional order division multiplexing was implemented, where a specific order of the FrFT was assigned to each users. Finally, the mathematical model of the proposed waveform for two encoding schemes as BFSK and BPSK was carried out, and it was compared in terms of Mean Square Error (MSE) of the amplitude and phase with which it was obtained by applying a discrete fractional Fourier transform.

In chapter 6 the radar and communication performance of the proposed joint radar and communication system were presented. The results obtained by the Ambiguity Function have shown that, when the BFSK encoding was used the radar performance appeared similar to the one obtained when an LFM pulse was transmitted. On the other hand, when the bits are mapped through the BPSK encoding, the radar performance was highly depending on the data information. Consequently, in an automotive environment, the BFSK encoding was fitted better for a joint radar and communication system based on the FrFT. Additionally, the simulation analysis was shown applying a fractional order division multiplexing it was possible to allocate two users in the same frequency band. Additionally, the simulation analysis has shown that by applying a fractional order division multiplexing, it is possible to allocate two users in the same frequency band without degrading the radar performance. The minimum difference between two orders of the FrFT preventing the radar performance to be degraded, can be obtained through the maximum value of the correlation between two waveforms, that is equal to the maximum value of the side lobe levels. Moreover, the proposed system was able to distinguish the targets in a range and in a Doppler frequency. However, in multi users scenarios the mutual radar interference was arisen also considering the multiplexing fraction techniques. Finally, the communication performance illustrated the capability of the proposed system to share information with other users.

In chapter 7 two interference mitigation frameworks based on a joint radar and communication system were presented. In the first framework, the subtraction between the reconstructed interference signal and the received radar signal was carried out in a coherent manner. While in the second framework,

the subtraction was carried out in a non-coherent manner. The performance of these two frameworks was assessed considering the SIR_{out} obtained when the interference was mitigated by using both frameworks. The results have shown that, when a coherent subtraction was carried out the performance depended highly on the estimation of the Doppler frequency. While, when the non-coherent framework was used, the performance did not depend highly on the estimation of the Doppler frequency. Finally, the performance of the non-coherent framework was assessed on the real signal, whereas a human target was also presented.

8.1 Future Work

In the presented work there are several topics worthy of future research. The drawbacks of the proposed system to embed data information into radar waveform are the following: a low bit/rate is achieved, synchronisation between the transmitter and receiver, and due to the fact that this system uses the FrFT, so it is necessary to estimate the time where the received communication signal starts.

The drawback related to the low bit/rate is presented due to the following aspects. The first aspect, it is that on the radar side, in order to increase the SNR, a coherent processing has been applied. So this means that the phase of the signals for a single CPI has to be the same. Due to the fact that the data are embedded in the radar waveform, in order to keep the phase constant in a single CPI, the same information bits have to be embedded. The second aspect is that in order to allocate more than one user in the same frequency band, a multiplexing fractional order is proposed. In this way, at each user a different order of the FrFT is assigned, this means that each users can use a single sub-carrier, rather than more than one as in OFDM or in Co-radar system. The future work may interest to analyse the radar performance when a non-coherent processing is applied, in this way it should be not necessary to embed the same data information in every CPI, but in the same waveform different data can be embedded. In addition, to allocate more than one user in the same frequency band, a different strategy may be proposed such that

a single user could use more than one sub-carriers.

The drawback related of the synchronisation in the proposed system is solved, by transmitting a sequence pilot and it is transmitted at the beginning of some CPIs. It is not transmitted at every CPI, due to the fact that the radar processing cannot be applied on it. However, when the pilot sequence is not transmitted a new user cannot demodulate the received data. In other words, this means that, when a new user shares the channel it can transmit the data information to other users, but cannot demodulate the received information, until the synchronisation has not been carried out. In the future work it could be interesting to analyse this issue and to find some solution such as the radar processing can be applied also on the sequence pilot. In this way, the pilot sequence can be transmitted at the beginning of every CPI and/or embed at the half duration of the CPI.

Last drawback of the proposed system is related to the FrFT. As mentioned in chapter the IFrFT can be applied in a correct way only, if the time where the received signal starts is, exactly, known with. In this research, this issue is solved selecting an opportunity pilot sequence, but in real scenario it is not easy to estimate parameters without some errors. In the future it could be interesting to find some techniques to avoid this aspect. Finally, in last part of this chapter the analytical model of the proposed waveform has been derived. It has been obtained without taking into account the RRC filter, so in the future it could be interesting to obtain the signal model considering the RRC filter, too.

The radar performance of the proposed system shows that when a BFSK is used to encode the data information into a sample, the radar performance does not depend highly on data information, but when a BPSK is used the radar performance depends on the bits information embedded in the radar waveform. However, the BPSK encoding is a very basic technique used in several wireless standards. It is considered to be more robust among all the modulation types, due to the difference of 180 degrees between two constellation points. In the future work it could be interesting to find some types of waveform based on the FrFT so that the BPSK encoding scheme can be used without to degrade the radar performance. In multi users scenarios, the targets are detected applying a CA-CFAR. It is used, because it is easy to implement.

In the future a more sophisticated CFAR technique could be applied. The communication performance has shown the ability of the proposed system to share information with other users. However, the results in terms of BER have shown that to obtain a low BER a high SINR and/or SNR is required. In an automotive environment, where more than one user shares the same channel, it is not easy to have a high SINR, consequently the BER is high. In the future work it could be interesting to apply some techniques, such that to decrease the BER.

In order to mitigate the mutual radar interference, in both frameworks the interference signal is reconstructed and then a subtraction between the received and reconstructed one is carried out. The main difference is that the subtraction is carried out in a coherent and non-coherent manner. The main drawback of both the frameworks is that the performance, in terms of the gain obtained after the processing, depends on the estimation of some parameters as Doppler frequency, delay, and amplitude. In the future work it could be interesting to realise how to increase the estimation of these parameters. In addition, when the reconstructed signal is obtained, by applying the analytical model, the gain in terms of the ratio between the SINR before and after interference mitigation is very low. It is due to the fact that the signal model is not equal to that one obtained when a Fast FrFT algorithm is used. In the future work, it can be improved; in this way the processing to reconstruct the signal will become faster. Finally, if the hardware introduces some non-linearity or impurity before the subtraction, the reconstructed signal has to be passed through it. In this research it has not been achieved, so after the interference mitigation processing some interferent components are still acting. In the future work the impulse response of the hardware may be taken into account and before the subtraction the reconstructed signal may pass through a filter, that has obtained the same impulse response of the hardware.

Appendix A

Design of signal-sharing for radar and communication

The proposed non-coherent interference mitigation framework is implemented by means of a SDR device, namely the National Instruments Universal Radio Peripheral (NI-USRP) 2943R. It has four in-phase and quadrature (IQ) channels, two receivers and two transmitters/receivers, and its working frequency range between 1.2 GHz and 6.6 GHz. It is used with three wideband LB-2675-15 multi octave horn antennas produced by A-Info. The maximum I/Q sample rate of the transmitter and receiver are both equal to 200 *MSs*. The resolution and Spurious-free dynamic range (sFDR) of the Digital-to-Analog Converter (DAC) are 16 bit and 80 dB, respectively. While the Resolution and sFDR of the Analog-to-Digital Converter (ADC) are 14 bit and 88 dB, respectively. The processed architecture design is illustrated in Fig. A.1. The SDR is used to transmit and receive the signals. Matlab is used to generate the waveforms, while the GNU Radio is used to read the file from Matlab and forwards the signal to the USRP. In this architecture, each user uses a different channel. When the antenna receives the signals, the GNU Radio reads the signal from the USRP and saves the sample in a file. Finally the processing is carried out in Matlab.

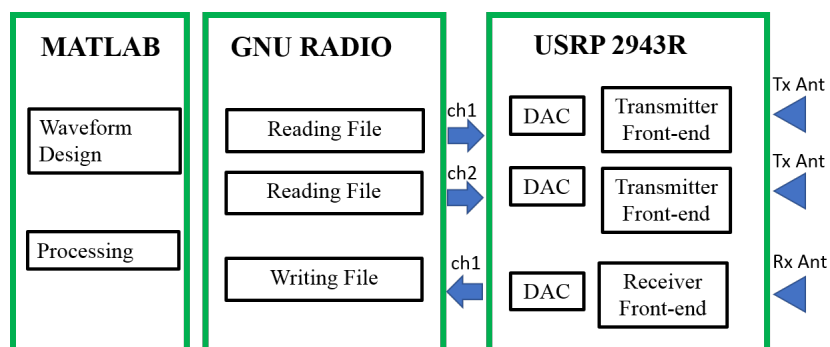


Fig. A.1. Architecture design.

References

- [1] (2013). *79 GHz : towards Vehicle and Road Automation development*.
- [2] Ahmed, A., Zhang, Y. D., and Himed, B. (2018). Multi-user dual-function radar-communications exploiting sidelobe control and waveform diversity. In *2018 IEEE Radar Conference (RadarConf18)*, pages 698–702.
- [3] Amein, A. S. and Soraghan, J. J. (2005). A new chirp scaling algorithm based on the fractional fourier transform. In *IEEE Signal Processing Letters*, volume 12, pages 705–708.
- [4] Bechter, J., Biswas, K. D., and Waldschmidt, C. (2017). Estimation and cancellation of interferences in automotive radar signals. In *2017 18th International Radar Symposium (IRS)*, pages 1–10.
- [5] Bechter, J., Eid, K., Roos, F., and Waldschmidt, C. (2016a). Digital beamforming to mitigate automotive radar interference. In *2016 IEEE MTT-S International Conference on Microwaves for Intelligent Mobility (ICMIM)*, pages 1–4.
- [6] Bechter, J., Sippel, C., and Waldschmidt, C. (2016b). Bats-inspired frequency hopping for mitigation of interference between automotive radars. In *2016 IEEE MTT-S International Conference on Microwaves for Intelligent Mobility (ICMIM)*, pages 1–10.
- [7] Bechter, J., Sippel, C., and Waldschmidt, C. (2016). Bats-inspired frequency hopping for mitigation of interference between automotive radars. pages 1–4.

References

- [8] Blunt, S. D., Cook, M. R., and Stiles, J. (2010a). Embedding information into radar emissions via waveform implementation. In *2010 International Waveform Diversity and Design Conference*, pages 195–199.
- [9] Blunt, S. D., Yatham, P., and Stiles, J. (2010b). Intrapulse radar-embedded communications. In *IEEE Transactions on Aerospace and Electronic Systems*, volume 46, pages 1185–1200.
- [10] Blunt, S. D., Yatham, P., and Stiles, J. (2010c). Intrapulse radar-embedded communications. In *IEEE Transactions on Aerospace and Electronic Systems*, volume 46, pages 1185–1200.
- [11] Brigham and Oran, E. (1974). *The fast Fourier transform*. Englewood Cliffs, N.J. : Prentice-Hall.
- [12] Bultheel, A. and Sulbaran, H. E. M. (2004). Computation of the fractional fourier transform. In *Applied Computational Harmonic Analysis*, volume 16, pages 182–202.
- [13] Cabric, D., O’Donnell, I. D., Chen, M. S. ., and Brodersen, R. W. (2006). Spectrum sharing radios. In *IEEE Circuits and Systems Magazine*, volume 6, pages 30–45.
- [14] Cager, R., LaFlame, D., and Parode, L. (1978). Orbiter ku-band integrated radar and communications subsystem. In *IEEE Transactions on Communications*, volume 26, pages 1604–1619.
- [15] Cariolaro, G., Erseghe, T., Kraniuskas, P., and Laurenti, N. (1998). A unified framework for the fractional fourier transform. *IEEE Transactions on Signal Processing*, 46(12):3206–3219.
- [16] Charvat, G. (2014). *Small and Short Range Radar Systems*. Taylor & Francis Group.
- [17] Chen, S., Zhang, S., Zhao, H., and Chen, Y. (2015). A new chirp scaling algorithm for highly squinted missile-borne sar based on frft. In *IEEE Journal of Selected Topics in Applied Earth Observations and Remote Sensing*, volume 8, pages 3977–3987.

References

- [18] Chen, V. C., Li, F., Ho, S. ., and Wechsler, H. (2006). Micro-doppler effect in radar: phenomenon, model, and simulation study. In *IEEE Transactions on Aerospace and Electronic Systems*, volume 42, pages 2–21.
- [19] Chen, X., Wang, X., Xu, S., and Zhang, J. (2011). A novel radar waveform compatible with communication. In *2011 International Conference on Computational Problem-Solving (ICCP)*, pages 177–181.
- [20] Cheng, L., Henty, B. E., Stancil, D. D., Bai, F., and Mudalige, P. (2007). Mobile vehicle-to-vehicle narrow-band channel measurement and characterization of the 5.9 ghz dedicated short range communication (dsrc) frequency band. In *IEEE Journal on Selected Areas in Communications*, volume 25, pages 1501–1516.
- [21] Choi, J., Va, V., Gonzalez-Prelcic, N., Daniels, R., Bhat, C. R., and Heath, R. W. (2016). Millimeter-wave vehicular communication to support massive automotive sensing. In *IEEE Communications Magazine*, volume 54, pages 160–167.
- [22] Clemente, C., Ilioudis, C., Gaglione, D., Thompson, K., Weiss, S., Proudler, I., and Soraghan, J. J. (2014a). Reuse of fractional waveform libraries for mimo radar and electronic countermeasures. In *2014 6th International Symposium on Communications, Control and Signal Processing (ISCCSP)*, pages 505–508.
- [23] Clemente, C., Shorokhov, I., Proudler, I., and Soraghan, J. J. (2014b). Radar waveform libraries using fractional fourier transform. In *2014 IEEE Radar Conference*, pages 855–858.
- [24] Clemente, C. and Soraghan, J. J. (2010a). Fractional range doppler algorithm for sar imaging. In *The 7th European Radar Conference*, pages 248–251.
- [25] Clemente, C. and Soraghan, J. J. (2010b). Fractional rda and enhanced frcsa for sar imaging. In *Sensor Signal Processing for Difence (SSPD 2010)*, pages 1–5.

References

- [26] Clemente, C. and Soraghan, J. J. (2010c). Range doppler sar processing using the fractional fourier transform. In *11-th INTERNATIONAL RADAR SYMPOSIUM*, pages 1–4.
- [27] Corazza, G. E., Ferrarelli, C., and Vatalaro, F. (1994). A rice-lognormal terrestrial and satellite channel model. In *Proceedings of 1994 3rd IEEE International Conference on Universal Personal Communications*, pages 155–159.
- [28] Cui, G., Li, H., and Rangaswamy, M. (2014). Mimo radar waveform design with constant modulus and similarity constraints. In *IEEE Transactions on Signal Processing*, volume 62, pages 343–353.
- [29] Devlin, C. A., Zhu, A., and Brazil, T. J. (2008). Peak to average power ratio reduction technique for ofdm using pilot tones and unused carriers. In *2008 IEEE Radio and Wireless Symposium*, pages 33–36.
- [30] Dokhanchi, S. H., Shankar, M. R. B., Stifter, T., and Ottersten, B. (2018). Ofdm-based automotive joint radar-communication system. In *2018 IEEE Radar Conference (RadarConf18)*, pages 902–907.
- [31] Donnet, B. J. and Longstaff, I. D. (2006a). Combining mimo radar with ofdm communications. In *2006 European Radar Conference*, pages 37–40.
- [32] Donnet, B. J. and Longstaff, I. D. (2006b). Combining mimo radar with ofdm communications. In *2006 European Radar Conference*, pages 37–40.
- [33] Engels, M. (2002). *Wireless OFDM Systems: How to Make Them Work*. Boston, MA: Kluwer Academic.
- [34] Erseghe, T., Laurenti, N., and Cellini, V. (2005). A multicarrier architecture based upon the affine fourier transform. In *IEEE Transactions on Communications*, volume 53, pages 853–862.
- [35] Euzière, J., Guinvarc’h, R., Lesturgie, M., Uguen, B., and Gillard, R. (2014). Dual function radar communication time-modulated array. In *2014 International Radar Conference*, pages 1–4.

References

- [36] Farhang, A., RezazadehReyhani, A., Doyle, L. E., and Farhang-Boroujeny, B. (2018). Low complexity modem structure for ofdm-based orthogonal time frequency space modulation. In *IEEE Wireless Communications Letters*, volume 7, pages 344–347.
- [37] Farina, A., De Maio, A., and Haykin, S. (2017). *The impact of cognition on radar technology*. Electromagnetics and radar. Institution of Engineering and Technology, Stevenage.
- [38] Fischer, C., Blöcher, H. L., Dickmann, J., and Menzel, W. (2015). Robust detection and mitigation of mutual interference in automotive radar. In *2015 16th International Radar Symposium (IRS)*, pages 143–148.
- [39] Franken, G. E. A., Nikookar, H., and Genderen, P. V. (2006). Doppler tolerance of ofdm-coded radar signals. In *2006 European Radar Conference*, pages 108–111.
- [40] Friis, H. T. (1946). A note on a simple transmission formula. In *Proceedings of the IRE*, volume 34, pages 254–256.
- [41] Gaglione, D., Clemente, C., Ilioudis, C. V., Persico, A. R., Proudler, I. K., and Soraghan, J. J. (2016a). Fractional fourier based waveform for a joint radar-communication system. In *2016 IEEE Radar Conference (RadarConf)*, pages 1–6.
- [42] Gaglione, D., Clemente, C., Ilioudis, C. V., Persico, A. R., Prouler, I. K., Soraghan, J. J., and Farina, A. (2018). Waveform design for communicating radar systems using fractional fourier transform. In *Digital Signal Processing*, volume 80.
- [43] Gaglione, D., Clemente, C., Persico, A. R., Ilioudis, C. V., Proudler, I. K., and Soraghan, J. J. (2016b). Fractional fourier transform based co-radar waveform: Experimental validation. In *2016 Sensor Signal Processing for Defence (SSPD)*, pages 1–5.
- [44] Gao, R. and Yan, R. (2006). Non-stationary signal processing for bearing health monitoring. In *IJMR*, volume 1, pages 18–40.

References

- [45] Garmatyuk, D., Schuerger, J., Morton, Y. T., Binns, K., Durbin, M., and Kimani, J. (2007). Feasibility study of a multi-carrier dual-use imaging radar and communication system. In *2007 European Radar Conference*, pages 194–197.
- [46] Ghasemi, A. and Sousa, E. S. (2008). Spectrum sensing in cognitive radio networks: requirements, challenges and design trade-offs. In *IEEE Communications Magazine*, volume 46, pages 32–39.
- [47] Griffiths, H., Cohen, L., Watts, S., Mokole, E., Baker, C., Wicks, M., and Blunt, S. (2015). Radar spectrum engineering and management: Technical and regulatory issues. In *Proceedings of the IEEE*, volume 103, pages 85–102.
- [48] Hadani, R., Rakib, S., Tsatsanis, M., Monk, A., Goldsmith, A. J., Molisch, A. F., and Calderbank, R. (2017). Orthogonal time frequency space modulation. In *2017 IEEE Wireless Communications and Networking Conference (WCNC)*, pages 1–6.
- [49] Han, L. and Wu, K. (2010). Radar and radio data fusion platform for future intelligent transportation system. In *The 7th European Radar Conference*, pages 65–68.
- [50] Hassanien, A., Amin, M. G., Zhang, Y. D., and Ahmad, F. (2016a). Dual-function radar-communications: Information embedding using sidelobe control and waveform diversity. In *IEEE Transactions on Signal Processing*, volume 64, pages 2168–2181.
- [51] Hassanien, A., Amin, M. G., Zhang, Y. D., Ahmad, F., and Himed, B. (2016b). Non-coherent psk-based dual-function radar-communication systems. In *2016 IEEE Radar Conference (RadarConf)*, pages 1–6.
- [52] Haykin, S. (2001). *Communication Systems*. Wiley, New York.
- [53] Heinzl, G., Rüdiger, A., and Schilling, R. (2002). Spectrum and spectral density estimation by the discrete fourier transform (dft), including a comprehensive list of window functions and some new at-top windows. In *Max Plank Inst.*

References

- [54] Hesar, F. and Roy, S. (2016). Spectrum sharing between a surveillance radar and secondary wi-fi networks. In *IEEE Transactions on Aerospace and Electronic Systems*, volume 52, pages 1434–1448.
- [55] Hong-Bo Sun, Guo-Sui Liu, Hong Gu, and Wei-Min Su (2002). Application of the fractional fourier transform to moving target detection in airborne sar. In *IEEE Transactions on Aerospace and Electronic Systems*, volume 38, pages 1416–1424.
- [56] Ilioudis, C. V., Clemente, C., Proudler, I., and Soraghan, J. J. (2014). Constant envelope fractional fourier transform based waveform libraries for mimo radar. In *2014 Sensor Signal Processing for Defence (SSPD)*, pages 1–5.
- [57] Ilioudis, C. V., Clemente, C., Proudler, I., and Soraghan, J. J. (2015). Performance analysis of fractional waveform libraries in mimo radar scenario. In *2015 IEEE Radar Conference (RadarCon)*, pages 1119–1124.
- [58] Jackson, C. A., Holloway, J. R., Pollard, R., Larson, R., Sarno, C., Baker, C., Woodbridge, K., Ormondroyd, R. F., Lewis, M. B., and Stove, A. G. (2007). Spectrally efficient radar systems in the l and s bands. In *2007 IET International Conference on Radar Systems*, pages 1–6.
- [59] Jakabosky, J., Blunt, S. D., and Himed, B. (2016). Spectral-shape optimized fm noise radar for pulse agility. In *2016 IEEE Radar Conference (RadarConf)*, pages 1–6.
- [60] Jamil, M., Zepernick, H., and Pettersson, M. I. (2008a). On integrated radar and communication systems using oppermann sequences. In *MILCOM 2008 - 2008 IEEE Military Communications Conference*, pages 1–6.
- [61] Jamil, M., Zepernick, H., and Pettersson, M. I. (2008b). Performance assessment of polyphase pulse compression codes. In *2008 IEEE 10th International Symposium on Spread Spectrum Techniques and Applications*, pages 166–172.

References

- [62] Jeong-Geun Kim, Sang-Hoon Sim, Sanghoon Cheon, and Songcheol Hong (2005). 24 ghz circularly polarized doppler radar with a single antenna. In *2005 European Microwave Conference*, volume 2, page 4 1386.
- [63] Jiang, D. and Delgrossi, L. (2008). Ieee 802.11p: Towards an international standard for wireless access in vehicular environments. In *VTC Spring 2008 - IEEE Vehicular Technology Conference*, pages 2036–2040.
- [64] Jin, F. and Cao, S. (2019). Automotive radar interference mitigation using adaptive noise canceller. In *IEEE Transactions on Vehicular Technology*, volume 68, pages 3747–3754.
- [65] Jung-Hwan , C., Han-Byul, L., Ji-Won and KIM, C., and Cheol, S. (2016). Mutual interference suppression using clipping and weighted-envelope normalization for automotive fmcw radar systems. In *IEICE Transactions on Communications*, volume E99.B, pages 280–287.
- [66] Khanna, R. and Saxena, R. (2009). Improved fractional fourier transform based receiver for spatial multiplexed mimo antenna systems. In *Wireless Personal Communications*, volume 50, pages 563–574.
- [67] Khoury, J., Ramanathan, R., McCloskey, D., Smith, R., and Campbell, T. (2016). Radarmac: Mitigating radar interference in self-driving cars. In *2016 13th Annual IEEE International Conference on Sensing, Communication, and Networking (SECON)*, pages 1–9.
- [68] Kim, E. H. and Kim, K. H. (2018). Random phase code for automotive mimo radars using combined frequency shift keying-linear fmcw waveform. In *IET Radar, Sonar Navigation*, volume 12, pages 1090–1095.
- [69] Konno, K. and Koshikawa, S. (1997). Millimeter-wave dual mode radar for headway control in ivhs. In *1997 IEEE MTT-S International Microwave Symposium Digest*, volume 3, pages 1261–1264.
- [70] Kumari, P., Choi, J., González-Prelcic, N., and Heath, R. W. (2018). Ieee 802.11ad-based radar: An approach to joint vehicular communication-radar system. In *IEEE Transactions on Vehicular Technology*, volume 67, pages 3012–3027.

References

- [71] Kunert, M. (2012). The eu project mosarim: A general overview of project objectives and conducted work. In *2012 9th European Radar Conference*, pages 1–5.
- [72] Kutay, A., Ozaktas, H. M., Ankan, O., and Onural, L. (1997). Optimal filtering in fractional fourier domains. In *IEEE Transactions on Signal Processing*, volume 45, pages 1129–1143.
- [73] Lakshminarayana, H. K., Bhat, J. S., Jagadale, B. N., and Mahesh, H. M. (2009). Improved chirp modulation spread spectrum receiver based on fractional fourier transform for multiple access. In *2009 International Conference on Signal Processing Systems*, pages 282–286.
- [74] Lellouch, G., Tran, P., Pribic, R., and van Genderen, P. (2008). Ofdm waveforms for frequency agility and opportunities for doppler processing in radar. In *2008 IEEE Radar Conference*, pages 1–6.
- [75] Levanon, N. and Mozeson, E. (2004). *Radar Signals*. Chichester: John Wiley and Sons.
- [76] Lin, Z. and Wei, P. (2006). Pulse position modulation time hopping ultra wideband sharing signal for radar and communication system. In *2006 CIE International Conference on Radar*, pages 1–4.
- [77] Liu, T., Cao, N., Mao, M., Wang, F., and Du, Y. (2014). Waveform design and optimization for ofdm radar signal based on fractional fourier transform. In *The 2014 2nd International Conference on Systems and Informatics (ICSAI 2014)*, pages 724–729.
- [78] Liu, Y., Liao, G., Xu, J., Yang, Z., and Zhang, Y. (2017). Adaptive ofdm integrated radar and communications waveform design based on information theory. In *IEEE Communications Letters*, volume 21, pages 2174–2177.
- [79] Mahmoud, H. A., Yucek, T., and Arslan, H. (2009). Ofdm for cognitive radio: merits and challenges. In *IEEE Wireless Communications*, volume 16, pages 6–15.

References

- [80] Manolakis, D. and Ingle, V. (2011). *Applied Digital Signal Processing: Theory and Practice*. Cambridge University Press.
- [81] Martone, M. (2001). A multicarrier system based on the fractional fourier transform for time-frequency-selective channels. In *IEEE Transactions on Communications*, volume 49, pages 1011–1020.
- [82] Mendlovic, D. and Ozaktas, H. M. (1993). Fractional fourier transforms and their optical implementation: I. In *Journal of the Optical Society of America A*, volume 10, pages 1875–1881. OSA.
- [83] Mishra, K. V. and Eldar, Y. C. (2017). Sub-nyquist channel estimation over ieee 802.11ad link. In *2017 International Conference on Sampling Theory and Applications (SampTA)*, pages 355–359.
- [84] Mizui, K., Uchida, M., and Nakagawa, M. (1993). Vehicle-to-vehicle communication and ranging system using spread spectrum technique (proposal of boomerang transmission system). In *IEEE 43rd Vehicular Technology Conference*, pages 335–338.
- [85] Moghaddasi, J. and Wu, K. (2016). Multifunctional transceiver for future radar sensing and radio communicating data-fusion platform. In *IEEE Access*, volume 4, pages 818–838.
- [86] Muhammad, A., Joaquim, F., and José, F. (2016). *Introduction to Intelligent Transportation Systems*. Springer International Publishing, Cham.
- [87] Muns, G. R., Mishra, K. V., Guerra, C. B., Eldar, Y. C., and Chowdhury, K. R. (2019). Beam alignment and tracking for autonomous vehicular communication using ieee 802.11ad-based radar. In *IEEE INFOCOM 2019 - IEEE Conference on Computer Communications Workshops (INFOCOM WKSHPS)*.
- [88] Namias, V. (1980). The fractional order transform and its application to quantum mechanics. In *IMA Journal of Applied Mathematics*, volume 65, pages 241–265.

References

- [89] Neemat, S., Krasnov, O., and Yarovoy, A. (2019). An interference mitigation technique for fmcw radar using beat-frequencies interpolation in the stft domain. In *IEEE Transactions on Microwave Theory and Techniques*, volume 67, pages 1207–1220.
- [90] Nozawa, T., Makino, Y., Takaya, N., Umehira, M., Takeda, S., Wang, X., and Kuroda, H. (2017). An anti-collision automotive fmcw radar using time-domain interference detection and suppression. In *International Conference on Radar Systems (Radar 2017)*, pages 1–5.
- [91] of Advisors on Science, P. C. and Technology (2012). Report to the president: Realizing the full potential of government-held spectrum to spur economic growth. In *Executive Office of the President of the USA Presidents Council of Advisor on Science and Technology, Tech. Rep.*
- [92] Ozaktas, H., Mendlovic, D., Kutay, M. A., and Z., Z. Z. (2001a). *The Fractional Fourier Transform: With Applications in Optics and Signal Processing*. Wiley.
- [93] Ozaktas, H. M., Arikan, O., Kutay, M. A., and Bozdogat, G. (1996). Digital computation of the fractional fourier transform. In *IEEE Transactions on Signal Processing*, volume 44, pages 2141–2150.
- [94] Ozaktas, H. M., Zalevsky, Z., and Kutay, M. A. (2001b). *The Fractional Fourier Transform with Applications in Optics and Signal Processing*. John Wiley & Sons.
- [95] Patole, S. M., Torlak, M., Wang, D., and Ali, M. (2017). Automotive radars: A review of signal processing techniques. In *IEEE Signal Processing Magazine*, volume 34, pages 22–35.
- [96] Peden, M., R.Scurfield, Sleet, D., Mohan, D., Hyder, A. A., Jarawan, E., and Mathers, C. (2004). World health organization (who). In *World report on road traffic injury prevention*.
- [97] Pelich, R., Longépé, N., Mercies, G., Hajduch, G., and Garello, R. (2015). Refocusing of ship signatures and azimuth speed estimation based on frft

References

- and sar slc imagery. In *2015 IEEE International Geoscience and Remote Sensing Symposium (IGARSS)*, pages 3699–3702.
- [98] Porcino, D. and Hirt, W. (2003). Ultra-wideband radio technology: potential and challenges ahead. In *IEEE Communications Magazine*, volume 41, pages 66–74.
- [99] Poularikas, A. (2010). *Transforms and Applications Handbook*. Electrical Engineering Handbook. CRC Press.
- [100] Proakis, J. (2000). *Digital Communications*. 4th ed., McGraw-Hill New York.
- [101] Raei, E., Modarres-Hashemi, M., and Bhavani Shankar, M. R. (2019). Range cell migration correction by fractional fourier transform in synthetic aperture radars. In *2019 20th International Radar Symposium (IRS)*, pages 1–10.
- [102] Rajappan, G. and Honig, M. (2002). Signature sequence adaptation for ds-cdma with multipath. *IEEE Journal on Selected Areas in Communications*, 20(2):384–395.
- [103] Rameez, M., Dahl, M., and Pettersson, M. I. (2018). Adaptive digital beamforming for interference suppression in automotive fmcw radars. In *2018 IEEE Radar Conference (RadarConf18)*, pages 252–256.
- [104] Rapajic, P. and Vucetic, R. (1994). Linear adaptive transmitter-receiver structures for asynchronous cdma systems. In *Proceedings of IEEE 3rd International Symposium on Spread Spectrum Techniques and Applications (ISSSTA '94)*, volume 1, pages 181–185.
- [105] Rappaport, T. S. (1996). *Wireless Communications: Principles and Practice*. IEEE Press, 1st edition.
- [106] Raviteja, P., Hong, Y., Viterbo, E., and Biglieri, E. (2019a). Practical pulse-shaping waveforms for reduced-cyclic-prefix ofts. In *IEEE Transactions on Vehicular Technology*, volume 68, pages 957–961.

References

- [107] Raviteja, P., Phan, K. T., Hong, Y., and Viterbo, E. (2019b). Orthogonal time frequency space (otfs) modulation based radar system. In *2019 IEEE Radar Conference (RadarConf)*, pages 1–6.
- [108] Reed, J. H., Clegg, A. W., Padaki, A. V., Yang, T., Nealy, R., Dietrich, C., Anderson, C. R., and Mearns, D. M. (2016). On the co-existence of td-lte and radar over 3.5 ghz band: An experimental study. In *IEEE Wireless Communications Letters*, volume 5, pages 368–371.
- [109] Reichardt, L., Sturm, C., Grünhaupt, F., and Zwick, T. (2012a). Demonstrating the use of the ieee 802.11p car-to-car communication standard for automotive radar. In *2012 6th European Conference on Antennas and Propagation (EUCAP)*, pages 1576–1580.
- [110] Reichardt, L., Sturm, C., Grünhaupt, F., and Zwick, T. (2012b). Demonstrating the use of the ieee 802.11p car-to-car communication standard for automotive radar. In *2012 6th European Conference on Antennas and Propagation (EUCAP)*, pages 1576–1580.
- [111] Richards, A. (2014). *Fundamental of Radar Signal Processing, Second Edition*. McGraw-Hill Education.
- [112] Richards, M. A. (2005). *Fundamentals of Radar Signal Processing*. McGraw-Hill, New York.
- [113] Richards, M. A. and Holm, J. A. S. W. A. (2010). *Principle of MODERN RADAR*. SciTech Publishing-An Imprint of the IET.
- [114] Robertson, M. and Brown, E. R. (2003). Integrated radar and communications based on chirped spread-spectrum techniques. In *IEEE MTT-S International Microwave Symposium Digest, 2003*, volume 1, pages 611–614.
- [115] Rock, J., Toth, M., Messner, E., Meissner, P., and Pernkopf, F. (2019). Complex signal denoising and interference mitigation for automotive radar using convolutional neural networks. In *2019 22th International Conference on Information Fusion (FUSION)*, pages 1–8.

References

- [116] Roh, W., Seol, J., Park, J., Lee, B., Lee, J., Kim, Y., Cho, J., Cheun, K., and Aryanfar, F. (2014). Millimeter-wave beamforming as an enabling technology for 5g cellular communications: theoretical feasibility and prototype results. In *IEEE Communications Magazine*, volume 52, pages 106–113.
- [117] Rohling, H. and Meinecke, M. . (2001). Waveform design principles for automotive radar systems. In *2001 CIE International Conference on Radar Proceedings (Cat No.01TH8559)*, pages 1–4.
- [118] Saddik, G. and Brown, E. R. (2005). Towards a multifunctional lfm waveform communication radar system: Single-crystal ain-on-sic saw filters for x-band. In *GOMA Tech. Conf.*, pages 399–402.
- [119] Sanders, F. A., Sole, R. L., Bedford, B. L., Franc, D., and Pawlowitz, T. (2006). Effects of rf interference on radar receivers. In *U.S. Dept. of Commerce, National Telecommunications and Information Administration, Tech. Rep.*
- [120] Seskar, I. and Mandayam, N. (1999a). Software-defined radio architectures for interference cancellation in ds-cdma systems. *IEEE Personal Communications*, 6(4):26–34.
- [121] Seskar, I. and Mandayam, N. (1999b). A software radio architecture for linear multiuser detection. *IEEE Journal on Selected Areas in Communications*, 17(5):814–823.
- [122] Seung Hee Han and Jae Hong Lee (2005). An overview of peak-to-average power ratio reduction techniques for multicarrier transmission. In *IEEE Wireless Communications*, volume 12, pages 56–65.
- [123] Shaojian, X., Bing, C., and Ping, Z. (2006). Radar-communication integration based on dsss techniques. In *2006 8th international Conference on Signal Processing*, volume 4.
- [124] Shiwen, C., Gongming, W., Xiaopeng, X., and Jie, H. (2019). A method of radar signal feature extraction based on fractional fourier transform. In

References

- 2019 IEEE 4th International Conference on Signal and Image Processing (ICSIP)*, pages 583–587.
- [125] Singh, Ashutosh, Saxena, and Rajiv (2013). Dfrft: A classified review of recent methods with its application. In *Journal of Engineering*, volume 2013.
- [126] Stelzer, A., Jahn, M., and Scheiblhofer, S. (2008). Precise distance measurement with cooperative fmcw radar units. In *2008 IEEE Radio and Wireless Symposium*, pages 771–774.
- [127] Stojanovic, D., Djurovic, I., and Vojcic, B. R. (2009). Interference analysis of multicarrier systems based on affine fourier transform. In *IEEE Transactions on Wireless Communications*, volume 8, pages 2877–2880.
- [128] Stüber, G. L. (1996). *Digital Signaling on Flat Fading Channels*. Springer US, Boston, MA.
- [129] Sturm, C., Braun, M., Zwick, T., and Wiesbeck, W. (2010). A multiple target doppler estimation algorithm for ofdm based intelligent radar systems. In *The 7th European Radar Conference*, pages 73–76.
- [130] Sturm, C., Pancera, E., Zwick, T., and Wiesbeck, W. (2009a). A novel approach to ofdm radar processing. In *2009 IEEE Radar Conference*, pages 1–4.
- [131] Sturm, C., Pancera, E., Zwick, T., and Wiesbeck, W. (2009b). A novel approach to ofdm radar processing. In *2009 IEEE Radar Conference*, pages 1–4.
- [132] Sturm, C. and Wiesbeck, W. (2011). Waveform design and signal processing aspects for fusion of wireless communications and radar sensing. In *Proceedings of the IEEE*, volume 99, pages 1236–1259.
- [133] Surender, S. C. and Narayanan, R. M. (2011). Uwb noise-ofdm netted radar: Physical layer design and analysis. In *IEEE Transactions on Aerospace and Electronic Systems*, volume 47, pages 1380–1400.

References

- [134] Surender, S. C., Narayanan, R. M., and Das, C. R. (2010). Performance analysis of communications and radar coexistence in a covert uwb system. In *2010 IEEE Global Telecommunications Conference GLOBECOM 2010*, pages 1–5.
- [135] Tatiana, A., Vicente, L., Agulló-López, Fernando, and Almeida, L. (1994). The fractional fourier transform in optical propagation problems. volume 41, pages 1037–1044.
- [136] Tavik, G. C., Hilterbrick, C. L., and all (2005). The advanced multifunction rf concept. In *IEEE Transactions on Microwave Theory and Techniques*, volume 53, pages 1009–1020.
- [137] Tranter, W., Shanmugan, K., Rappaport, T., and Kosbar, K. (2003). *Principles of Communication Systems Simulation with Wireless Applications*. Prentice Hall Press.
- [138] Uchida, M., Kagawa, Y., and Okuno, A. (1994). A vehicle-to-vehicle communication and ranging system based on spread spectrum technique-ss communication radar. In *Proceedings of VNIS'94 - 1994 Vehicle Navigation and Information Systems Conference*, pages 169–174.
- [139] Umehira, M., Nozawa, T., Makino, Y., Wang, X., Takeda, S., and Kuranda, H. (2018). A novel iterative inter-radar interference reduction scheme for densely deployed automotive fmcw radars. In *2018 19th International Radar Symposium (IRS)*, pages 1–10.
- [140] Uysal, F. and Sanka, S. (2018). Mitigation of automotive radar interference. In *2018 IEEE Radar Conference (RadarConf18)*, pages 405–410.
- [141] Van Loan, C. (1992). *Computational Frameworks for the Fast Fourier Transform*. Society for Industrial and Applied Mathematics, USA.
- [142] Wang, H., Johnson, J. T., and Baker, C. J. (2017). Spectrum sharing between communications and atc radar systems. In *IET Radar, Sonar Navigation*, volume 11, pages 994–1001.

References

- [143] Winkler, V. and Detlefsen, J. (2007). Automotive 24 ghz pulse radar extended by a dqpsk communication channel. In *2007 European Radar Conference*, pages 138–141.
- [144] Woll, J. D. (1995). Vorad collision warning radar. In *Proceedings International Radar Conference*, pages 369–372.
- [145] Wymeersch, H., Seco-Granados, G., Destino, G., Dardari, D., and Tufvesson, F. (2017). 5g mmwave positioning for vehicular networks. In *IEEE Wireless Communications*, volume 24, pages 80–86.
- [146] Xu, S. J., Chen, Y., and Zhang, P. (2006). Integrated radar and communication based on ds-uw. In *2006 3rd International Conference on Ultrawideband and Ultrashort Impulse Signals*, pages 142–144.
- [147] Yang, C. and Shao, H. (2015). Wifi-based indoor positioning. In *IEEE Communications Magazine*, volume 53, pages 150–157.
- [148] Yates, R. (1995). A framework for uplink power control in cellular radio systems. *IEEE Journal on Selected Areas in Communications*, 13(7):1341–1347.
- [149] Yattoun, I., Labia, T., Peden, A., Landrac, G., Ney, M., Resibois, M., Bonnin, J., Baghdadi, A., Montavont, N., Fujise, M., and Le Roux, Y. (2007). A millimetre communication system for ivc. In *2007 7th International Conference on ITS Telecommunications*, pages 1–6.
- [150] Youn-Sik, S., Hyuk-Kee, S., and Seo, H. (2018). Automotive frequency modulated continuous wave radar interference reduction using per-vehicle chirp sequences. In *Sensors*, volume 18, page 2831. MDPI AG.
- [151] Zepemick, H.-J. (2005). Pseudo random signal processing : theory and application. In *Chichester, England : John Wiley and Sons*.
- [152] Zhang, H., Li, L., and Wu, K. (2007). 24ghz software-defined radar system for automotive applications. In *2007 European Conference on Wireless Technologies*, pages 138–141.

References

- [153] Zhang, R. and Cao, S. (2018). Support vector machines for classification of automotive radar interference. In *2018 IEEE Radar Conference (RadarConf18)*, pages 366–371.
- [154] Zhang Chaozhu and Chen Qiang (2013). Design of signal-sharing for radar and communication. In *Proceedings 2013 International Conference on Mechatronic Sciences, Electric Engineering and Computer (MEC)*, pages 1250–1253.
- [155] Zheng, L., Lops, M., Wang, X., and Grossi, E. (2018). Joint design of overlaid communication systems and pulsed radars. In *IEEE Transactions on Signal Processing*, volume 66, pages 139–154.
- [156] Zhou, H., Li, X., Tang, M., Wu, Q., X. Chen, Luo, M., Fu, S., and Liu, D. (2016). Joint timing/frequency offset estimation and correlation based on frft encoded training symbols for pdm co-ofdm systems. In *Optical Express*, volume 24.
- [157] Z.Xu and Shi, Q. (2018). Interference mitigation for automotive radar using orthogonal noise waveforms. In *IEEE Geoscience and Remote Sensing Letters*, volume 15, pages 137–141.